Abstract

LAMBERT, JEREMY BRANDON. A Miniaturized Device For Blood Typing Using A Simplified Spectrophotometric Approach. (Under the direction of Dr. M. K. Ramasubramanian.)

A new blood typing technology has been developed by Narayanan et al. using ultraviolet and visible light spectroscopy. Blood groups can be typed using changes in the UV and visible spectra between antibody treated and non-treated samples. These changes can be observed by optical density measurements in the 665 to 1000 nm region. Comparison of the slopes between the optical densities of control samples and antibody treated samples can be used to calculate an agglutination index number (A.I.) that describes whether or not the sample reacts to the antibody treatment.

A simplified system using a discrete LED/photodiode system to take the place of the monochromator/photodiode array system in the spectrophotometer has been developed by Anthony and Ramasubramanian that has shown promising results reproducing the measurements of the spectrophotometer. This system was used as a starting point for the proposed research.

The purpose of this research is to evaluate the scattering/absorption effects of red blood cells, designing a miniaturized system, and investigate this approach. The miniaturized system has been able to reproduce similar results to the spectrophotometer and is consistent with the simplified method of Anthony and Ramasubramanian. The miniaturized system also explores the use of fiber optics to improve repeatability of source mounting. A plano-convex lens is used to collimate the source beam incident on

the detector and eliminate the need for specific placement of the sample that would be necessary for the converging/diverging beam used previously. This allows the components to be placed closer together and further miniaturize the setup.

Packaging of this system into a compact device has been investigated and a device configuration is proposed. This packaged device could be modified further to include fluid handling that would yield a fully automated system.

It is concluded that an automated blood typing system or a possible bedside pretransfusion safety device using the spectrophotometric approach is a possibility.

A MINIATURIZED DEVICE FOR BLOOD TYPING USING A SIMPLIFIED SPECTROPHOTOMETRIC APPROACH

By

Jeremy Brandon Lambert

A thesis submitted to the Graduate Faculty of
North Carolina State University
in partial fulfillment of the
requirements for the Degree of
Master of Science

MECHANICAL ENGINEERING

Raleigh
2006

APPROVED BY:

Dr. W. L. Roberts	Dr. K. J. Peters

Dr. M.K. Ramasubramanian
(Committee Chair)

Dedication

To my Mother and Father, who always believed in me and sacrificed their own comforts in order to give me a chance at attaining my dreams

And

To God above, whose loving hand has given me the strength to take on the challenges that life presents

Biography

On November 1st, 1980, Jeremy Brandon Lambert was brought into the world in Raleigh, N.C. by his two loving parents, Buddy and Beverly Lambert. Jeremy was not an only child for long as his lone sibling, Jacob, was born a few years later on June 2nd, 1983 which was also their fourth wedding anniversary. Jacob would later go into engineering as well and is pursuing a double major in Computer and Electrical Engineering. Jeremy and Jacob had a happy childhood growing up in a very loving home. Jeremy graduated from Garner Senior High School in spring 1999 and was accepted into the Mechanical Engineering program at North Carolina State University for the following fall. He later began dating Crystal Hanifer, who he knew in high school, and is still currently dating. Jeremy did an extensive Co-Op at Advanced Energy Corporation that prolonged his undergraduate degree for an additional year. He still currently works part-time there and has enjoyed an excellent working relationship with the company. Jeremy graduated with his Bachelor of Science degree in Mechanical Engineering in spring 2004. Just before graduation, Jeremy was accepted into the Mechanical Engineering Masters program and decided to concentrate in the Mechatronics program. Jeremy intends to graduate in summer 2006 and work on a contract basis with Advanced Energy. It is during this time that he hopes to find a fulfilling career.

Acknowledgments

It is with sincere gratitude that I thank Dr. Ranga Krishnan, Chair of the Department of Psychiatry & Behavioural Sciences at Duke University as well as Dr. Steven Bredehoeft and the staff at the Duke University Medical Center Transfusion Services Laboratory. I would also like to give a special thanks to Mr. Donald Bennett, Technical Director of the Duke University Medical Center Transfusion Service Laboratory, for giving me everything I needed to conduct tests as well as providing some technical insight on the project. If it was not for the gracious support of all involved, this testing would not have been possible.

I would like to thank Dr. M.K. Ramasubramanian ("Dr. Ram") for giving me a project and helping me secure funding as well as providing a job for me during the summer. Without Dr. Ram, I could not have had the rewarding and enjoyable experience that I have had in Graduate School.

I would also like to thank Dr. Roberts and Dr. Peters for serving on my committee and providing helpful technical advice. Thanks to Dr. Chang for access to his equipment in the Pulp and Paper Science Department. Thanks to Dr. Aspnes for his helpful input. Thanks to Steve Anthony for his helpful advice.

I also want to thank to my colleagues Stewart Alexander, Joey Cochran, Vinay Swaminathan, Kalyan Katuri, and Sarah Fisher for their friendship along this journey. Thanks to Stewart and Joey for fabrication help and Sarah for taking care of ordering supplies.

Last but not least, I would like to thank my family. Thanks to Mom and Dad for their love and support. Thanks to my brother Jacob for programming help and friendship. Thanks to my grandparents, Ed and Dot Lambert and John and Frances Patterson, for their loving support. Thanks to Aunt Sarah, Uncle Mike, Uncle Brent, and Aunt Kim for all of their love and support.

I also need to thank my girlfriend, Crystal Hanifer, who always understands when I have to work and gives me a refuge of loving support when I am feeling down. I look forward to the future ahead.

Table of Contents

List of Figures vii

List of Tables x

Chapter 1 1

Chapter 2 2

2.1 General Properties of Human Blood 2

2.2 The ABO Blood Group System 3

2.3 ABO Grouping Errors 5

2.4 The Rh Blood Group 5

2.5 Complications Associated with Transfusions 6

2.6 Blood Donors 7

2.7 Collection and Storage 7

2.8 Immune Response to Blood Products 8

2.9 Pretransfusion Testing 10

Chapter 3 13

3.1 Automation Techniques 13

3.2 Manual Techniques 13

3.3 Flow Cytometry 15

3.4 UV and Visible Spectrophotometric Approach 15

Chapter 4 18

4.1 The Spectrophotometer 18

4.1.1 Optical Design 18

4.1.2 Electronic Design 19

4.2 Spectrophotometric Characteristics 20

4.2.1 Properties of Spectrophotometric Measurement 20

4.2.2 Sources of Error in Absorbance Measurement 21

Chapter 5 23

5.1 Spectroscopic Method for Blood Typing 23

5.2 Scattering Theory 25

5.3 Numerical Model and Results 31

5.4 Scattering Theory Application 36

Chapter 6 38

6.1 Optoelectronic Miniaturization 38
6.1.1 Light Sources and Detection 38
6.1.2 Fiber Optic Theory 41
6.1.3 Optical System 45
6.2 Current to Voltage Amplifiers 48
6.3 Data Acquisition 50
6.4 Experimental System 51
Chapter 7 53
7.1 Blood Typing Procedure 53
7.2 System Evaluation 55
7.3 Fiber Optic Characteristics 59
7.4 Collimation of the Beam Incident to the Detector 62
7.5 Source Intensity Effects 69
7.6 Sample Concentration 71
7.7 Sample Transience 72
7.8 Optimal Configuration 75
7.9 Full ABO/Rh Results 76
7.10 Reactive and Non-Reactive Thresholds 84
7.11 Economic Analysis 87
Chapter 8 89
8.1 Discussion of Testing 89
8.2 Future Recommendations 89
8.2.1 Whole Blood System 90
8.2.2 The Antisera Method 90
8.2.3 A Packaged Device with Manual Fluid Handling 90
Chapter 9 93
References 94
Appendix A 97
Appendix B 122
Appendix C 125
Appendix D 127
Appendix E 139

List of Figures

Figure 2.1 - Red Blood Cells with a White Blood Cell 3
Figure 2.2 – Acute Hemolytic Transfusion Reactions 7
Figure 3.1 – Micronics ABO Card 14
Figure 3.2 – ID-MTS Gel Test System (Ortho-Clinical Diagnostics, Inc.) 14
Figure 3.3 – Optical Configuration for Previous Sensor 16
Figure 4.1 – Agilent 8453 Optical System 18
Figure 4.2 – Transmittance Through a Homogeneous Mixture 20
Figure 4.3 – Cuvettes Containing Saline, Control, and Antibody Treated Samples 22
Figure 5.1 – Spectra of A- Blood 25
Figure 5.2 – Particle Exhibiting Rayleigh Scattering 25
Figure 5.3 – Particle Exhibiting Mie Scattering 26
Figure 5.4 – Coordinate System for Plane Electromagnetic Wave 27
Figure 5.5 – Spherical Coordinate System 28
Figure 5.6 – Single Particle Scenario with Detector 29
Figure 5.7 (a) and (b) – Non Reactive Cells (a) and Reactive Cells (b) 32
Figure 5.8 – Particle Size Distributions 33
Figure 5.9 - $\langle C_{ext} \rangle$ vs Wavelength 34
Figure 5.10 – Differential Scattering Cross Section 35
Figure 5.11 – Asymmetry Parameter vs. Wavelength 36
Figure 5.12 – B- Blood Spectrum 37
Figure 6.1 – LED/IRED Schematic 39
Figure 6.2 – Combined LED and Photodiode Response 41
Figure 6.3 – Light Wave 42
Figure 6.4 – Electromagnetic Spectrum 42
Figure 6.5 – Snell's Law 43
Figure 6.6 – Total Internal Reflection 44
Figure 6.7 – Acceptance Angle 45
Figure 6.8 – Initial Optical System 46
Figure 6.9 – Optimal Configuration 47
Figure 6.10 – Photodiode Amplifier Circuit 48

Figure 6.11 – Step Response 49
Figure 6.12 – Bode Plot 49
Figure 6.13 – LabView User Interface 50
Figure 6.14 – Automated Test System Configuration 51
Figure 6.15 – Miniaturized Optical System 51
Figure 6.16 (a) and (b) – Amplifiers (a) and Power Supplies (b) 52
Figure 6.17 (a) and (b) – Light Sources (a) and Data Acquisition (b) 52
Figure 7.1 – Flow Chart of Sample Preparation 54
Figure 7.2 – Absorption of Antibody Background 55
Figure 7.3 – Amplifier Linearity with Neutral Density Filter 56
Figure 7.4 – Amplifier Linearity with no Obstruction 57
Figure 7.5 – Combined Electrical System Response over time 58
Figure 7.6 – Normalized Cuvette Mount Repeatablility Versus Time 59
Figure 7.7 – Output Voltage Versus Optical Fiber Angle 60
Figure 7.8 – Normalized Output Voltage Versus Time for Fiber Coupling Repeatability 61
Figure 7.9 – System Collimation 62
Figure 7.10 – Normalized Optical Density vs. Aperture Size at 660 nm Wavelength 63
Figure 7.11 – Normalized Optical Density vs. Aperture Size at 870 nm Wavelength 64
Figure 7.12- Normalized Optical Density vs. Aperture Size at 950 nm Wavelength 64
Figure 7.13– Optical Density vs. Detector Distance at 660 nm Wavelength 65
Figure 7.14 – Optical Density vs. Detector Distance at 870 nm Wavelength 66
Figure 7.15 – Optical Density vs. Detector Distance at 950 nm Wavelength 66
Figure 7.16 – Measured Spectra of A- Control and Antibody Treated Samples 68
Figure 7.17 - Measured Spectra of B- Control and Antibody Treated Samples 68
Figure 7.18– Optical Density vs. Source Intensity for 660 nm LED 69
Figure 7.19 – Optical Density vs. Source Intensity for 870 nm LED 70
Figure 7.20 – Optical Density vs. Source Intensity for 950 nm LED 70
Figure 7.21 – Spectra of 10 – 80 μL A+ Concentrations 71
Figure 7.22 – Comparison of Control and Antibody Treated Spectra at 950 nm 72
Figure 7.23 – Normalized Output Voltage Over Time for Saline and A- Samples With 660 nm Source 73

Figure 7.24 – Agglutination Index over Time 74
Figure 7.25 – Full Spectra of A+ Type Blood on Spectrophotometer 77
Figure 7.26 – Full Spectra of A+ Type Blood on LED Device 77
Figure 7.27 – Full Spectra of A- Type Blood on Spectrophotometer 78
Figure 7.28 – Full Spectra of A- Type Blood on LED Device 78
Figure 7.29 – Full Spectra of B+ Type Blood on Spectrophotometer 79
Figure 7.30 – Full Spectra of B+ Type Blood on LED Device 79
Figure 7.31 – Full Spectra of B- Type Blood on Spectrophotometer 80
Figure 7.32 – Full Spectra of B- Type Blood on LED Device 80
Figure 7.33 – Full Spectra of O+ Type Blood on Spectrophotometer 81
Figure 7.34 – Full Spectra of O+ Type Blood on LED Device 81
Figure 7.35 – Full Spectra of O- Type Blood on Spectrophotometer 82
Figure 7.36 – Full Spectra of O- Type Blood on LED Device 82
Figure 8.1 – Solid Model of Proposed Sensor with Manual Fluid Handling 91
Figure 8.2 – Collimating Lens Integrated Into Fiber 91

List of Tables

Table 2.1 – ABO Blood Grouping System 3
Table 2.2 – ABO Reactions..... 4
Table 2.3 – Interpretations of Agglutination Reactions 11
Table 7.1 – Comparison of the Agglutination Indeces between the Spectrophotometer and Experimental System..... 83
Table 7.2 – Agglutination Index Distribution for Agglutinated Samples 85
Table 7.3 – Agglutination Index Distribution for Non-Agglutinated Samples..... 85
Table 7.4 – Agglutination Index Thresholds for Slope Calculation Methods 86
Table 7.5 – Approximated Cost of Packaged Unit..... 87

Chapter 1

Introduction

Bedside blood typing techniques in use today rely on subjective evaluation of reactions to determine the type of blood [1]. The accuracy of this type of testing has proven to be a function of the person's experience who is administering the test [2,3]. The administration of blood to anyone other than the intended patient could have catastrophic effects due to adverse reactions caused by incompatible ABO groups [3]. It has been proven that the amount of mistakes made during pre-transfusion testing, which leads to incompatible transfusions, can be attributed to human error and may be able to be significantly reduced with new methods [2,3].

The final crossmatch or bedside compatibility test provides the last check before a transfusion is administered. In order to reduce errors, improvements in bedside test kits have been pursued as well towards automating the procedure[4]. Currently, there are no automated bedside crossmatching devices in use although there have been many techniques proposed to accomplish this feat. The automated devices in use today are employed in the laboratory and come at a high cost [5].

A new method of blood typing has been introduced recently that uses the transmission spectra of blood cell suspensions in saline to detect agglutination using a spectrophotometer [6,7]. The results published using this method have shown a high level of accuracy. Research was initiated at NCSU to create a cost effective sensor that could replicate laboratory results using the spectrophotometer [8]. This method employed a discrete LED array and a photodetector.

The research in this paper builds on the previous research at NCSU by employing different methods such as fiber optics and a small lens to create a simplified and miniaturized the setup. The scope of this work will address the fundamental light scattering properties of the red blood cells, design a miniaturized sensor, and evaluate this approach through various testing methods.

Chapter 2

Blood Background

In order to provide a basis for the composition of blood, the blood group systems, and the effects of agglutination, this section will provide a brief discussion of these topics.

2.1 General Properties of Human Blood

Red blood cells, also known as erythrocytes, average about 7.5 μm in diameter with a thickness of about 2.4 μm at the edges and 1.0 μm in the center [9]. Red blood cells make up about 40 – 50% of the composition of blood. A normal human will have about 5 million red blood cells per cubic millimeter of blood. The red blood cell is composed of about 64% water, 28% hemoglobin, 7% lipids or fatty materials, and the rest consists of sugars, salts, enzymes, and other proteins. The main purpose of red blood cells is to carry oxygen throughout the body from the lungs and return carbon dioxide to the lungs. They are able to do this because they contain a protein known as hemoglobin which is able to carry out the oxygen-carbon dioxide exchange [10].

White blood cells, also known as leukocytes, are colorless cells that are not always confined to the blood channel. Leukocytes consist of neutrophils, eosinophils, basophils, monocytes, and lymphocytes which range in size from 7.5 – 22 μm[10]. They can easily pass through unruptured blood cells through a process called diapedesis. They are attracted to inflammation or infection due to tissue damage. White blood cells engulf the infection and digest them with lysosomal hydrolytic enzymes. They make up roughly 1% of the blood and are present in numbers of about 5,000 to 10,000 per cubic millimeter [10].

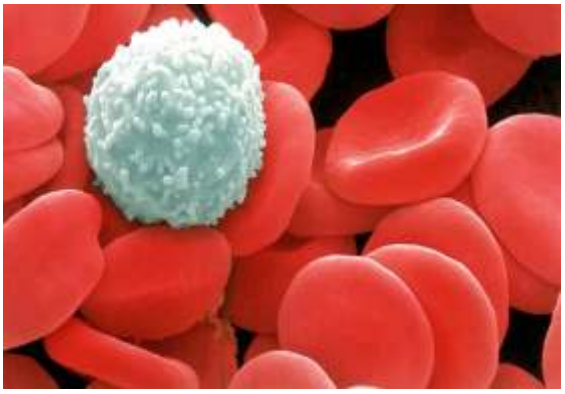


Figure 2.1 - Red Blood Cells with a White Blood Cell

Platelets, also known as thromocytes, are the smallest of the cells present in blood. They measure about 2-3 μm and form platelet membranes in to order clot and avoid blood loss. They also assist in providing protection for damaged tissue and fighting infection [10].

Plasma is the remaining major component of blood and makes up roughly 55 – 60% of the blood. Plasma is 90% water and 10% solids. The solids are made up of about 7% proteins while the rest is organic matter [10].

2.2 The ABO Blood Group System

The most important blood group system in use today is the ABO blood group system [11-13]. A person's blood type is categorized based on the antigens present on the red cells with the reciprocal antibody present in the plasma. The table below shows the ABO system at its simplest level [11].

Table 2.1 – ABO Blood Grouping System

ABO Group	Antigens on Red Cells	Antibodies in Plasma
O	None	Anti A and Anti B
A	A antigen	Anti B
B	B antigen	Anti A
AB	A and B antigen	None

A simple way to see the effects of the ABO system is mixing RBC's with plasma or serum. There are also reagents produced by monoclonal technology that can be used for ABO typing. These monoclonal reagents are utilized in typing experiments later in this paper. The incompatible combinations will react in a process called hemagglutination which

will be discussed later. The reactions can be summarized in table 2.2 with a positive reaction denoted by a "+" and negative reaction denoted by a "-" [10].

Table 2.2 – ABO Reactions

Blood Group	Forward Grouping Reaction with:		Reverse Grouping Reaction with:	
	Anti A	Anti B	A cells	B cells
O	-	-	+	+
A	+	-	-	+
B	-	+	+	-
AB	+	+	-	-

There are exceptions to these relations and a famous example of this is the Bombay phenotype. These individuals lacked the A and B antigens on the surface of the RBCs, but had antibodies to A, B, and O antigens. This is very rare and is isolated to the Bombay area.

The A and B blood types also have subgroups with varying phenotypes and genotypes [11-13]. Subgroups of A are phenotypes that differ quantitatively or qualitatively from the A antigen found on the RBCs. A_1 and A_2 account for about 99% of all type A patients tested. Both are found to react strongly with reagent anti A when tested. It has been found that type A_2 patients carry about 25% as many A antigen sites as A_1 cells. A_2 patients also demonstrated a reduction in the amount of N-acetylgalactosaminyltransferase which results in a larger amount of H antigen on the surface of their RBCs. Rare, weaker subgroups of A such as $A_{int,}$ A_3, A_x, A_m, or A_{el} are present in the population and are sometimes mistaken as type O patients [19].

There are also rare and weak subgroups of B that are seen even less frequently than the A subgroups. They are classified as B_3, B_x, B_m, and B_{el}.

Antibodies are Y shaped proteins also known as Immunoglobins (Ig) and arise shortly after birth. The antibodies of the ABO system are typically type IgM although some IgG and IgA antibodies may also be present. Antibodies are present in various bodily secretions and are mostly influenced by environmental factors [11].

2.3 ABO Grouping Errors

ABO grouping consists of a cell grouping and a serum grouping [11]. This is also known as forward and reverse grouping. Comparing the results of the two should support a common conclusion so that they confirm each other. There is a wide range of causes for these errors which are described below.

Technical errors committed by inexperienced personnel occur often and can produce discrepancies. Establishing and following test protocol can help eliminate errors of this type. When an error occurs, repetition of the procedure can help alleviate the errors.

Weak or missing antibodies that occur in adolescents and older patients can lead to incorrect typing [11,13]. Disease and weakness are also culprits for these errors. These problems can be addressed by testing the samples at a temperature lower than room temperature. This procedure can cause problems if cold reacting antibodies begin to react. This can also be said for weak or absent antigens[11].

Cold reactive antibodies and autoantibodies can also cause errors. Panagglutination or the ability for a serum to agglutinate all or almost all the cells in a sample can occur in a person with a strong auto anti-I. This occurs with adults because the I antigen is strong in almost all adults. This is more apparent the colder the temperature is. These antigens must be identified using other procedures to avoid an error in typing.

Rouleax is a phenomenon that can cause cells to stick together in a phenomenon that resembles agglutination [11]. This is caused by elevated protein levels or can occur in the presence of Dextran and Wharton's Jelly.

Other factors that can contribute to incorrect typing include alterations in normal blood samples such as increased blood group specific soluble substances(BGSS). Acquired B phenomenon or a source reagent that will demonstrate an antibody to a private antigen will also result in errors.

2.4 The Rh Blood Group

The Rh blood group was discovered in 1940 where about 85% of the population can be characterized as Rh positive and the remaining 15% as Rh negative [12]. There are about 40 different Rh antigens making the Rh system one of the most complex blood group systems. The term Rh positive or negative only corresponds to the presence of one Rh antigen in the

system known as Rh_O or D. For the purpose of simplicity and the fact that routine blood bank procedure does not account for the rest of the antigens, the D antigen will be the focus of this paper.

The D antigen is the most significant antigen after A and B. This antigen is so strong that about 50% of Rh negative people will form anti D after a single exposure. The D antigen can cause severe problems in transfusions and therefore should never be given to patients with anti D in their blood [12].

2.5 Complications Associated with Transfusions

An incompatible ABO transfusion can have horrifying effects on the patient. The worst of which is the immediate (acute) hemolytic reaction. This results in intravascular destruction of transfused red blood cells. The biological systems activated are complement, coagulation, and kinin[11].

Upon activation of the classical pathway, C3a and C5a are released into the plasma and act as potent anaphylatoxins. This leads to vascular permeability, delicate blood cells, polymorphonuclear leukocyte chemotaxis, and releases vasoactive amines such as serotonin and histamine. This leads to hypotension and shock. The compliment membrane attack can lead to activation of C9 and cause hemolysis of the RBC which causes hemoglobinuria and elevated plasma hemoglobin. The removal of the hemolglobin, which is released by the RBC, results in an increase of bilirubin. Haptoglobin binds to free hemoglobin in an effort to remove it.

The activated complement system can release thromboplastic substances from the RBC stroma. This activates the coagulation cascade and produces disseminated intravascular coagulation. (DIC) Excessive bleeding can be expected from the site.

Hageman factor initiates the coagulation cascade which can act on the kinin system to produce bradykinin. This increases capillary permeability and dilates arterioles. This produces hypotension which stimulates the nervous system to increase levels of norepinephrine and other catecholamines in the circulation. This can produce vascoconstriction in the kidneys.

The damaging effects result in systemic hypotension, DIC, renal vasoconstriction, and renal intravascular thrombi, leading to shock, renal failure, and occasionally death. The figure below maps out the effects [11]:

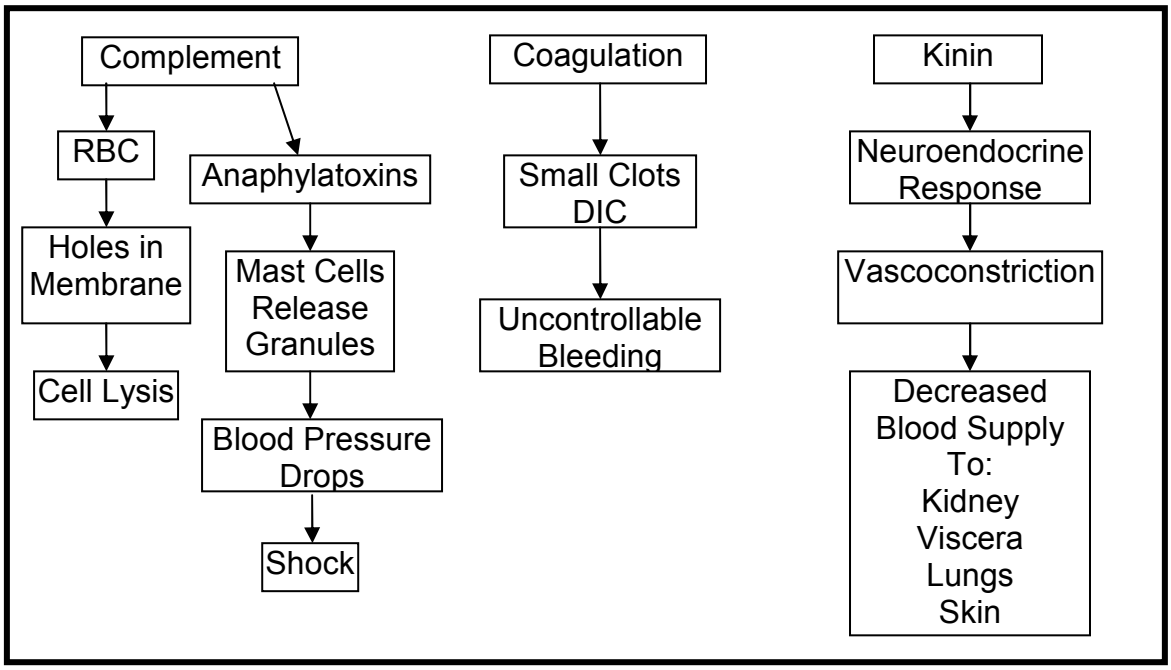


Figure 2.2 – Acute Hemolytic Transfusion Reactions

2.6 Blood Donors

Blood centers or blood banks try to provide an environment that is as pleasant and simple as possible for the prospective donors so that they continue to donate in the future. The American Association of Blood Banks (AABB) and the Food and Drug Administration (FDA) have set controlled manufacturing practices and standard operating procedures to govern the process of blood collection [11]. Donors are required to register contact information and medical history so that the blood can be traced and pulled from the supply if necessary. Donors are required to answer questions about lifestyle and recent health issues. Donors are notified of tests performed on their blood and possible complications that are revealed from these tests. The information collected is confidential and donors are given the opportunity to have their blood pulled from the supply if they believe there is a risk when using their blood.

2.7 Collection and Storage

Collection is undertaken by trained personel under the supervision of a qualified physician. Blood is removed through an aseptic technique using a sterile, closed system. All instruments and materials are single use, sterile, and disposable. All containers are FDA approved and must contain enough anticoagulant for the amount of blood being collected. The average amount of blood collected from a donor is about 450 +/- 45 ml with about 65 ml

of anti coagulant [11]. Each donation is assigned a unique number and is placed on the donation record. This is applicable to all blood components prepared.

RBCs are usually prepared soon after collection although they can be prepared anytime over the shelf life of the blood. The hematocrit or percentage of red cells in whole blood must be found to exist at a level of no less than 38% and no more than 80%. Patients with hematocrit levels over 80% must be evaluated by a physician. If the hematocrit levels are below 38% then the patient may be anemic and is unsuitable to donate. The RBCs are then separated from other blood components and placed in an additive solution. It is important that the white blood cells are removed because they could have adverse affects on the transfusion.

Anticoagulants used are citrate-phosphate- dextrose (CPD), citrate-phosphate-2-dextrose (CP2D), and citrate-phosphate-dextrose plus 0.25 mmol/L adenine (CPDA-1). These all contain citrate which prevents coagulation. Sodium biphosphate is also in the solution to maintain a high pH during storage. This helps maintain necessary levels of 2,3-DPG for oxygen dissociation. The concentration of 2,3-DPG influences release of oxygen to the tissues [10].

The shelf life of blood can be extended to 42 days when stored between 1 and 6ºC. The additive solutions contain saline, adenine, dextrose, and other substances that enhance RBC life. The blood is closely monitored in storage and alarms sound if the temperature of the blood exceeds the 6 ºC limit [11].

2.8 Immune Response to Blood Products

The immune response consists of antigen presentation and formation of antibodies. Concerns arise from the B-cell antibody made in response to antigenic material such as allogeneic or foreign red cells. This sometimes applies to platelets, white cells, and drugs. Immunization or sensitivity to these substances occurs through transfusion or pregnancy. The antibodies made in response to foreign blood products may be of IgG or IgM subclasses. IgM antibodies are usually the result of the primary exposure and are of low concentration. A secondary exposure could lead to IgG antibodies in much higher concentrations. This is known as the anamnestic response. Many factors such as age and condition of the immune system play a role in the strength of the response [11].

The mechanisms of agglutination can be described by antigen-antibody reactions that follow the law of mass action. Early work on this subject was done by Hughes-Jones in 1963 [14]. A simple combination equation shows the reaction between the antigen and antibody. This is considered to be a reversible bimolecular reaction:

$$Ab + Ag \underset{k_2, k_1}{\Leftrightarrow} AbAg$$

Where k_1 and k_2 are rate constants for the forward and reverse reactions. The law of mass action then dictates the following relationship:

$$\frac{[AbAg]}{[Ab] \times [Ag]} = \frac{k_1}{k_2} = K$$

Where [Ab], [Ag] and [AbAg] represent the concentration of reactants and products, and K is the equilibrium or association constant.

To observe an agglutination reaction through red cell-antibody binding a minimum number of antibody molecules must be bound to an antigen. The more antibodies present on a red cell, the stronger the reaction. The same can also be said if the serum concentration is increased. Increasing antigen concentration by increasing the strength of the RBC concentration will weaken the reaction and decrease sensitivity.

The law of mass action can also describe binding. Primary reactions are simply recognition in which an antigen and antibody have complementary structures and come in close opposition to one another. They can then be held together by weak intermolecular bonds which may or may not hold the complex together. Hydrogen bonds also result from sharing of hydrogen atoms between protons. Van der Waals forces are present from shifting of various positive cations and resultant attraction of negative ions.

The second stage of the red cell-antibody reaction is hemagglutination. Hemagglutination is dependent on amount and type of antibody present; the size, the number, and location of available antigen sites; and the pH, temperature, and ionic strength of the system. Most blood groups react in the pH range of 6.5 to 7.5 and a temperature range of 4 to 37ºC. The rate of dissociation increases as the temperature is raised.

The final stage in red cell-antibody binding includes complement activation, phagocytosis, opsonization, chemotaxis, immune adherence, and cellular degranulation, causing the destruction of the red cell (hemolysis).

2.9 Pretransfusion Testing

In the 1908, Ottenburg reported the importance of blood grouping and crossmatching prior to transfusion[11]. The crossmatch included the testing of recipient serum against donor red blood cells. Today the crossmatch is just one precaution taken before a transfusion. Pretransfusion protocols have been put in place and consist of the following fundamental practices:

1. A request to perform testing and prepare components
2. Receipt of an acceptable blood sample
3. Performance of an ABO blood group, Rh type, and antibody screen
4. Review of previous records of blood type and expected antibodies
5. Selection of crossmatch procedure
6. Selection of blood for transfusion
7. Performance of a crossmatch

Patient identity is maintained by wearing a wristband. Workers will ask the patient for their identity and confirm it. When taking samples from a patient, they are labeled before leaving the patient's side. The tube is then compared to the requisition and the wristband [11].

Forward ABO grouping is performed by adding anti A or anti B to a test tube and adding one drop of 4 to 6% serum or saline suspension of RBCs. This mixture is centrifuged, gently resuspended, and observed for clumping which could represent the presence of A and/or B antigen on the surface of the patient's RBCs. The reverse grouping is performed by mixing the patients serum or plasma with A_1 or B red blood cells. This mixture is processed the same as the forward grouping and observed for hemolysis or agglutination. To avoid error most facilties require a 2+ grading before the ABO/Rh can be determined. If an unresolvable discrepancy arises, group O blood will be used. The following chart shows the grating scale.

Table 2.3 – Interpretations of Agglutination Reactions

Strength of Reaction	Appearance
4+	Single agglutinate, no free cells
3+	Strong reaction, many large agglutinates
2+	Large agglutinates with smaller clumps, no free cells
1+	Many small agglutinates with a background of free cells
+/-	Few agglutinates and weak agglutinates microscopically
0	An even cell supspension, no agglutinates detected

The Rh test is basically the same procedure as the ABO test. In this case the saline or serum suspension is mixed with an anti D reagent. If a patient is possibly AB positive, a commercial Rh control serum or 6% albumin control should be included and should be negative. This must be done because a negative control is not present in the forward grouping.

An antibody screen is used to detect clinically significant antibodies in the patient's serum. The screening cells used contain antigenic expressions of D, C, d, E, e, Kell, k, Le^a, Le^b, Jk^a, Jk^b, Fy^a, Fy^b, P1, M, N, S, and s.

Finally, the crossmatch can be employed to determine compatibility of recipient serum with donor RBCs. Two serologic methods are used, the immediate spin crossmatch (IS) and the indirect antiglobulin test crossmatch (IAT).

The IS crossmatch [11] detects most ABO incompatibility and can be used if the antibody screen is nonreactive. The IS crossmatch is performed by making a 2 to 3% suspension of donor RBCs and mixing with patient serum. After centrifugation, the cell button is gently dislodged and inspected for agglutination or hemolysis.

The IAT crossmatch [11] consists of testing donor cells and patient serum with an enhancement medium such as albumin or LISS at a 37ºC incubation phase and includes addition of an antiglobulin phase.

Now that blood properties and blood handling have been introduced, the next chapter will discuss blood typing machines and methods.

Chapter 3

Current Technology and Previous Research

This section will discuss blood typing methods from the past and present. Automating, manual, and experimental techniques will be discussed leading up to the basis for the current research.

3.1 Automation Techniques

The TIC Auto Analyzer was introduced in 1967 and was the first machine to attempt automation of routine donor testing. This machine utilized continuous flow technology. The machine automatically sampled and performed ABO and Rh tests, but relied on the operator to identify samples, read reactions, and interpret and record results [5,15].

The Groupamatic was a French machine designed at the Centre National de Transfusion Sanguine in Paris. It mimicked manual test procedures with robotics, yet had great speed and accuracy. Data processing was incorporated easily to this setup and it enjoyed rapid success [5].

In order to compete with the Groupamatic, TIC released a new version of the Auto Analyzer and called it the Auto Grouper. This machine included a laser for reading sample numbers and integration of those with machine interpreted results [5].

The Olympus was introduced in the late 1980's that utilized a unique micro-plate technology that does not require centrifugation [5]. .

3.2 Manual Techniques

Card tests have become popular bedside and home blood typing techniques. Micronics, Inc. and Eldon Biologicals, Inc. market card tests presently. Both of these test methods require someone to interpret the results.

The Micronics ABO^{TM} card requires that the person apply blood to the card and push a small on-card bellows that draws the reagents and sample together. A viewing window shows whether the agglutination occurs and a reference table allows the user to determine the blood type. All waste is stored on the card which allows for easy cleanup [16].

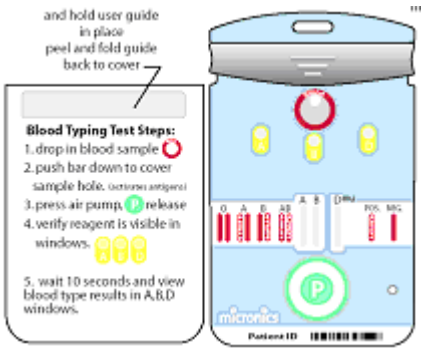


Figure 3.1 – Micronics ABO Card

The Eldon Biologicals Eldon Card™ requires more effort to prepare because water must be applied to the test areas before testing. The sample is then drawn and collected. The blood must then be spread across the test areas with a comb that is provided. The samples are then compared to a chart provided with the card [17].

Gel testing was developed in the late 1980's and is still a reliable test method for transfusion laboratories [11]. This test uses six microtubes contained in a 2.0 x 2.75 inch card. Predispensed in the tubes is a mixture of gel particles, the AHG serum, and diluent. The gel particles are Dextran acrylamide spheres that function as filters that trap red cell agglutinates. This is one of the main manual tests used at the Duke Transfusion Services lab and a picture is shown in figure 3.2.



Figure 3.2 – ID-MTS Gel Test System (Ortho-Clinical Diagnostics, Inc.)

A measured amount of the desired red blood cell suspension is added first, followed by a measured volume of serum or plasma. The gel card is incubated at 37°C for a predetermined time and then centrifuged. After centrifugation, the test results are read and graded [11].

The ID-MTS is available with a variety of automation platforms, such as the TECAN Megaflex-ID™ used at Duke University Hospital, which is designed for high-volume throughput in centralized blood bank testing [8].

3.3 Flow Cytometry

Flow cytometry is basically the use of forward light scattering to estimate the size of individual biological cells [18]. These biological cells are flowing single file in a single stream of fluid. Light scattering at different angles can distinguish differences in size and internal complexity. This makes flow cytometry a good tool for detailed analysis of complex populations. Characteristics that can be observed from this analysis include cell size, cytoplasmic complexity, DNA or RNA content, and a wide range of membrane bound and intracellular proteins [19]. Although a great tool for research, flow cytometry's complexity and expense make it less feasible for routine blood typing.

3.4 UV and Visible Spectrophotometric Approach

A new method of blood typing based on UV and visible light spectroscopy was developed by S. Narayanan, S. et al. of the Departments of Chemistry and Chemical Engineering at the University of South Florida [6,7]. This research determined blood types by quantifying reproducible changes in UV and visible light spectra of blood in the presence of agglutination. This was done using a spectrophotometer to give a spectrum between 665 and 1000 nm. This range was found to reveal a large difference between reactive and non-reactive samples. An algorithm was derived to compare the relative slopes between control and antibody treated samples to output an agglutination index that describes whether the sample is reactive or non-reactive.

Steve Anthony presented a partially automated method that simplified the method by using three discrete wavelength light sources in the 600-1000 nm range [8]. The transmitted light intensity was measured through the use of a photodiode and the blood type was determined using the agglutination index computation [6,7].

This system is quite flexible in that it allows for adjustment of all of the components in the system [8]. Light sources chosen for the system fell within the 600 – 1000 nm wavelength range of interest for the blood samples. Instead of using a monochromator to generate these light sources, discrete light emitting diodes of 660, 880, and 940 nm with spectral bandwidths of 60 nm, 30 nm, and 30 nm were used. These LEDs implemented

dome lenses producing narrow half power emission angles of 12°, 22°, and 22°, respectively. These sources were mounted to aluminum blocks and interchanged for measurements. A photodiode was selected as the detector whose output voltage can be made directly proportional to light intensity received. The photodiode selected has a wide range of sensitivity (320 nm – 1100 nm) as well as low dark current, high shunt resistance, and low terminal capacitance. These qualities make this Hammamatsu photodiode an ideal component for analytical instruments (see appendix D).

The optical configuration was a convergent light path focused inside the cuvette which was mounted on a precision machined holder to reduce movement and increase consistency of the cuvette position. The convergent light path was created by focusing the narrow beam from the source with two bi-convex lenses having a focal length of 50mm. These lenses were mounted in a lens tube to reduce the overall effective focal length. A ½" variable aperture restricted the light and allowed for adjustment to the source beam. Adjustment to the system was done with ½" posts and holders that allowed movement of all components in the system. All of these mounts were fixed to an optical breadboard so that all mounts would be secure. This system proved to be effective, yet the size of the system was larger than desirable. The optical configuration schematic is shown in figure 3.3 [8]:

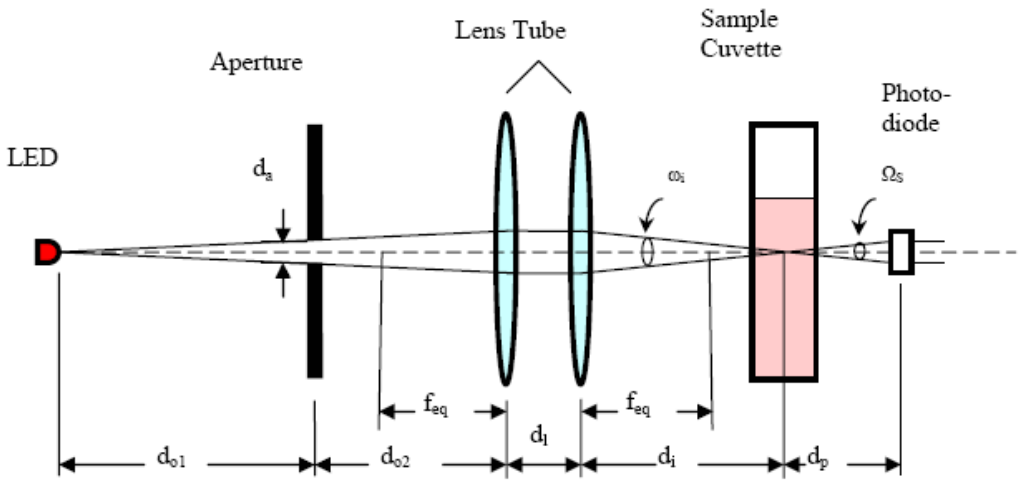


Figure 3.3 – Optical Configuration for Previous Sensor

The experimentation with this configuration focused on varying the d_a and d_p parameters to find an optimal configuration. Scattering angle was also investigated because of the ability rotate to components about the optical axis. The lens tube allowed for a

separation of 8 mm between the lenses which gave an effective focal length shown by the equation below [20]:

$$f_{eq} = \frac{f_1 f_2}{f_1 + f_2 - d_1} = 27.439mm$$

The position of the image as a function of $d_{o1} + d_{o2}$ is solved with the simple thin lens equation:

$$d_i = \frac{(d_{o1} + d_{o2}) f_{eq}}{d_{o1} + d_{o2} + f_{eq}}$$

The resulting solid angle ω_i entering the cuvette is [21]:

$$\omega_i = 2\pi(1 - \cos\theta_i) \quad [sr]$$

The projected solid angle detected by the photodiode is [21]:

$$\Omega_s = \pi \sin^2 \theta_i \quad [sr]$$

Where:

$$\theta_i = \tan^{-1}\left(\frac{(2d_{o1} + 2d_{o2} + d_l)\sin\theta_o}{2d_i + d_l}\right) \quad [rad]$$

And:

$$\theta_o = \tan^{-1}\left(\frac{d_a}{2d_{ol}}\right) \quad [rad]$$

This system created the basis for the research in this paper because it gave insight on things to consider before miniaturization. This setup and the spectrophotometer show that the forward scattering direction is the optimal direction to focus on. Light sources need to share a common axis and lenses with smaller focal lengths need to be utilized to create a miniaturized version of this setup.

Now that previous and current blood typing techniques have been discussed a basic understanding of the fundamental concepts that govern this project will be presented in the following chapter.

Chapter 4

The Spectrophotometric Approach

4.1 The Spectrophotometer

A schematic of the Agilent 8453 diode array spectrophotometer is shown in Figure 4.1 [22].

4.1.1 Optical Design

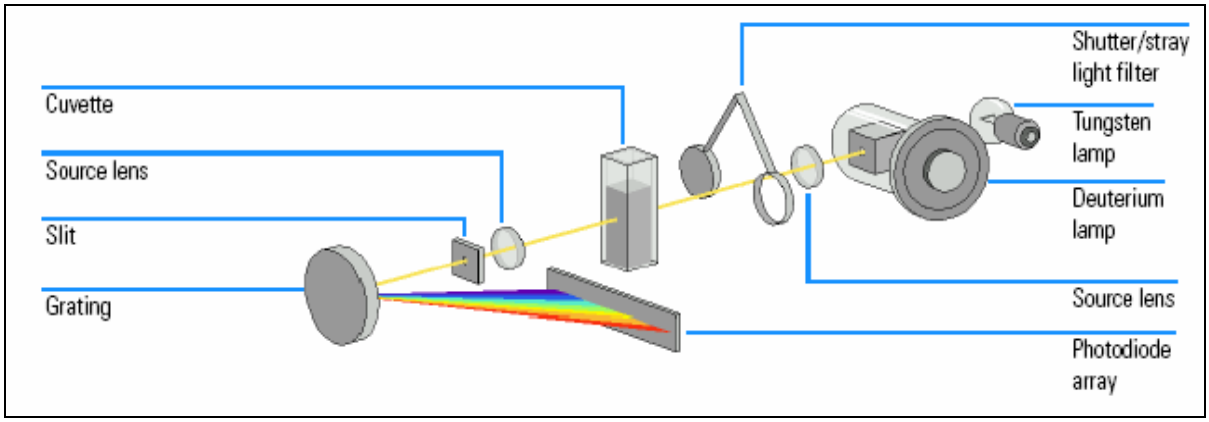


Figure 4.1 – Agilent 8453 Optical System

The light source is a dual lamp arrangement, a deuterium-discharge lamp and a tungsten lamp. The deuterium lamp provides the ultraviolet wavelength range which is about 190 nm to 800 nm. The tungsten lamp provides the visible and short wave near-infrared range of about 370-1100 nm. The two sources share a common axis to the source lens which collimates the light into a single beam. This beam is passed through a shutter/stray-light correction filter and through the sample to the spectrograph lens. This light is focused onto a slit aperture that is the size of a single photodiode on the photodiode array. This allows the light to be focused only on the appropriate photodiode. A holographic grating disperses the light beam onto the photodiode at an angle proportional to the wavelength to handle the dispersion and spectral imaging. There are 1024 photodiodes etched to a single chip which allows a nominal sampling interval of 0.9 nm from 190 to 1100 nm [22].

4.1.2 Electronic Design

The photodiode array mentioned above forms spectra derived from intensity counts through the use of several processing steps and hardware boards. There is a built in data acquisition board that adjust signals from the photodiode array and converts them to digital values with a 16 bit, 160 kHz, A/D converter. Temperature compensation is done using a table of correction factors.

The main processor board contains a spectra and signal processor that uses a ASIC and RAM of 3 ×128 KB and converts 1024 raw data values from the data acquisition board to intensity and absorbance values. The process goes as follows:

1. dark current correction
2. offset correction
3. photodiode array temperature compensation
4. stray light correction
5. absorbance calculation
6. signal averaging over an integration time, and
7. variance calculation

The lamp supply board provides controls for the light sources. The deuterium lamp is powered with a constant current of 320 mA and voltage of 50 and 105 VDC. The tungsten lamp requires a constant voltage of 6 VDC and currents between 0.7 and 0.9 A [22].

4.2 Spectrophotometric Characteristics

A beam of radiation can pass through a medium and change in one of four fundamental processes: reflection, refraction, absorption, and transmission. The spectrophotometer measures absorption of a solvent and eliminates or compensates for other effects. The prototypes that have been designed at NCSU give up some of these compensation features in the interest of cost, but the strength of the reactions make up for these sources of error.

4.2.1 Properties of Spectrophotometric Measurement

Absorbance only applies to a solution so optical density will be used to define this process. Optical density is a general term that is measured in absorbance units (AU) and are calculated from transmittance using the Beer-Lambert law [23].

$$T = \left(\frac{I_O}{I}\right) \; and \; OD = -\log_{10} T$$

where T is transmittance, I is incident radiation, and I_O is transmitted radiation. The spectrophotometer reads the transmitted radiation in the manner shown below:

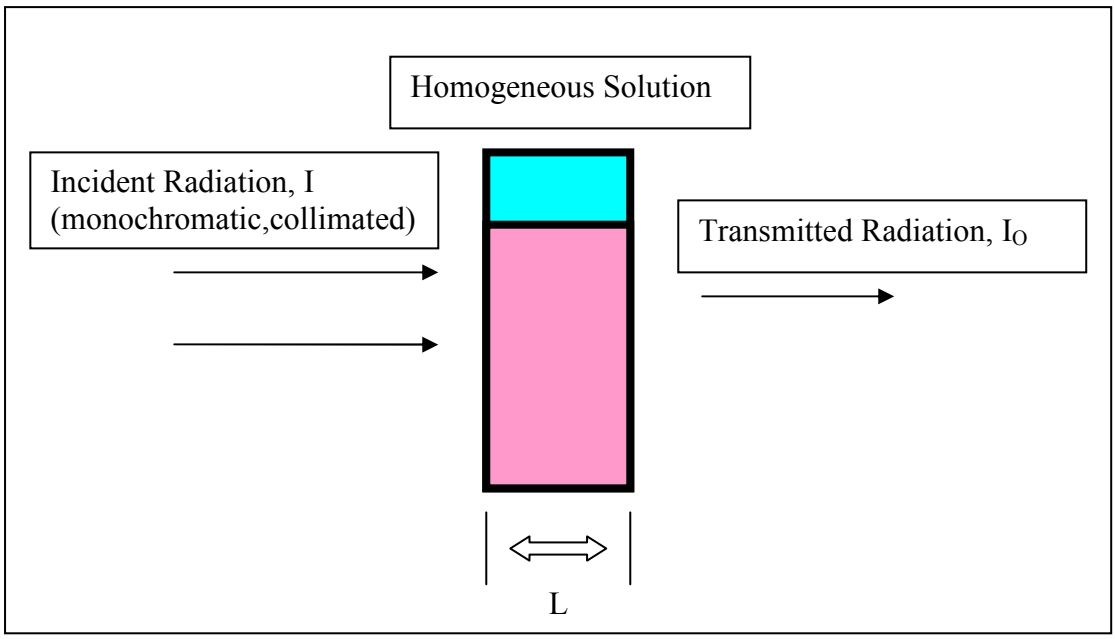


Figure 4.2 – Transmittance Through a Homogeneous Mixture

4.2.2 Sources of Error in Absorbance Measurement

Errors associated with absorbance measurement can be attributed to the spectrophotometer or device and the way they are used. The transmittance or absorption as outlined by Jones and Sandorfy that is seen by the spectrophotometer or device in reality for parallel radiation of intensity I incident on the cuvette:

I_r = reflection losses at cuvette interfaces

I_s= scattering losses at cuvette surfaces and from solution

I_b = absorption losses by solvent

I_a = absorption by solute

The true transmittance of the solute is shown below:

$$T = \frac{I - (I_a + I_b + I_r + I_s)}{I - (I_b + I_r + I_s)}$$

Sample and reference cuvettes made to a high specification will minimize the reflection losses that can occur and outer face reflections will cancel. Scattering losses are usually attributed to short wavelength measurements that exhibit Tyndall scattering. Solvent absorption is also a small factor because the number of solvent absorbing particles in each beam is almost identical. It can be concluded that the transmittance and absorbance measurements for the purpose of this experiment will be accurate enough to provide sufficient readings [24].

4.2.3 Cuvette Handling

The cuvettes used throughout the experimentation were manufactured by Plastibrand® and were purchased through Fisher Scientific®. These cuvettes are manufactured to high tolerances and have a large bandwidth which allows them to be useful in the wavelength range of interest. Their volume of 12.5 x 12.5 x 45mm was selected to hold necessary concentration of solute to acquire measurements within the 0.1 AU to 1.0 AU range of optimal accuracy [24]. The volume of the solution was determined with initial tests on the Agilent 8453 which will be discussed in chapter 7.

Cuvette surfaces are required to be clean so that measurement is not compromised [25]. All cuvettes used in an experiment should be identical in order to maintain uniform measurements. The Fresnel relationship governs the ratio of reflected light intensity I_r to incident light intensity I on the surface of the cuvette [24]:

$$\frac{I_r}{I} = \left(\frac{n_1 - n_2}{n_1 + n_2} \right)^2$$

Where n_1 and n_2 are refractive indeces of the two media.

Accuracy is acquired in the placement and repeatability of placement of the cuvette in the beam of light. With an angle θ normal to the beam and a beam refractive index of n, the fractional error in path length, δ can be given by the following relationship [24]:

$$\delta = \frac{0.123\theta}{n}$$

This relationship suggests that error can be introduced with small amounts of play in the cuvette holder and placement. When building a device that will utilize a cuvette mount, it is wise to conduct experiments on the reproducibility of the cuvette placement. The cuvettes used in the experimentation were disposable to eliminate possible errors associated with cleaning and wear associated with a reusable cuvette. This is addressed in chapter 7

The cuvette used for testing filled with saline, a control sample and a reactive sample, respectively, will be shown in figure 4.3.

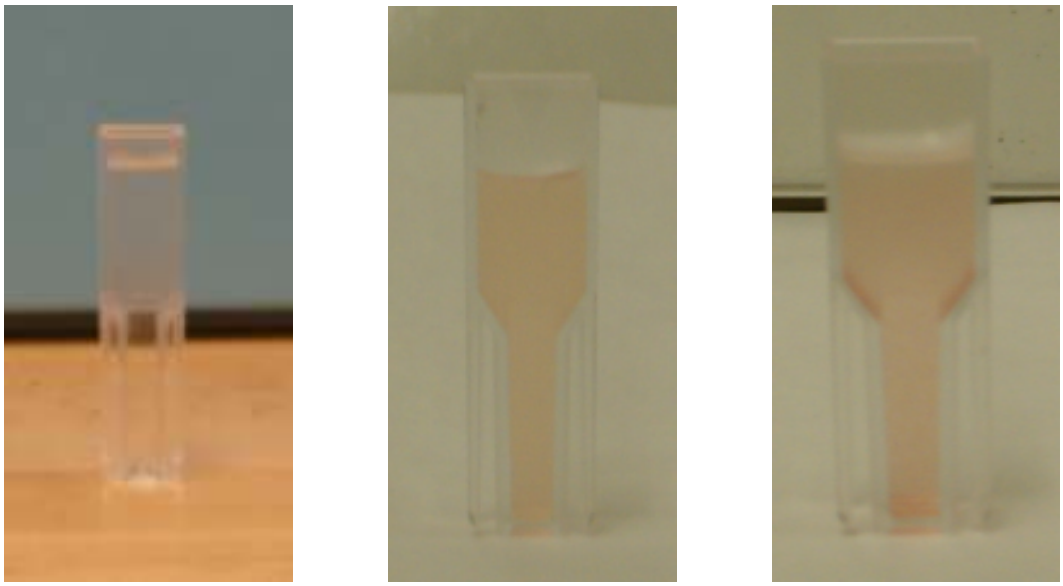


Figure 4.3 – Cuvettes Containing Saline, Control, and Antibody Treated Samples

The spectrophotometer is able to provide an accurate measurement of the blood spectrum. This instrument will be used as a reference for the instrument developed for this experimentation. Now that the operating principles of the spectrophotometer have been explored, the spectral measurements of blood will now be addressed in the next chapter.

Chapter 5

Spectrophotometric Application to Biological Solutions

The current bedside blood typing methods outlined in Chapter 3 all rely on serological testing methods to determine the presence of agglutination in blood. This requires a skilled technician or nurse to judge what the reaction is showing. An automated spectroscopic method would allow for less experienced personnel to type blood because the human judgment would be eliminated and the burden would be placed on the device to type the blood.

5.1 Spectroscopic Method for Blood Typing

Blood typing through spectroscopy is a new blood typing method with potential applications to bedside testing and the laboratory [6,7]. This method utilizes the absorption spectra of blood treated with antibody serums to determine blood type and compute an agglutination index [6,7]. This agglutination index or AI is a number that indicates a reaction or no reaction. The Agilent 8453 diode array spectrophotometer was used. The light scattering component of the spectrum from 660-1000 nm changed significantly between reactive and non-reactive samples. These effects, which can be modeled using the Mie Scattering Theory, provide the basis for the method.

In this procedure, either the RBC or the whole blood sample is used. In the case of RBC, it is diluted 1:16 whereas the whole blood sample is diluted 1:8. Monoclonal anti A and anti B serums are diluted 1:16 and 1:8, respectively. Polyclonal anti D is not diluted. The serums are diluted to reduce the strength of the reaction. A reaction of high strength tends to produce rapid sedimentation that would not allow the spectra to be measured in a reasonable amount of time. The anti D reaction is significantly weaker and does not require dilution; however the D blood group introduces a high amount of variability to the test procedure because reaction strengths and effects from other blood groups affect its reaction strength. The ABO group was observed to be much more uniform in its test behavior and therefore became the main focus of this paper even though group D reactions will be presented.

Antibody backgrounds are made by adding 100 μL of antibody solution and 100 μL of phosphate buffered saline to a culture tube. The contents are mixed by inversion and 25 μL of the solution are added to 2.5 mL of saline and mixed by inversion. The spectra is measured and subtracted from all subsequent readings with that particular antibody acting as a blank for those samples.

The RBC control sample is prepared mixing 100 μL of diluted blood and 100 μL of phosphate buffered saline by inversion in a culture tube. 25 μL of the contents are added to 2.5 ml of phosphate buffered saline and mixed by inversion. Saline is used as the background or blank for these samples.

The antibody treated samples are prepared mixing 100 μL of diluted blood and 100 μL of diluted antibody in a culture tube. This mixture is incubated for 1minute and 25 μL of the contents are added to 2.5 mL of phosphate buffered saline and incubated for 5 minutes. After incubation, the spectra are measured and the antibody background will serve as the blank.

Once the spectra are recorded, transmission and absorbance values are calculated at the 665 and 1000 nm wavelengths. The slope between the absorbance values at these wavelengths is noted for the RBC, Anti A, Anti B, and Anti D. The RBC serves as a control and the serum treated samples are compared to the control in the following relationship [6,7]:

$$AI = 100 - \frac{slope\ of\ test\ sample}{slope\ of\ control\ sample} \times 100$$

This relationship is the agglutination index (AI) algorithm which compares the differences of the ratios of absorbance between two wavelengths between the control and test sample. The AI was found through statistical analysis of the normal distribution of non-reactive samples to be a negative reaction if the AI was less than 17. This process is repeated for each antibody treated sample to determine the blood type, using the Agilent 8453 diode array spectrophotometer.

Microcosms of donor packed whole blood were provided by Duke University Medical Center Transfusion Services Laboratory throughout the study. Figure 5.1 shows that agglutinated and non-agglutinated spectral slopes significantly differ in the 660-1000 nm wavelength range of interest. The spectra shown are of A- blood treated with anti A and anti B serums.

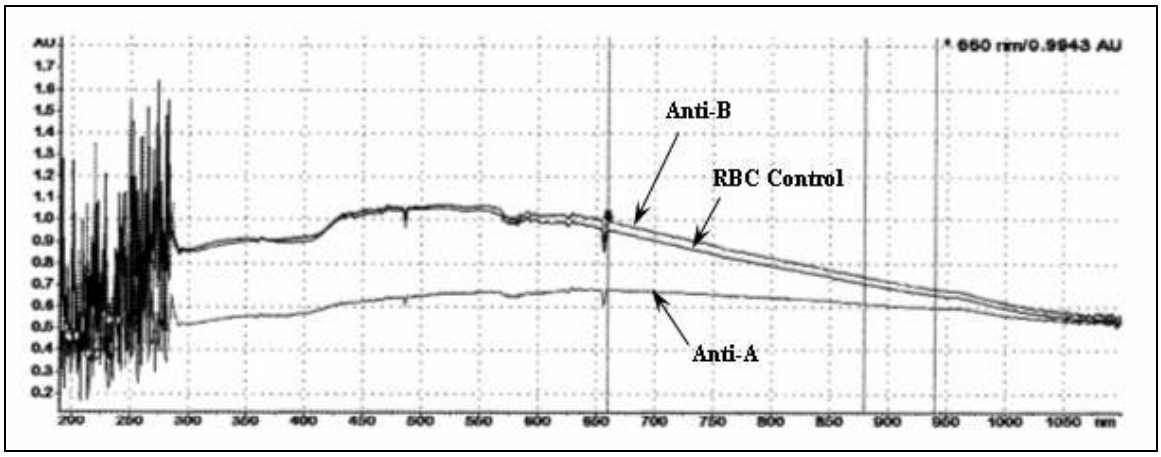


Figure 5.1 – Spectra of A- Blood

The figure shows that the spectrum of the agglutinated sample shows a significantly lower absorption and a flattened slope. This is much different from the non-agglutinated samples.

Narayanan et al. suggests this light scattering phenomenon can be explained by the Mie scattering theory. Simulation of Mie scattering on red blood cells was done at NCSU and can help further clarify this phenomenon.

5.2 Scattering Theory

When a particle diameter is less than one tenth of the wavelength of the incident light this phenomenon is known as Rayleigh scattering [26]. Rayleigh scattering demonstrates symmetrical forward and back scattering where the intensity of the scattered light is inversely proportional to the fourth power of wavelength. This means that light at shorter wavelengths will be scattered more than light at longer wavelengths. This explains the blue color of the sky because the air particles scatter the short blue visible wavelengths stronger than longer wavelengths [26]. This also makes Rayleigh scattering highly dependent on wavelength. Figure 5.2 shows the symmetrical scattering characteristics of Rayleigh scattering.

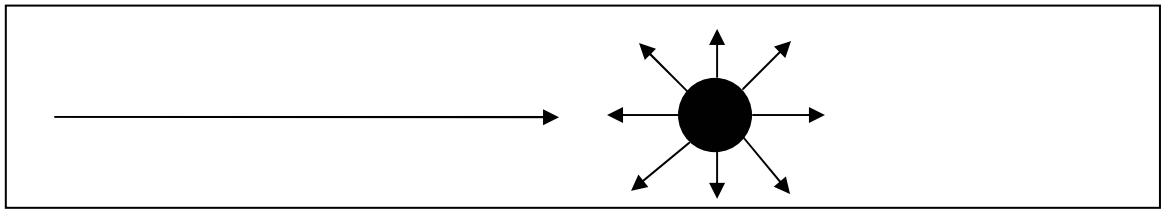


Figure 5.2 – Particle Exhibiting Rayleigh Scattering

When particles are larger than about one third of a wavelength, the light may be out of phase with light scattered from another point. The two then interfere and the light distribution is no longer symmetrical. As particle size increases, the forward scattered light becomes more concentrated in the forward direction as shown in the figure below:

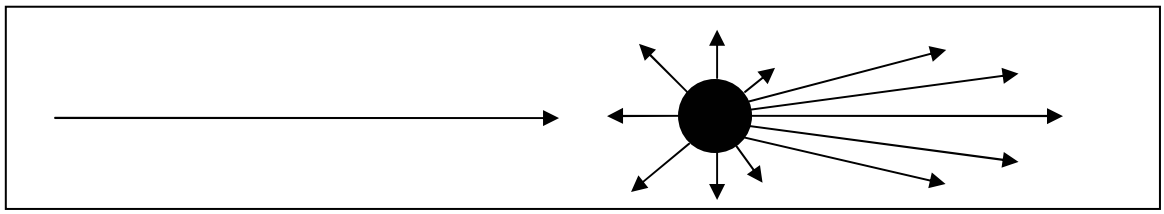


Figure 5.3 – Particle Exhibiting Mie Scattering

Unlike Rayleigh scattering theory which only takes into account the size of the particles, Mie scattering theory also takes into account also the particle's refractive index and the refractive index of the surrounding medium. Mie scattering also includes the shape, dielectric constant, and absorptivity of the particle to create a model. Mie scattering is also not wavelength dependent which explains why most clouds are white [20].

Mie scattering theory can be applied to any particle, but the drawback is that it is a much more complicated theory to evaluate than Rayleigh scattering. The equations to build a Mie scattering approximation were explored at the NASA Goddard Institute for Space Studies by Dr. Mishenko and his group of researchers. A brief description of their approach is shown on the following pages.

A plane electromagnetic wave propagating in a medium with constant ε, μ, and k can be represent by four real and linearly independent quantities known as the Stokes parameters as shown given the coordinate system shown in figure 5.3 [27]. The Stokes parameters are defined in a 4 x 1 column vector known as the Stokes column vector:

$$\mathbf{E}_c(\mathbf{r},t) = \mathbf{E}_0 \exp(i\,k\,\hat{\mathbf{n}}\cdot\mathbf{r} - i\,\omega t)$$

$$\mathbf{I} = \begin{bmatrix} I \\ Q \\ U \\ V \end{bmatrix} = \frac{1}{2}\sqrt{\frac{\varepsilon}{\mu}} \begin{bmatrix} E_{0,\vartheta}E_{0,\vartheta}^* + E_{0\varphi}E_{0\varphi}^* \\ E_{0,\vartheta}E_{0,\vartheta}^* - E_{0\varphi}E_{0\varphi}^* \\ -E_{0,\vartheta}E_{0\varphi}^* - E_{0\varphi}E_{0,\vartheta}^* \\ i\left(E_{0\varphi}E_{0,\vartheta}^* + E_{0,\vartheta}E_{0\varphi}^*\right) \end{bmatrix}$$

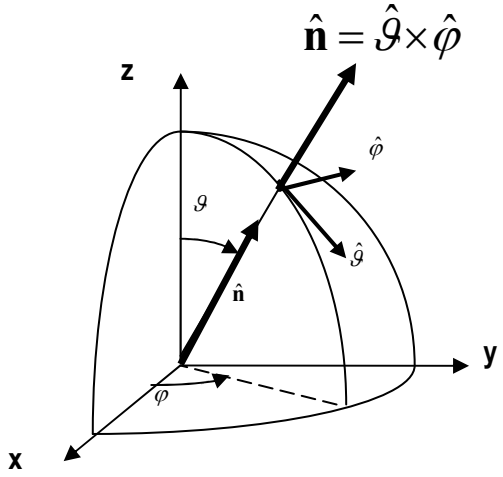


Figure 5.4 – Coordinate System for Plane Electromagnetic Wave

The first Stokes parameter , I , is the intensity of the electromagnetic wave while the parameters Q, U, and V describe the polarization state with the dimension of monochromatic energy flux. The irradiance recorded by the detector with no polarizing obstruction can be related to Q, U, and V by [27]:

$$I^2 \geq Q^2 + U^2 + V$$

Where P is degrees of polarization, P_L is linear polarization, and P_C is circular polarization, respectively [27]:

$$P = \frac{\sqrt{Q^2 + U^2 + V}}{I} \quad P_L = \frac{\sqrt{Q^2 + U^2}}{I} \quad P_C = \frac{V}{I}$$

With scattering a spherical coordinate system centered at the origin of a scattering particle is shown in figure 5.4:

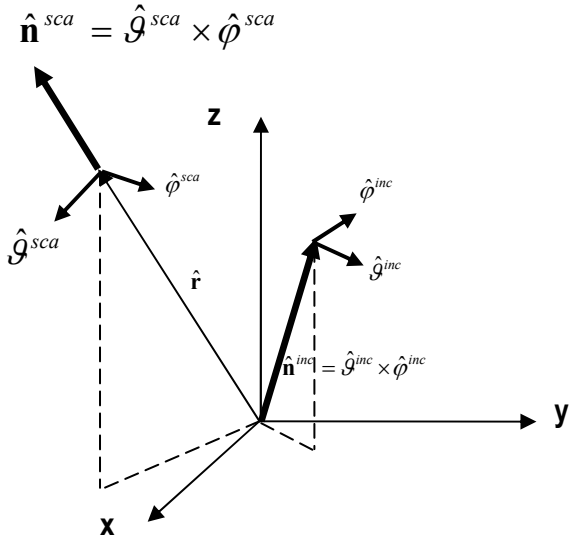


Figure 5.5 – Spherical Coordinate System

The 2 x 2 so-called amplitude scattering matrix represents the component transformation of the incident plane wave into the resulting scattered spherical wave [27]:

$$\begin{bmatrix} E_{\vartheta}^{sca}(r\hat{\mathbf{n}}^{sca}) \\ E_{\varphi}^{sca}(r\hat{\mathbf{n}}^{sca}) \end{bmatrix} = \frac{e^{ik_1 r}}{r} \mathbf{S}(\hat{\mathbf{n}}^{sca}, \hat{\mathbf{n}}^{inc}) \begin{bmatrix} E_{0\vartheta}^{inc} \\ E_{0\varphi}^{inc} \end{bmatrix}$$

In relation to the Stokes parameters, the analogous representation is formulated by the quadratic combinations of the **S** matrix created above to form the matrix **Z** where [27]:

$$\mathbf{I}^{sca}(r\hat{\mathbf{n}}^{sca}) = \frac{1}{r^2} \mathbf{Z}(\hat{\mathbf{n}}^{sca}, \hat{\mathbf{n}}^{inc}) \mathbf{I}^{inc}$$

In order to describe the scattering by a small volume of a collection of independent, randomly oriented particles, the scattering matrix **F** is introduced. The **Z** matrix relates the Stokes parameters of the incident and scattered beams relative to their respective meridonal planes. The **F** matrix relates the Stokes parameters of the incident and scattered beams with respect to the scattering plane, through unit vectors $\mathbf{n}^{inc}$ and $\mathbf{n}^{sca}$, or [27]:

$$\mathbf{F}(\vartheta^{sca}) = \mathbf{Z}(\vartheta^{sca}, \varphi^{sca} = 0; \vartheta^{inc} = 0, \varphi^{inc} = 0)$$

With randomly oriented mirror symmetric macroscopically isotropic particles, the scattering matrix reduces to eight non- zero elements [27]:

$$\mathbf{F}(\Theta) = \begin{bmatrix} F_{11}(\Theta) & F_{12}(\Theta) & 0 & 0 \\ F_{12}(\Theta) & F_{11}(\Theta) & 0 & 0 \\ 0 & 0 & F_{33}(\Theta) & F_{34}(\Theta) \\ 0 & 0 & -F_{34}(\Theta) & F_{33}(\Theta) \end{bmatrix} = N < \mathbf{F}(\Theta) >$$

$$\Theta = \arccos(\hat{\mathbf{n}}^{inc} \cdot \hat{\mathbf{n}}^{sca}) \qquad \Theta \in [0, \pi]$$

Where Θ is the scattering angle, N is the number of particles, and <**F**(Θ)> is the ensemble-averaged scattering matrix per particle. The corresponding amplitude matrix elements and expansion coefficients can be evaluated numerically.

Again, consider the single particle scenario in an incident plane wave and add a collimated detector with a sensitive area ΔS focused at the scattering particle the power received by the detector can be calculated integrating the time averaged Poynting vector across the surface of the detector [27]:

$$W_{\Delta S}(r) = \int_{\Delta S} dS\hat{\mathbf{r}} \cdot < \mathbf{S}(r') >$$

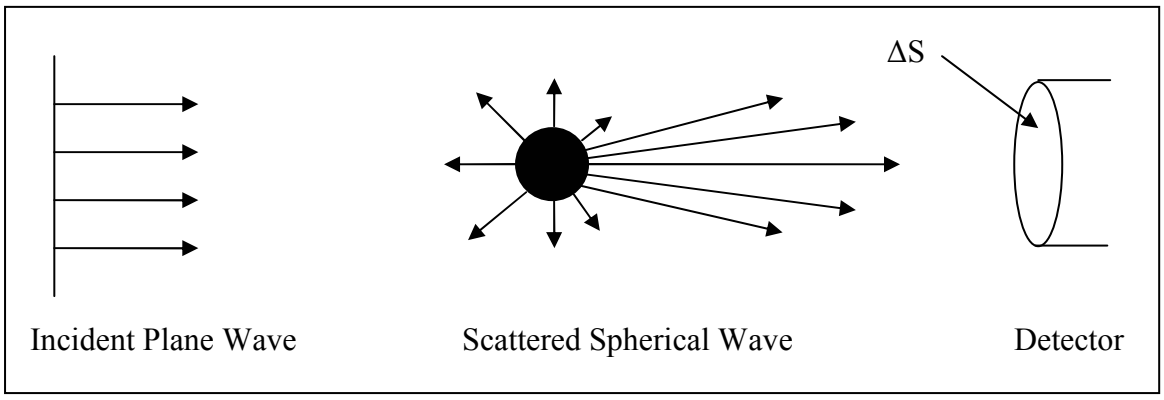


Figure 5.6 – Single Particle Scenario with Detector

Being in the forward scattering direction, the power incident on the detector can be shown as [27]:

$$W_{\Delta S}(\hat{\mathbf{n}}^{inc}) \approx \frac{1}{2}\Delta S\sqrt{\frac{\varepsilon_1}{\mu_0}}\left|\mathbf{E}_0^{inc}\right|^2 - \frac{2\pi}{k_1}\sqrt{\frac{\varepsilon_1}{\mu_0}}\,\mathrm{Im}\left[\mathbf{E}_1^{sca}(\hat{\mathbf{n}}^{inc}) \cdot \mathbf{E}_0^{inc^*}\right] + \frac{1}{2}\sqrt{\frac{\varepsilon_1}{\mu_0}}\frac{\Delta S}{r^2}\left|\mathbf{E}_1^{sca}(\hat{\mathbf{n}}^{inc})\right|^2 \quad (Eqn\ 1)$$

The first term is equal to the power received with no particle, the second term is the attenuation caused by the particle between the source and the detector, and the third term is

the contribution from forward scattered light. From this calculation, the scattering, absorption, and extinction cross sections C_{sca}, C_{abs}, and C_{ext} can be realized. The cross sections have units of area, and by multiplying with the incident monochromatic energy flux, the total monochromatic power removed form the incident wave as a result of the corresponding scattering and absorption processes are produced. The extinction cross section is the sum of C_{sca} and C_{abs} and product of C_{ext} with the incident flux give the total power removed from the effect of scattering and absorption:

$$C_{ext} = \frac{W_{ext}}{I_i} \;\; and \;\; C_{sca} = \frac{W_{sca}}{I_i} \;\; and \;\; C_{ext} = \frac{4\pi}{k_1 \left|\mathbf{E}_0^{inc}\right|^2} \mathrm{Im}\left[\mathbf{E}_1^{sca}(\hat{\mathbf{n}}^{inc}) \cdot \mathbf{E}_0^{inc^*}\right]$$

Inserting C_{ext} into Eqn 1, gives the power received by a detector in the forward scattering direction of a particle:

$$W_{\Delta S}(\hat{\mathbf{n}}^{inc}) = \frac{1}{2}\sqrt{\frac{\varepsilon_1}{\mu}}\left|\mathbf{E}_0^{inc}\right|^2 (\Delta S - C_{ext}) + \frac{1}{2}\sqrt{\frac{\varepsilon_1}{\mu}}\frac{\Delta S}{r^2}\left|\mathbf{E}_1^{sca}(\hat{\mathbf{r}})\right|^2 \quad (Eqn\,2)$$

The power received by the detector is proportional to the difference of detector area and the extinction cross section as well as forward scattered light [27].

C_{ext} and C_{sca} are equal with a nonabsorbent media. The scattering cross section is:

$$C_{sca} = \frac{W_{sca}}{I_i} = \frac{1}{I^{inc}}\int_{4\pi} d\hat{\mathbf{r}}[Z_{11}(\hat{\mathbf{r}},\hat{\mathbf{n}}^{inc})I^{inc} + Z_{12}(\hat{\mathbf{r}},\hat{\mathbf{n}}^{inc})Q^{inc} + Z_{13}(\hat{\mathbf{r}},\hat{\mathbf{n}}^{inc})U^{inc} + Z_{14}(\hat{\mathbf{r}},\hat{\mathbf{n}}^{inc})V^{inc}]$$

The angular distribution of the scattered light is described by the differential scattering cross section as shown:

$$\frac{dC_{sca}}{d\Omega} = \frac{1}{I^{inc}}[Z_{11}(\hat{\mathbf{r}},\hat{\mathbf{n}}^{inc})I^{inc} + Z_{12}(\hat{\mathbf{r}},\hat{\mathbf{n}}^{inc})Q^{inc} + Z_{13}(\hat{\mathbf{r}},\hat{\mathbf{n}}^{inc})U^{inc} + Z_{14}(\hat{\mathbf{r}},\hat{\mathbf{n}}^{inc})V^{inc}]$$

The asymmetry parameter <cosΘ> defines the average cosine of the scattering angle as shown:

$$<\cos\Theta> = \frac{1}{C_{sca}}\int_{4\pi} d\hat{\mathbf{r}}\frac{dC_{sca}}{d\Omega}\hat{\mathbf{r}}\cdot\hat{\mathbf{n}}^{inc}$$

The scattering coefficient is relevant in eqn 2 because it describes the attenuation of light by the red blood cells suspended in saline measured in the forward direction. C_{sca},

$dC_{sca}/d\Omega$, and <cosΘ> affect the transmission measurement s of the second term in equation 2 the same way. If the scattered light is distributed primarily in the forward direction it becomes more difficult for the detector to exclude scattered light at small angles from the incident direction.

5.3 Numerical Model and Results

The important parameters to evaluate when modeling the Mie scattering of a particle is the approximate ensemble-averaged extinction cross sections for various wavelengths, the particle size distributions, the differential scattering cross sections, and asymmetry parameters which will be discussed in this section. Steve Anthony used Lorentz-Mie scattering FORTRAN code developed by Mishchenko at the NASA Goddard Institute for Space Studies, New York to model these properties and use them to develop a theoretical basis for this method [8]. This code is available at http://www.giss.nasa.gov/~crmim.

The software evaluates the normalized scattering matrix <F(Θ)> for a polysdispersion of randomly oriented spherical particles, which is related to the regular scattering matrix by:

$$\tilde{F}(\Theta) = \frac{4\pi}{C_{sca}} F(\Theta) = \frac{4\pi}{< C_{sca} >} < F(\Theta) >= \begin{bmatrix} a_1(\Theta) & b_1(\Theta) & 0 & 0 \\ b_1(\Theta) & a_2(\Theta) & 0 & 0 \\ 0 & 0 & a_3(\Theta) & b_2(\Theta) \\ 0 & 0 & -b_2(\Theta) & a_4(\Theta) \end{bmatrix}$$

In obtaining the total scattering matrix, the normalized matrix has the additive properties for N number of M particle types of :

$$\tilde{F} = \frac{\sum_{m=1}^{M} N_m < C_{sca,m} > \tilde{F}_m}{\sum_{m=1}^{M} N_m < C_{sca,m} >}$$

Elements of the scattering matrix were numerically evaluated by expanding the elements in generalized spherical functions. The derivation of these solutions is described in detail by Mishchenko [27].

The properties of the human red blood cell are needed to properly construct the model and were investigated. The real part of the refractive index of a red blood cell at 632.8 nm is the product of hemoglobin (1.615) and water(1.333), which results in a refractive index of about 1.40 [9,28,29]. The particle will be suspended in saline which is approximated as that of water (1.333) so a relative refractive index of 1.058 was used. The imaginary part of the

refractive index was assumed negligible since it represented the absorbance of the medium. Human blood cells have a mean diameter of 7.65 μm and a thickness ranging from 1.42-2.74 μm.

Agglutination is the result of red blood cells being attracted to each of other because of antibody reactions that bond the cells together. In order to visualize this reaction, pictures of reactive and non reactive cells should be compared. Figure 5.3 shows agglutinated and unagglutinated cells side by side to demonstrate the reaction:

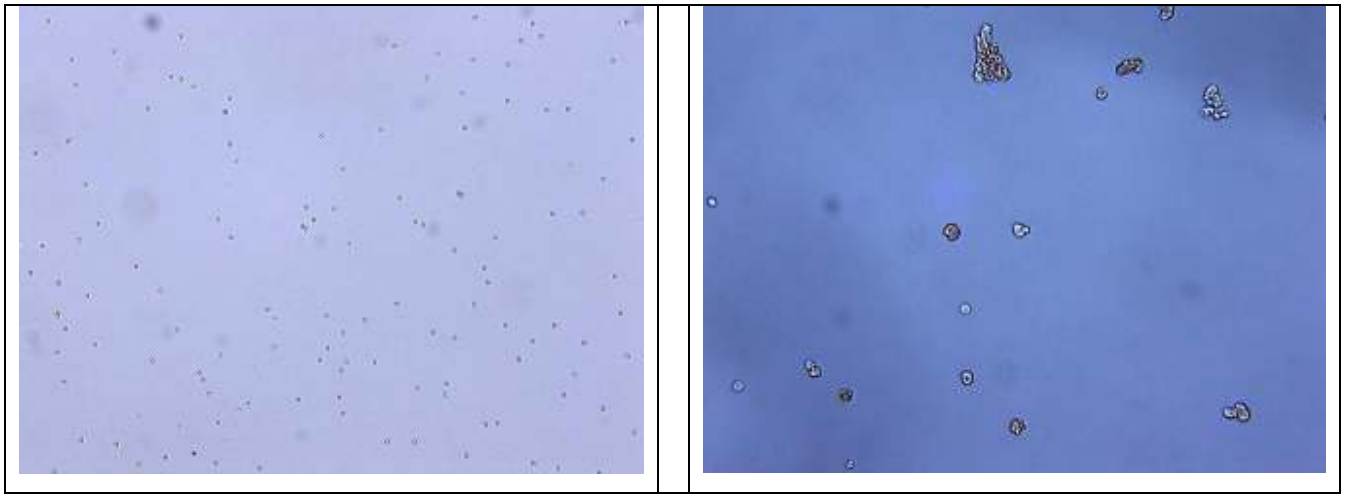


Figure 5.7 (a) and (b) – Non Reactive Cells (a) and Reactive Cells (b)

The non-reactive cells exhibit a uniform distribution where there is not large difference in size between each individual particle. The reactive cells show clumping and the cells are not evenly distributed through the suspension. The clumps are made up of groups that contain roughly 2-20 cells each. The size average of the particles is about 10 μm but can be as large as 50 μm.

The simulation modeled a subtle increase in agglutination for the numerical model. Normal distributions with mean particle radii of 3.5, 3.75, 4.0, 4.25, and 4.5 μm and variances of 0.04, 0.06, 0.08, 0.10m, and 0.12, respectively, were examined. The distributions are shown in figure 5.4 [8].

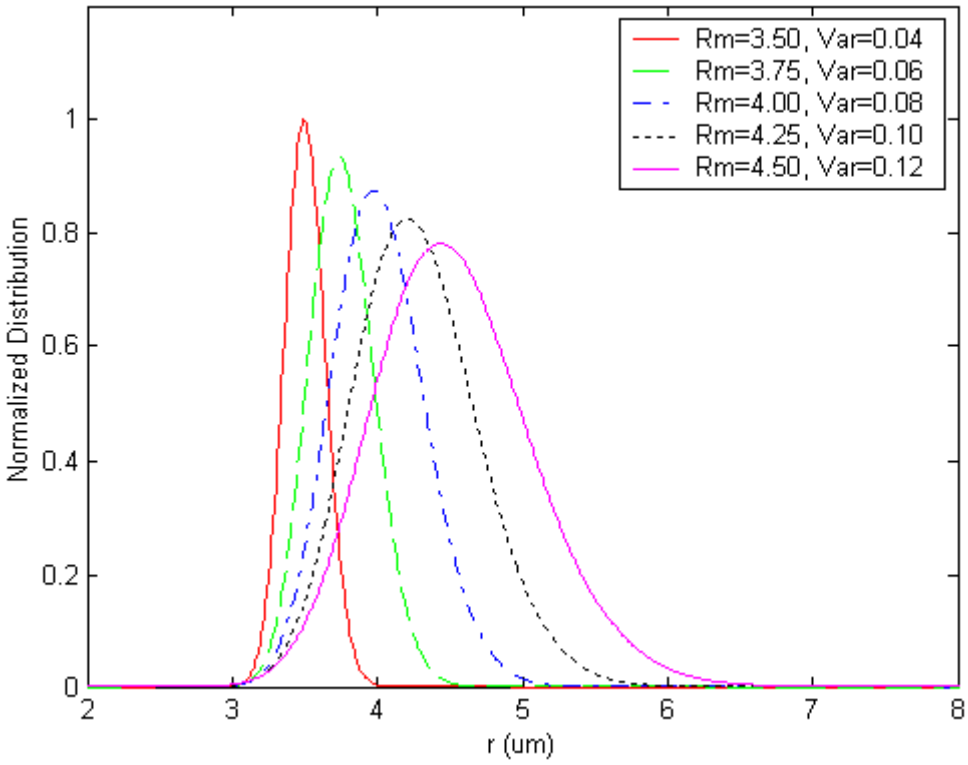


Figure 5.8 – Particle Size Distributions

The first parameter that was analyzed was the extinction cross section per particle, as a function of wavelength, for each particle size distribution that was generated above. Extinction is attenuation of light by both absorption and scattering. Extinction of a particle is higher than what can be expected from its physical size. The extinction cross section that is modeled in the following plot shows how the extinction cross section is affected by particle size [8].

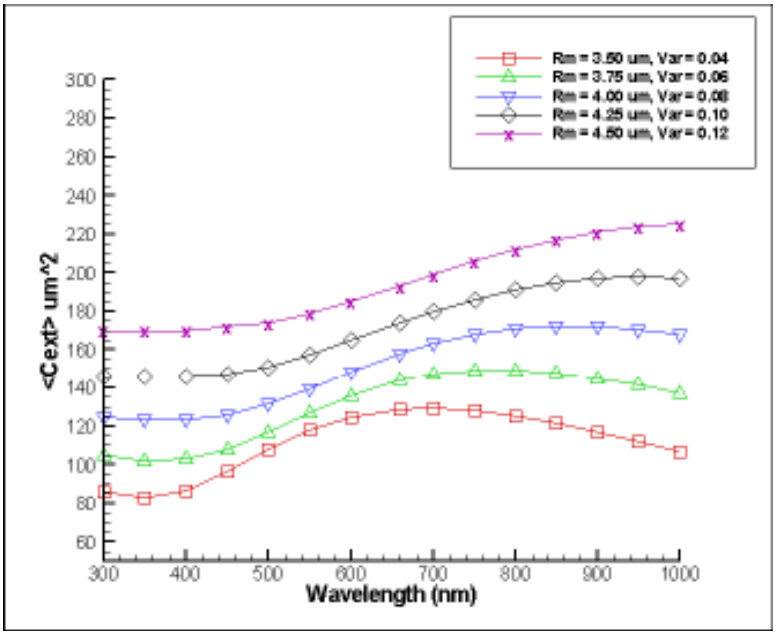


Figure 5.9 - $<C_{ext}>$ vs Wavelength

The 3.5 μm radius gives a shape similar to that measured on the spectrophotometer. As the particle size increases, there is an increase in $<C_{ext}>$ at the higher wavelengths as opposed to the 660 nm wavelength. This helps explain why the slope flattens with the agglutinated samples. These magnitudes can be misleading because the number of particles in the test samples will decrease because of the blood cells agglutinating. A simple relation can be used to predict this possibility:

$$\frac{V_{particle}}{V_{cell}} = \frac{r^3}{r_0^3}$$

This relation shows that the total extinction cross section would decrease by r^{-3} for $r > r_0$. The energy collected by a detector in the forward scattering direction of a light source will increase as the mixture agglutinates [29]. This was observed in the testing and is a valid claim to make. The agglutinated samples showed a flattened slope, but also recorded significantly lower absorption values as a result of this effect.

The next parameter that was analyzed was the angular distribution of scattered light for particle distributions generated. An incident wavelength of 660 nm was used to create the plot as shown below [8]:

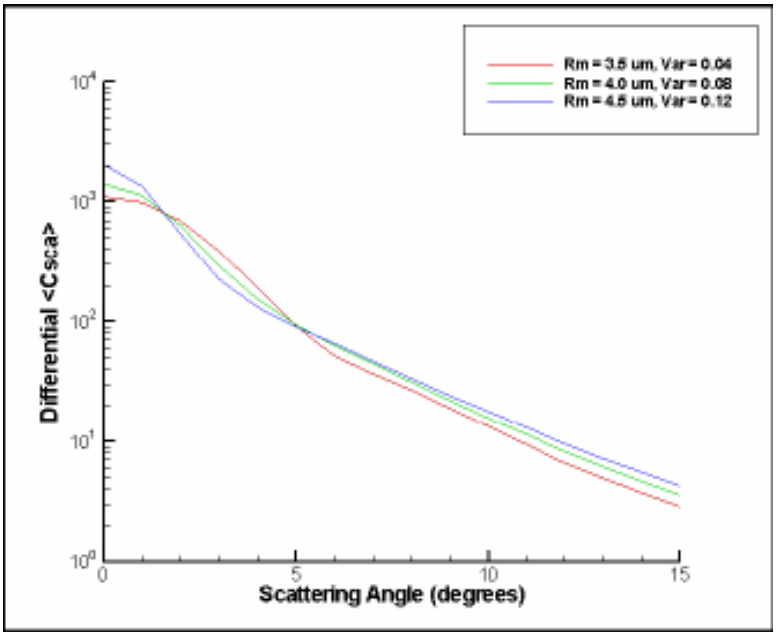


Figure 5.10 – Differential Scattering Cross Section

The larger particle sizes exhibit an increase in intensity in the forward scattering direction. As the scattering angle increases, the distribution narrows. This increase in forward scattered light helps offset the increase in extinction cross section measured by a forward detector.

The asymmetry parameter was the final element modeled using the Lorentz-Mie Fortran Code and is shown in figure 5.10 [8]:

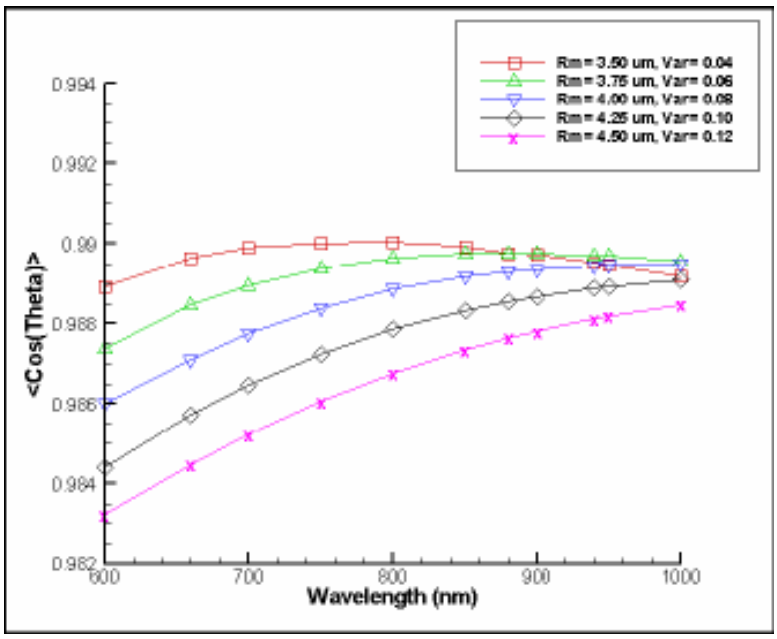


Figure 5.11 – Asymmetry Parameter vs. Wavelength

The asymmetry parameter was generated using average scattering angles of about 10.5º - 8º from the incident direction. As the particle size increases, the angular distribution of the scattered light narrows, thus showing that increasing particle size will cause the light to scatter at higher angles.

5.4 Scattering Theory Application

Now that scattering theory has been explained and modeled, this section will discuss their application to this research. An important note is when a sample is demonstrating Rayleigh scattering, the amount of scattered light at shorter wavelengths will be greater which results in a higher optical density. A sample demonstrating Mie scattering will scatter asymmetrically resulting in more forward scattered light. This results in large amount of incident light on the detector and nearly identical optical densities in the range of interest. Figure 5.12 shows a B- sample reading that demonstrates the phenomenon described.

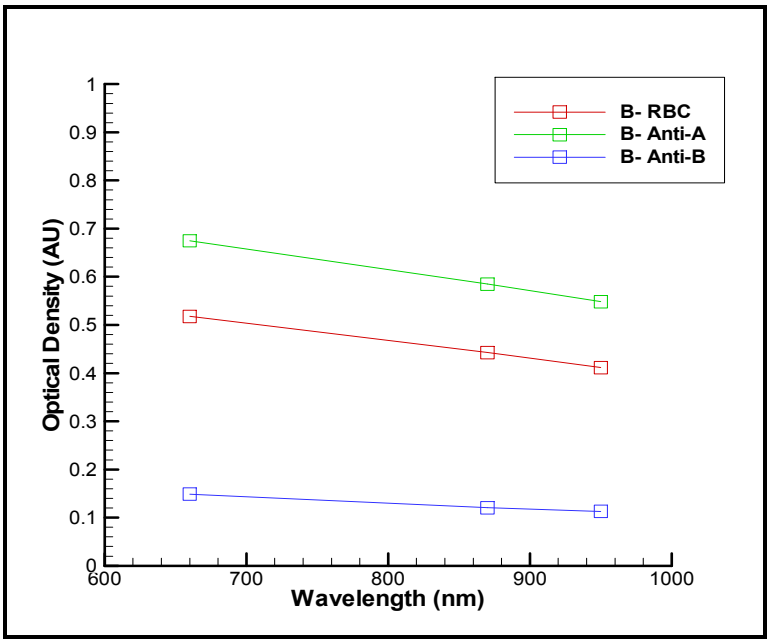


Figure 5.12 – B- Blood Spectrum

The figure above shows B- blood control and antibody treated spectra. The control and anti-A treated samples do not react and also show higher optical densities at the shorter wavelengths as a result of more light being scattered at those wavelengths. These samples appear to demonstrate a Rayleigh or wavelength dependent scattering phenomenon as a result of the mixtures being more homogeneous and containing much smaller particles. The reactive sample demonstrates more of a Mie scattering phenomenon due to its more uniform optical density measurements over the wavelength range of interest due to strong forward scattering. The reactive mixture is also not homogeneous like the non-reactive mixtures because of the particles bonding to each other. This allows more forward light on the detector which contributes to the low optical density measurements of reactive samples.

Now that the scattering effects of blood cells have been investigated, sensor design will be explored in the following chapter.

Chapter 6
Sensor Design and Considerations

The sensor design process consisted of considering the previous design, choosing light sources and detectors, selecting an optical configuration, implementing a signal processing method, and combining these components to produce a miniaturized system capable of reproducing the results of the previous system as well as the Agilent 8453 diode array spectrophotometer.

6.1 Optoelectronic Miniaturization

The miniaturization of a system requires analyzing the system being miniaturized and finding the factors that contribute to the increased size of the system being miniaturized. The light sources and detection, optical components, and data acquisition will be analyzed and solutions will be discussed.

6.1.1 Light Sources and Detection

The Narayanan study based their algorithm on measuring slopes between visible and near-infrared wavelengths in the 660 – 1000 nm range. For this reason, three methods of measurement were used to verify the spectra of the blood tested. The methods utilized were 660 – 870 nm, 660 – 950 nm, and a linear regression of 660, 870, and 950 nm in order to compare results.

The first attempt to integrate the three desired wavelengths was to attempt to find a multi wavelength LED. This LED would incorporate three desired wavelengths into a single unit so that the mounting inconsistencies would be eliminated. Clairex Technologies was contacted to find a model that could produce the desired outputs. Clairex recommended the CLE400F which is a surface mount multiple emitter chip that can be outfitted with chips of different wavelengths at an additional cost. This package would allow for the emitters to be switched on and off so that the desired wavelength would be on at the appropriate time.

Problems with the CLE400F are that each of the chips emit light from the top and sides of the die. They are not true point source or surface emitters so the light would be emitted from top side emission and side emission from all four sides. A lens could not used on this package to focus the light because the orientation of the chips so very little of the radiation could be focused ahead with a focal point lens.

The feasibility of accomplishing a narrow emission from the CLE400F is not good because the tooling required would be very expensive and does not guarantee that the radiation from each chip would be transmitted identically. Clairex also stated that they doubt that the CLE400F could accomplish the desired task and that none of the multi wavelength LEDs available could accomplish the task.

Therefore, this approach was abandoned in favor of using three separate sources that could be terminated into a single fiber optic wire.

The next step in reducing the size of the system is to find a more compact way of packaging the light sources. The approach used in this study was coupling the source with a fiber optic cable to allow placement of the sources in more desirable locations and not having to consider alignment each time the light source is changed out. Cost was also an issue so inexpensive sources were also desirable. After contacting manufacturers about low cost fiber optic sources the IF-E96, IF-E91D, and IF-E91A, which are manufactured by Industrial Fiber Optics Inc., were selected as sources for the system. These sources put out 660, 870, and 950 nm wavelengths, respectively. Each requires a low forward current of about 40 mA and are housed in plastic enclosures that focus the light into 1000 μm core plastic fiber multimode cable and allow for easy connection and disconnection of the fiber. A schematic of the LED/IREDs are shown in figure 6.2:

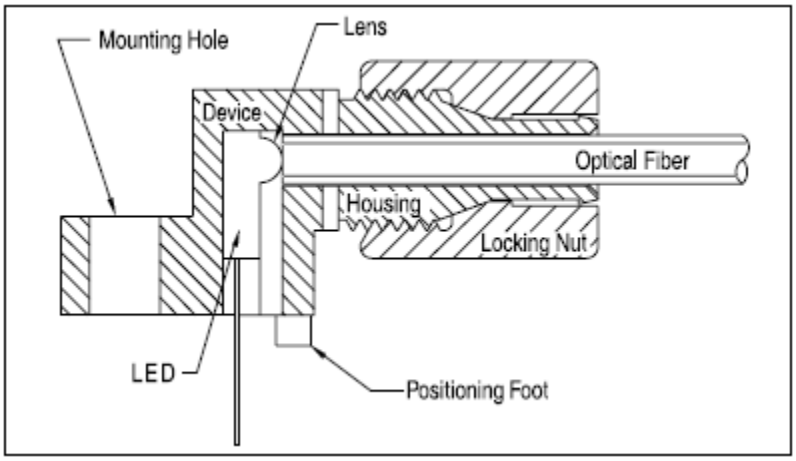


Figure 6.1 – LED/IRED Schematic

This unit was very useful in the development of the sensor because it did not require much effort to set up. The units are mounted in a breadboard and powered by a HP E3611A

constant current DC power supply. The power supply maintained a constant current to the LEDs to eliminate noise and errors associated with variable power sources.

A photodiode is selected as the detector because of their sensitivity and ability to sense in a wide bandwidth. Photodiodes can be specified in a wide range of spectral responses and sensitivities although it is tough to find any that perform well above 1100 nm. The Hamamatsu model S2386-45K was chosen because of its sensitivity in the desired bandwidth (320 – 1100 nm) as well as its low dark current, high shunt resistance, and low terminal capacitance. These qualities make this detector ideal for the experiment as well as the fact that this detector has been proven effective in previous experiments and are readily available in the research lab. The full data sheets for the LED/IREDs and the photodiode are in Appendix D.

The LEDs can be classified as an exponential intensity source as shown [30]:

$$I_\theta = I_O \cos^n \theta$$

The exponent can be calculated from half power angle [30]:

$$\theta_{1/2} = \arccos\left(0.5^{1/n}\right)$$

It is important to note that the spectral distribution of the light source should be considered when calculating the total flux the LED emits into an angle θ as shown [28]:

$$\Phi_s = \int_\lambda \int_0^\theta I_\theta(\lambda) 2\pi \sin\theta \, d\theta \, d\lambda = \int_\lambda \frac{2\pi I_O(\lambda)[1-\cos^{n+1}\theta]}{n+1}$$

The photodiode sensitivity is the next parameter to consider. The photodiode sensitivity is a function of wavelength and is an important parameter to consider when selecting one. The photodiode relative spectral response function (R(λ)) is the ratio of output signal voltage and the radiant power incident on the detector. When within the radiance of light source, the effective flux incident on the detector can be calculated through integration of geometric and spectral distributions of the radiant source and area of the detector [21]:

$$\Phi_{eff} = \tau_p \tau_e \int_\lambda \int_\theta \int_\phi \Phi_s(\lambda, \theta, \phi) R(\lambda) d\lambda \, d\theta \, d\phi$$

τ_p represents the path transmittance from scattering and absorption of the medium while τ_e is the optical efficiency from reflective and refractive losses. The spectral emission of the LEDs and response of the photodiode are plotted in Figure 6.3 based on the spec sheets of the components:

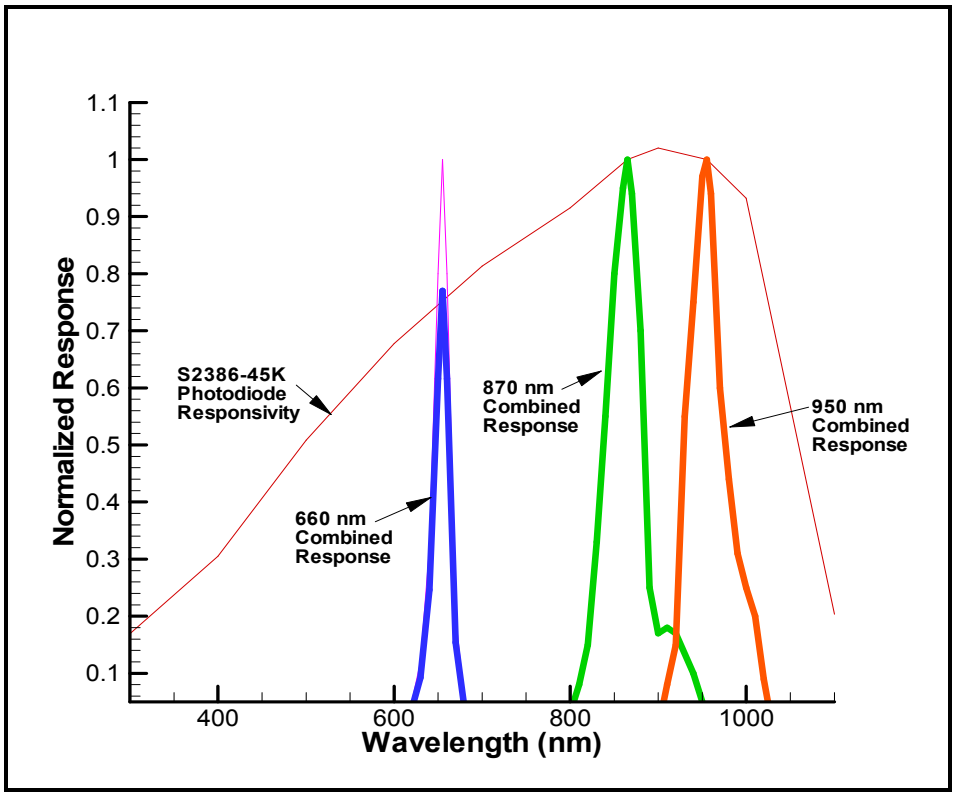


Figure 6.2 – Combined LED and Photodiode Response

Transmission measurements should cancel the geometric and spectral distributions. The spectral bandwidths and resolutions are important to consider because they can contribute to differences in the measurements between the experimental device and the monochromatic light used in the spectrophotometer. These LEDs can also have varying peak emission wavelengths based on the forward current being supplied. The spectrophotometer showed that the behavior of the blood spectra in this region is linear and therefore these effects should not greatly affect the slopes.

6.1.2 Fiber Optic Theory

Light is an electromagnetic wave composed of electric and magnetic fields. These fields vary sinusoidally rising from zero, hitting a positive peak, going back to zero, hitting a negative peak, and returning to zero. The distance light travels during this cycle is called a wavelength. The number of cycles per second is frequency and is measured in hertz (hz). A conceptual drawing of an electromagnetic wave of light is shown below where the magnetic and electric field sinusoids are 90° out of phase [31]:

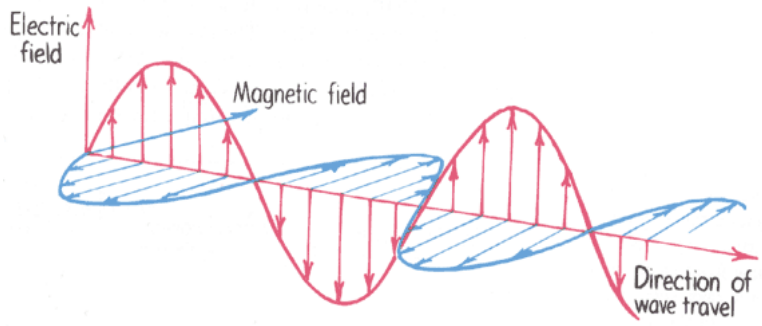


Figure 6.3 – Light Wave

The electromagnetic spectrum is shown below where the area of interest is the optical and near infrared spectrum which ranges from about 400 – 1000 nm [24].

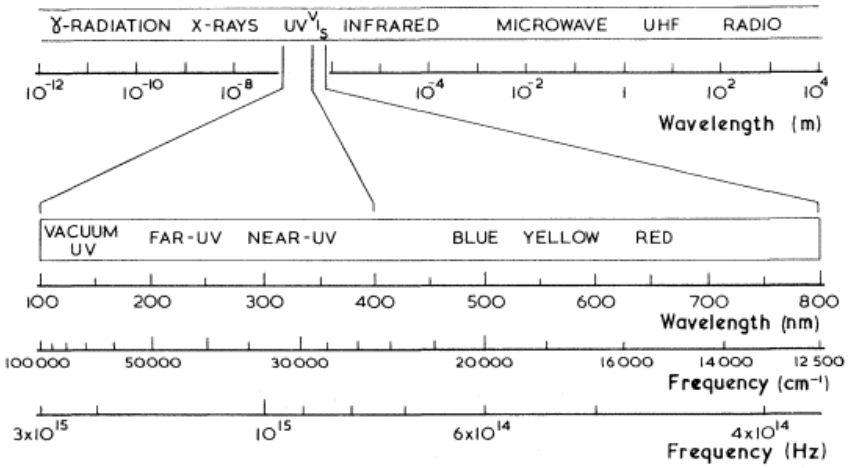


Figure 6.4 – Electromagnetic Spectrum

Wavelength and frequency are inversely proportional to each other through the following relation where λ is wavelength, c is the speed of light (180,000 miles per second) and ν is frequency [32]:

$$\lambda = \frac{c}{\nu}$$

Photon energy (E) can also be calculated from this relation using Plank's constant (h = 6.63 x 10^{-34} J-s) from Plank's law:

$$E\ (eV) = \text{h}\,\nu \text{ or } E(eV) = \frac{1.2399}{\lambda(\mu m)}$$

Which gives energy in electron-volts.

The refractive index of a material describes the effect light slowing down in a material. This is the ratio of the speed of light in a vacuum and the speed of light in that material and is denoted in optics by the letter **n** [32]:

$$n = \frac{c_{vac}}{c_{mat}}$$

Light is bent when it passes through a media where refractive index changes. The amount of bending depends on the refractive indices of the two media and angle at which light strikes the surface between them. The figure below shows this phenomenon known as Snell's Law [32,33]:

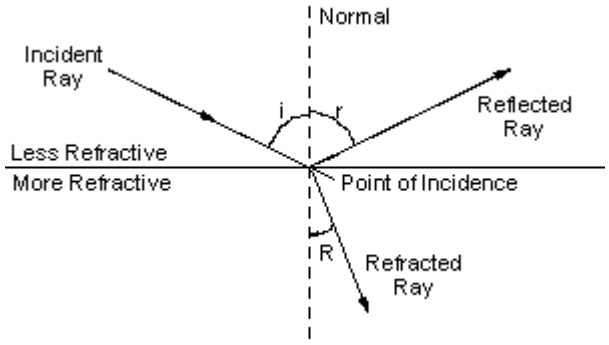


Figure 6.5 – Snell's Law

This relationship can be written as:

$$n_i \sin I = n_r \sin R$$

Where n_i and n_r are the refractive indices of the initial medium and medium into which light is refracted. R is the angle of refraction, I is the angle of incidence, and R is the angle of reflection.

This applies to fiber optics because when the angle of incidence is too large, light cannot refract out of the glass. The angle where this becomes true is known as the critical angle θ_c where Snell's Law is manipulated to compute the critical angle as a function of the ratio of refractive indices [32]:

$$\theta_c = \arcsin(n_r / n_i)$$

The light is bounced back into the glass at the same angle which is known as total internal reflection as shown in the figure below [32,33]:

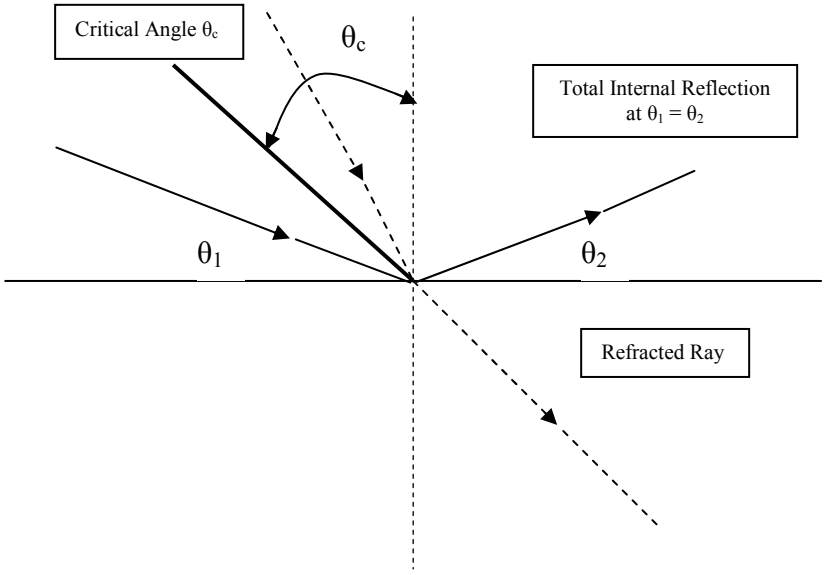


Figure 6.6 – Total Internal Reflection

Now that the total internal reflection principle has been investigated, light guiding can now be explained. Optical fiber consists of three main components, the protective sheath, cladding, and core. From an optical standpoint, the core and cladding are the only components that need to be analyzed. The refractive index of the core is higher than that of the cladding so that light in the core will strike the cladding at a glancing angle and is confined in the core by the total internal reflection principle. The difference between these refractive indices does not have to be large and can differ by as little as 1%. The critical angle of the Mitsubishi GH4001 1000 μm core jacketed step-index optical fiber used in the experiment is calculated below:

$$\theta_{critcal} = \arcsin(n_r / n_i) = \arcsin(1.402/1.492) = 70°$$

This value indicates that any light ray that meets the boundary between the core and cladding must be less than 20° to be internally reflected or any light beam must have a half angle of less than 20°.

Acceptance angle is another method used to analyze light guiding in a fiber. Acceptance angle is the angle over which light rays entering the fiber will be guided along its core and not attenuated. The acceptance angle is different from the critical angle because it is evaluated in air before the beam is refracted into the fiber. The acceptance angle is measured as numerical aperture (NA) which in the case of the fiber used is shown below [32]:

$$NA = \sqrt{\left(n_O{}^2 - n_l^2\right)} = \sqrt{\left(1.492^2 - 1.402^2\right)} = 0.51$$

Two definitions where the NA to can be applied are shown below:

$$NA = \sin\theta \quad where\ \theta = 30.7°$$

Where the sine of the half angle, θ, is evaluated and:

$$NA = n_O \sin\theta_c$$

Where θ_c is the confinement angle. The figure below gives a visual basis for these parameters [32,33]:

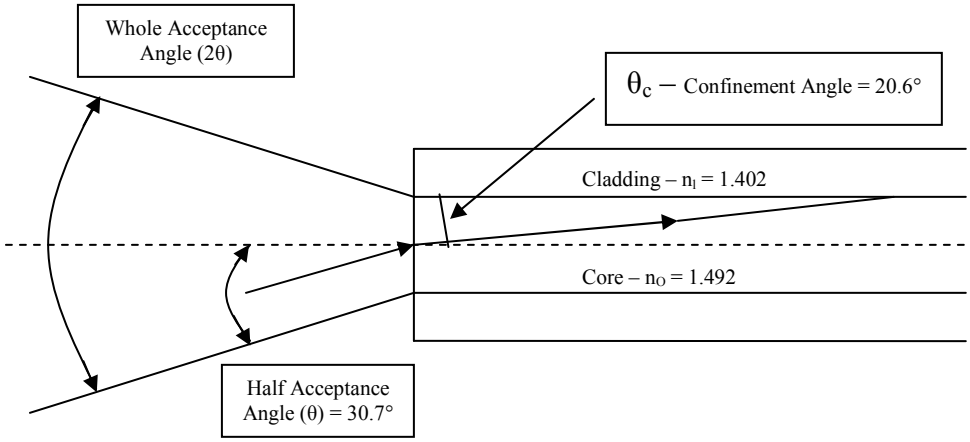


Figure 6.7 – Acceptance Angle

The half acceptance angle is larger than the largest confinement angle that the rays must remain inside of to be reflected. Snell's law shows that these rays will be accepted because refraction between air and the core will bend the rays inside the confinement angle.

Fiber attenuation is a factor that should be considered when transmitting over long distances. The fiber used in this project is rated at a low attenuation of 0.15 dB/m attenuation (650 nm). Attenuation usually occurs when the light escapes into the cladding. This is usually negligible unless the fiber is bent at sharp angles that allow the light to hit the core-cladding boundary at an angle steep enough to avoid the internal reflection [34].

The fundamentals of fiber optics have been discussed such as light entering the fiber, total internal reflection, and optical relationships that allow fiber optics to carry light.

6.1.3 Optical System

One way to begin miniaturizing the system is to collimate the incident light before it reaches the sample to eliminate the need to place the sample in order to focus the image of the converging/diverging beam. Thor Labs was contacted to select a lens that could accept the light from the fiber and collimate the light through the sample and on the detector. A BK-7 plano-convex lens was suggested with an AR coating that could reduce reflections below 0.5% per surface within the 650-1050 nm range. This lens also has a short focal length of 12 mm which is desirable for miniaturization. Two ½" apertures were also obtained (ID12) to limit the size of the beam into the sample and block stray and scattered light incident on the detector. A sample cuvette mount was made to fit the cuvette tightly and eliminate mounting errors. Mounts were fabricated and shimmed to hold the apertures precisely on the forward optical axis. A fiber mount was also obtained from Thor Labs (VH1) to hold the fiber steady and eliminate movement. This mount was bolted to an adjustable fabricated mount that allowed for maximum movement, but was very stiff when tightened. All components were bolted to an optical breadboard with 1" spacing. Great care was taken in aligning the system as precisely as possible, yet more precision could be realized with better equipment.

Initially, a simple system was attempted with one exit aperture as shown in figure 6.9:

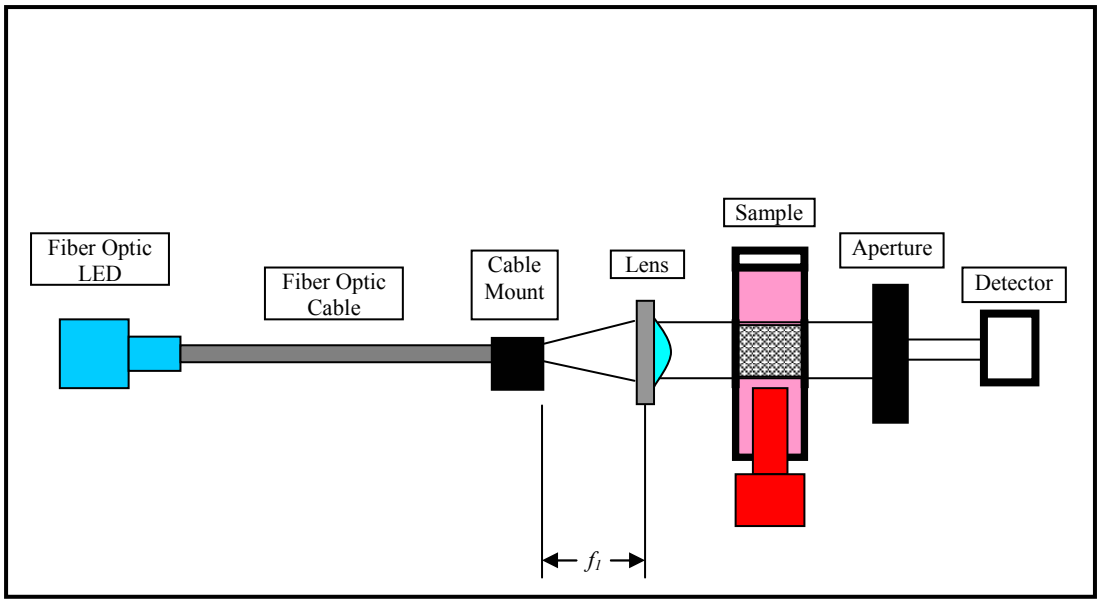


Figure 6.8 – Initial Optical System

This system failed to give satisfactory results because it allowed a large amount of reflection off of the cuvette walls to dilute absorption measurements and reduce the system effectiveness. The optimal configuration which included an entrance aperture is shown in figure 6.10:

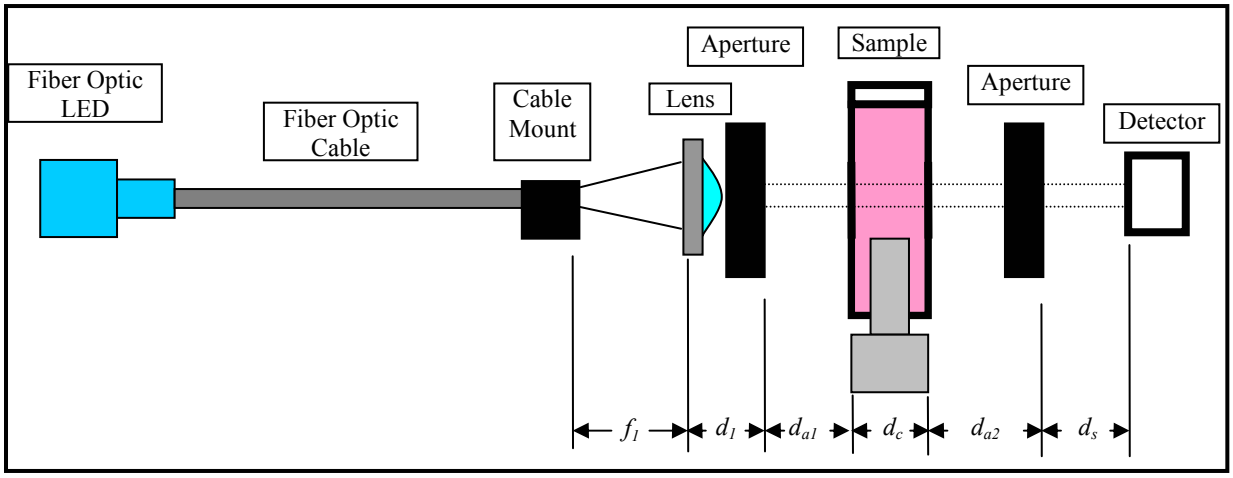


Figure 6.9 – Optimal Configuration

In this configuration the aperture diameter and detector distance d_s were changed until acceptable measurements were made.

The focal length of the plano-convex lens with radii of curvature $r_1 = \infty$ and $r_2 = 6.2$ mm can be calculated with its refractive index of n = 1.515082 by [35]:

$$\frac{1}{f} = (n-1)\left(\frac{1}{r_1} - \frac{1}{r_2}\right)$$

Where f is equal to a -12 mm focal length because divergent light enters on its planar side and is collimated.

The geometry of this system is very simple because in theory the beam is a uniform, constant beam whose diameter is controlled by the entrance aperture. The beam area of 7.065 mm^2 falls within the 17.9 mm^2 sensitive area of the detector. In reality it is impossible to produce a perfectly collimated beam so this factor could be considered as a source of error in the system because divergent beams could reach the detector and dilute measurements.

An important factor to consider in this design is the fact that three wavelengths are being bent in a monochromatic singlet lens. The point at which the image focuses is a factor of wavelength and measurements could be compromised. Based on the results obtained in

Chapter 7, this is a factor that may be present, but is greatly reduced by the short focal length of the lens. There did not appear to be any adverse affects of the image focusing.

6.2 Current to Voltage Amplifiers

The S2386-45K photodiode converts the incident radiation from the sources to a 0.01 – 100 μA current depending on the magnitude of the irradiance. With that being said, an amplifier with a significant gain will be required to produce a 0-5 V or 0 – 10V signal that is suitable for the data acquisition system. The photodiode was operated in photovoltaic mode for its linearity, low noise, lack of dark current, and simplicity. The photodiode can be operated in photoconductive mode, which gives a reverse bias to allow for a high speed response. This bias produces dominant noise and offset errors and was not used in favor of the photovoltaic mode.

For the amplifier needed for this device does not require a wide bandwidth or fast response, a simple RC feedback will be used to adjust gain and reduce noise. The resulting configuration is shown in Figure 6.11 [36].

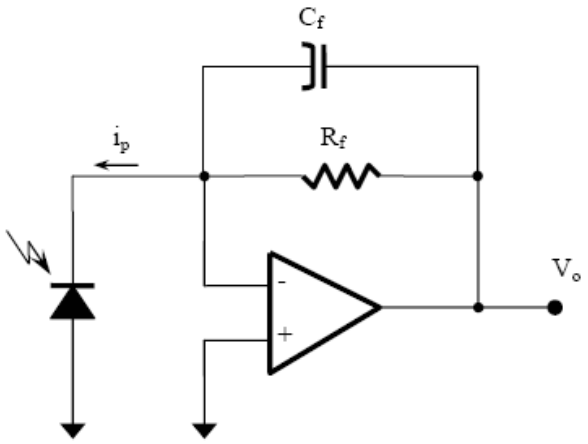


Figure 6.10 – Photodiode Amplifier Circuit

The basic transfer function is given:

$$\frac{V_O}{i_p} = \frac{R_f}{C_f R_f s + 1}$$

The feedback capacitor was selected with a capacitance of 0.1 μF. Precision 10 kΩ and 500 kΩ potentiometers with a ceramic resistor placed in series creates the total R_f so that

fine tuning of the gains is possible. With these values, the resulting step response and bode plots are shown in figure 6.12 and 6.13.

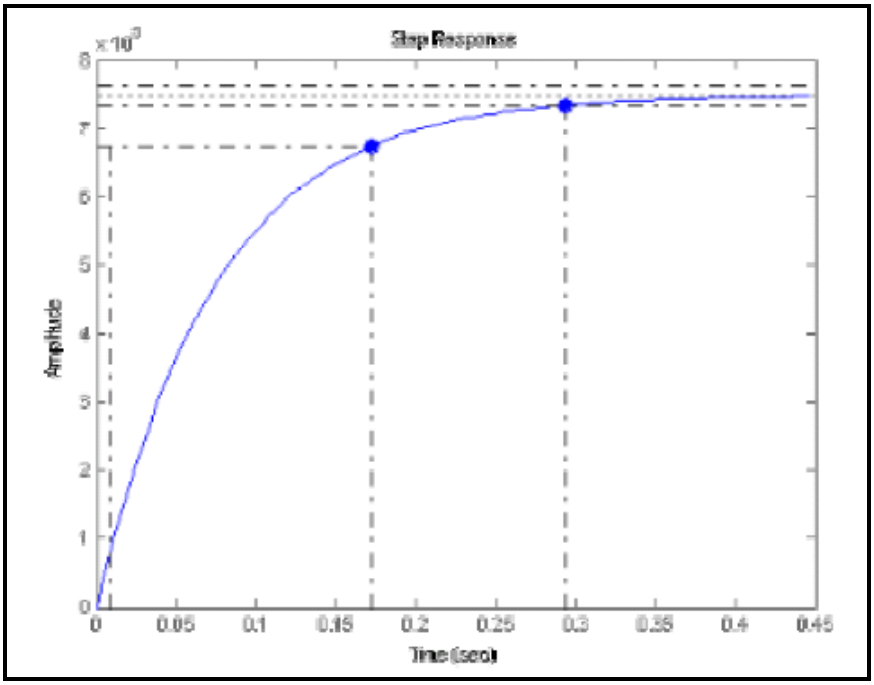


Figure 6.11 – Step Response

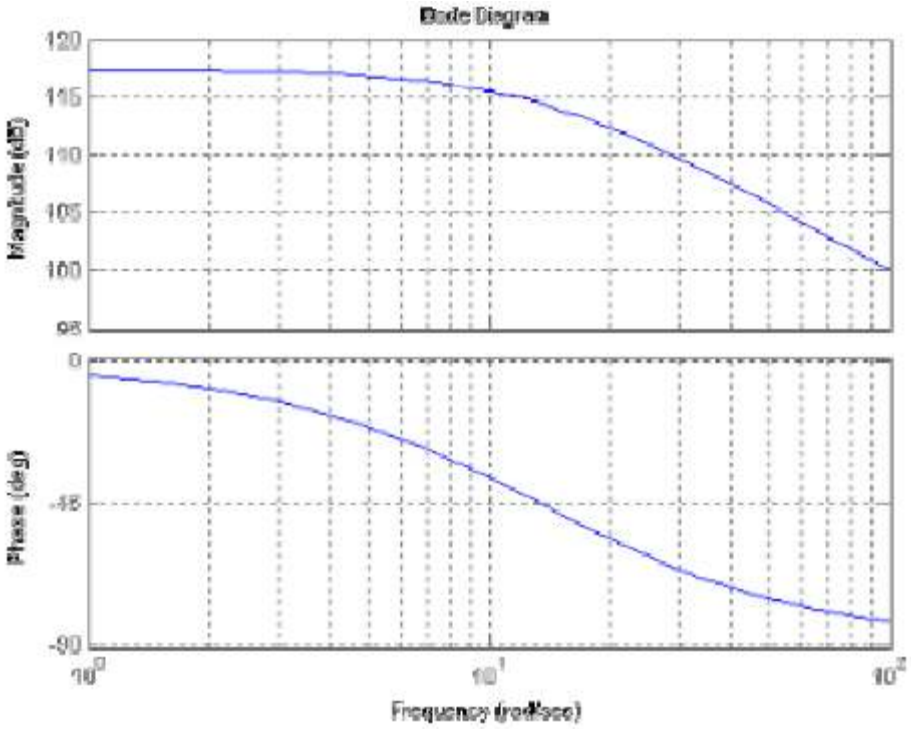


Figure 6.12 – Bode Plot

Matlab outputs a rise time, settling time, and corner frequency of 0.165 sec, 0.293 sec, and 2.15 Hz respectively. The op-amp is a Texas Instruments JFET – Input low noise op-amp. A total of three amplifier channels were made to accommodate the three source inputs.

6.3 Data Acquisition

The output voltage of the amplifier system described above is read by a National Instruments USB – 6008 board. This board has many capabilities, but only it's analog to digital conversion capabilities were needed for the scope of this project. The data acquisition board is a National Instruments USB-6008 board that couples to a computer through a USB connection. A LabView program was written to prompt the user for measurement and acquire the output voltages to calculate transmission, optical density, slopes, agglutination index, and type the blood using thresholds acquired through a normal distribution of non-agglutinated samples. The program uses case statements to choose the ABO type and Rh type. Sample Code is provided in Appendix B. The user interface is shown in figure 6.14:

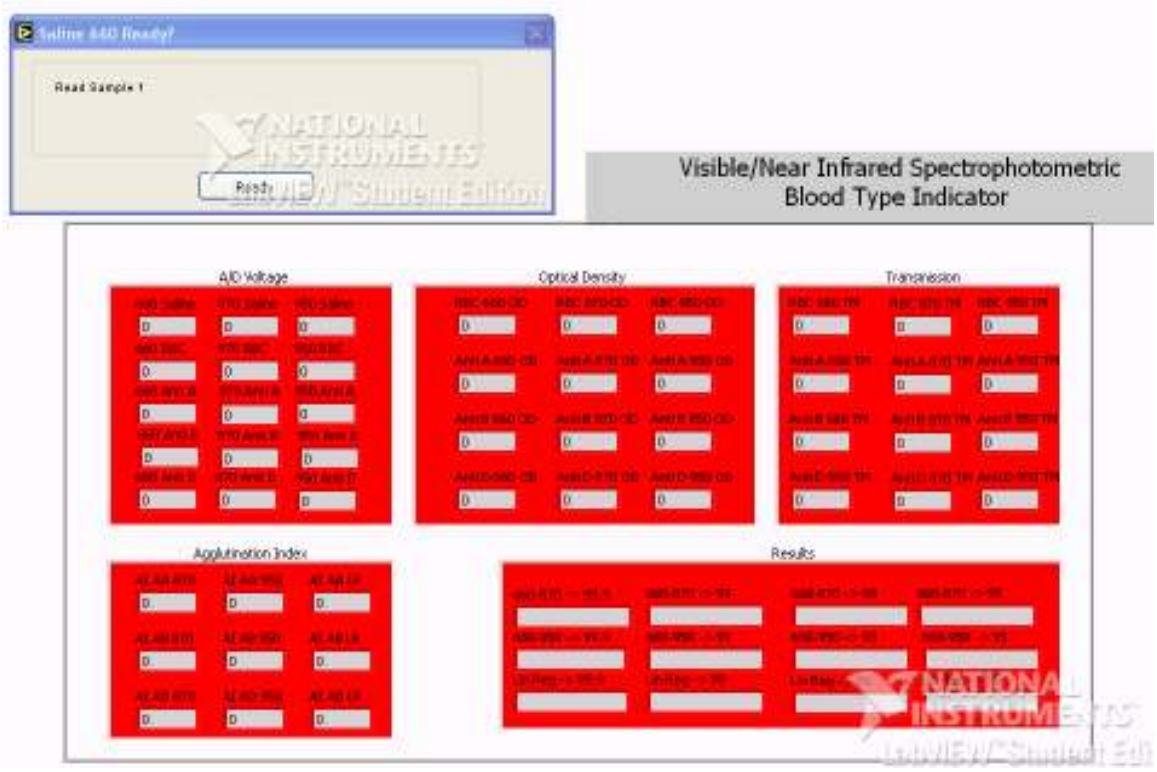


Figure 6.13 – LabView User Interface

This interface allowed the user to see the test results immediately and make necessary adjustments. This proved to be useful during sensor development.

6.4 Experimental System

The experimental system was assembled using affordable parts and some fabricated pieces to save time and resources. A schematic of the system is shown in figure 6.15:

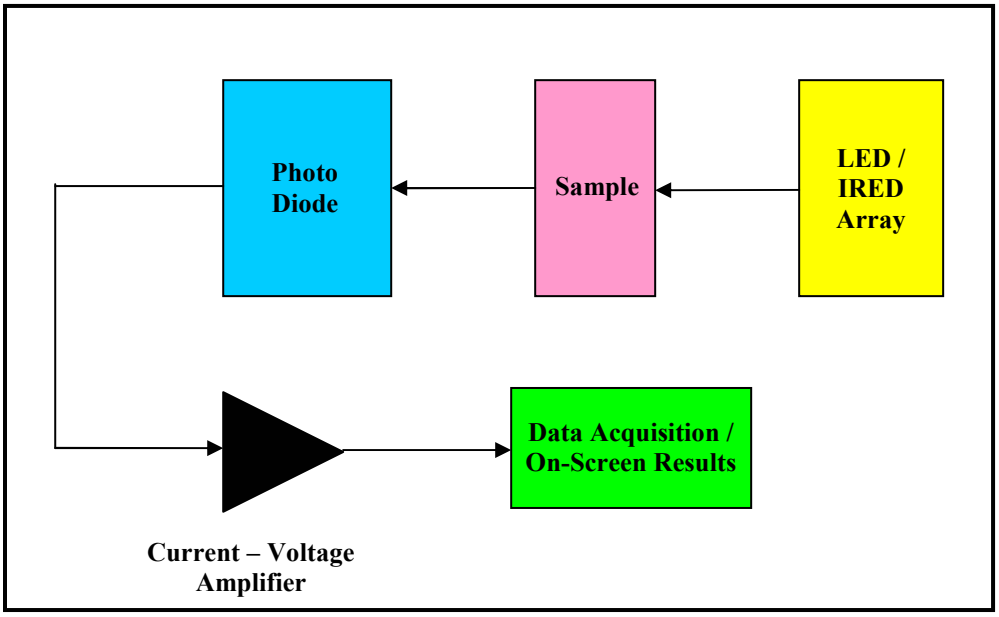


Figure 6.14 – Automated Test System Configuration

The optical system is shown figure 6.15 with the fiber termination mount, lens, entrance and exit aperture, and photodiode:

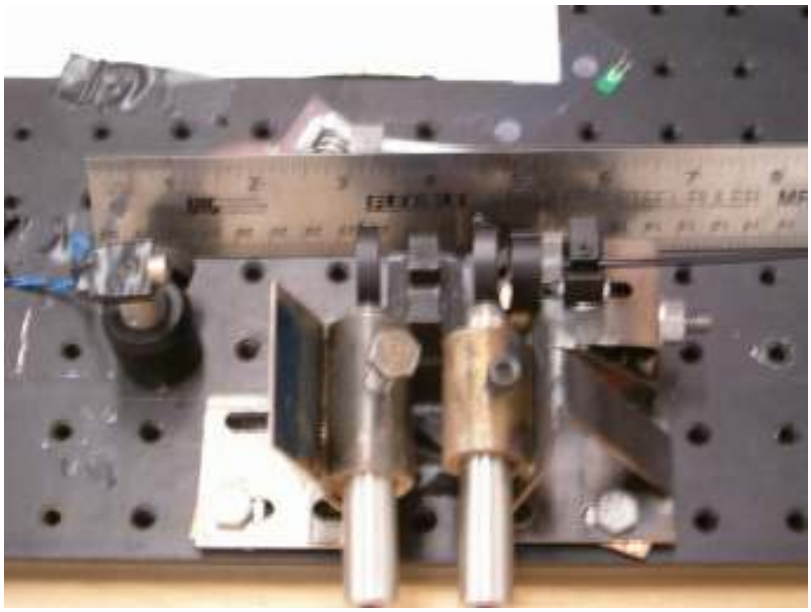


Figure 6.15 – Miniaturized Optical System

The amplifier and power supply setup is shown in figures 6.17 (a) and (b):

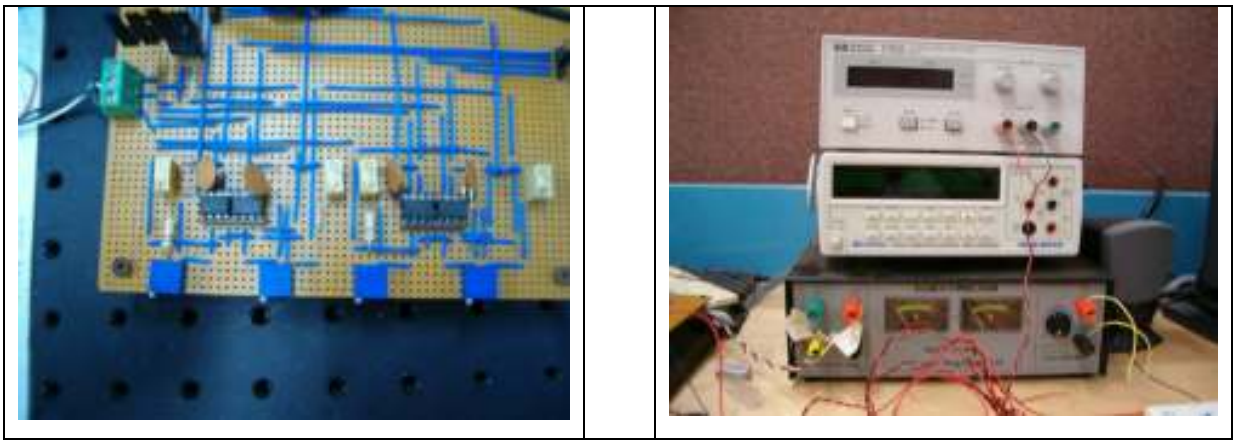


Figure 6.16 (a) and (b) – Amplifiers (a) and Power Supplies (b)

The light sources and data acquisition unit are shown in figures 6.18 (a) and (b):

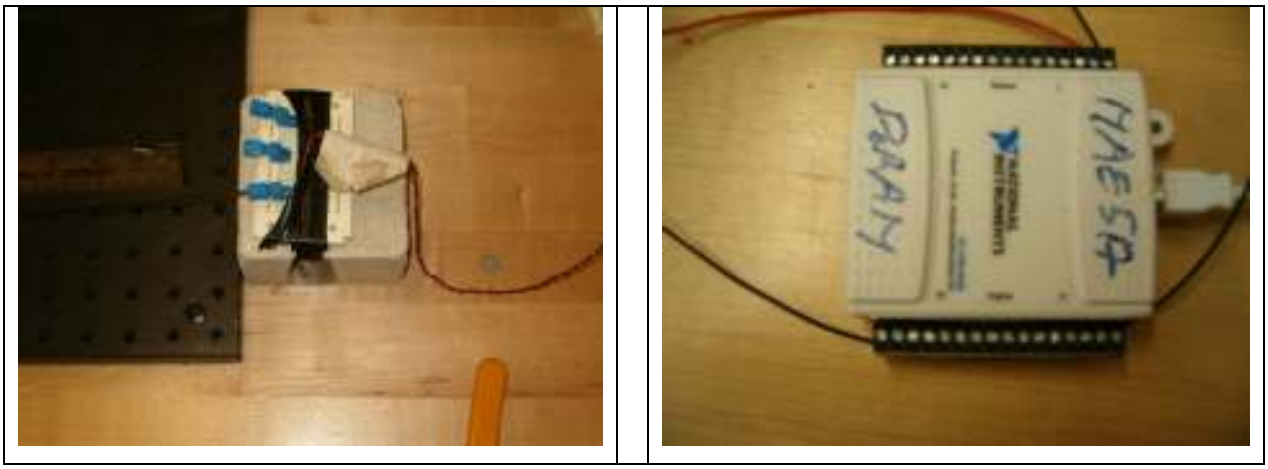


Figure 6.17 (a) and (b) – Light Sources (a) and Data Acquisition (b)

The light sources are anchored to a heavy block to minimize the chance of movement in the fiber optic cable. The data acquisition board is obviously capable of more than it was used for, but provided a nice measurement device for laboratory conditions.

The system component selection and theory has been presented so procedures and test results will be discussed in the next chapter.

Chapter 7

Experimental Procedures and Results

Once the system was designed and built, experiments were conducted and the system was modified based on the problems revealed by the experiments. This section will outline the blood typing procedure, evaluate the system performance, and present the blood typing results.

7.1 Blood Typing Procedure

A forward typing procedure using donor packed microcosms of whole blood from the Duke University Medical Center Transfusion Services Center was implemented in the research. Diluted commercial antibody was used for reactive samples while the control was mixed with saline. Anti-A and Anti-B are monoclonal blends marketed under the label Seraclone® and are manufactured by Biotest Inc. of Dreieich, Germany. Anti-D is a polyclonal blend marketed under the label Bioclone® and is manufactured by Ortho-Clinical Diagnostics of Raritan, New Jersey. Samples were evaluated using a method adopted from the Narayanan et al. research outlined in Chapter 5.

The control sample was made mixing whole blood 1:8 in phosphate buffered saline. Next, 100 μL of the diluted blood is added to 100 μL of saline in a culture tube and incubated at 37°C in a dry bath incubator for 1 minute to simulate body conditions and allow the reactions to take place if any. A small, 20 μL sample of this mixture is added to 2 ml of saline and the spectra is measured.

The treated samples also use 100 μL of the diluted whole blood and mix it with 100 μL of diluted antibody in a culture tube. The anti-A is diluted 1:8 in saline, the anti-B is diluted 1:2 in saline, and the anti-D is undiluted. The mixture is incubated for 1 minute at 37°C and 20 μL is added to 2 mL of saline. The spectra is measured and recorded.

The blank for all of the samples is simply a cuvette filled with saline. This blank allows for transmission calculations and helps eliminate error associated with the output voltage of the LEDs. A flow chart of the procedure is shown below:

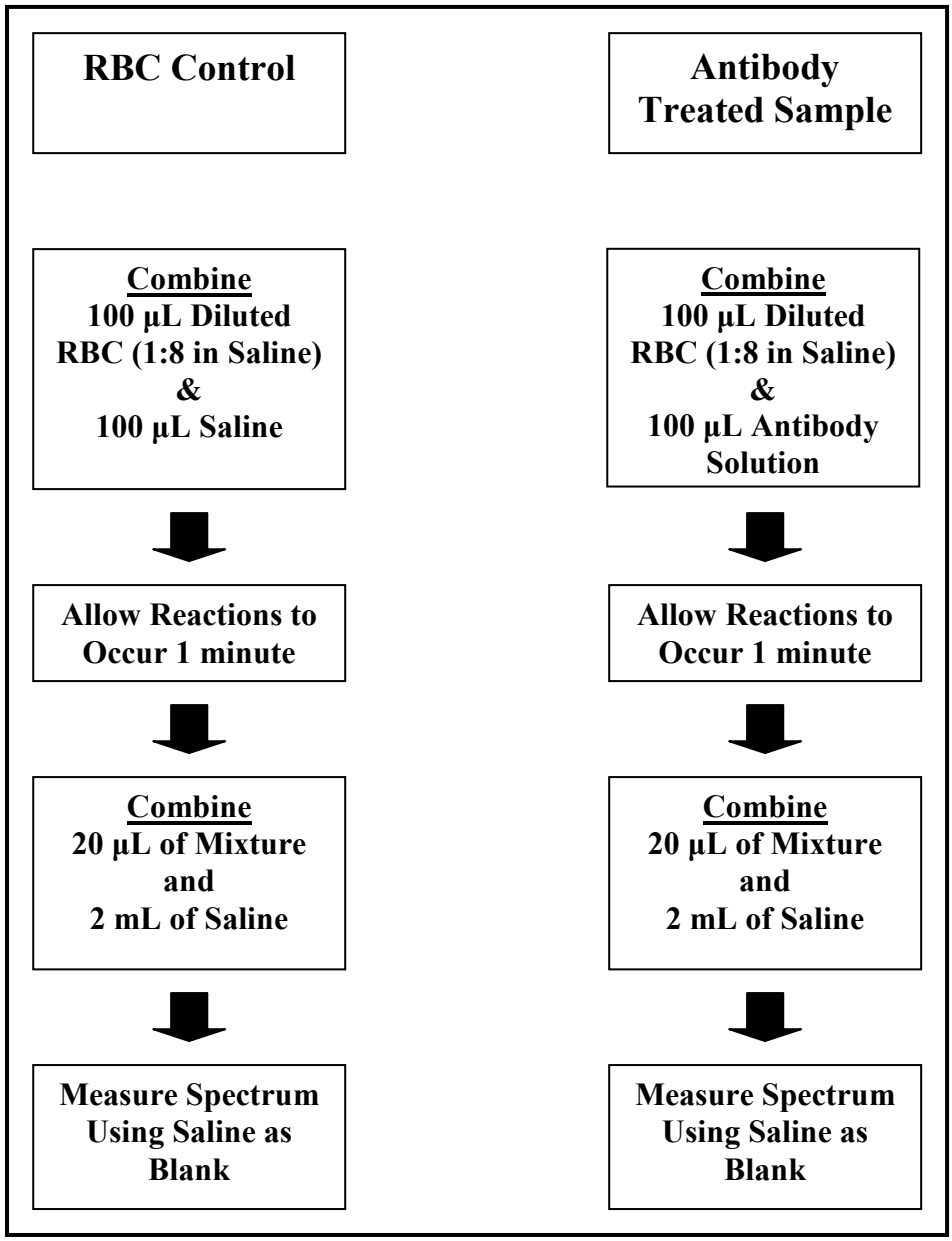


Figure 7.1 – Flow Chart of Sample Preparation

The concentration of the antibodies was determined during initial testing and allows for the strength of the blood reaction to be controlled. The concentrations were suggested by the Narayanan et al. research and proved to be effective for the sensor. Increasing concentration to strengthen the reaction is considered to be a valid approach when typing the blood.

Absorption spectroscopy standards require that when measuring a solution, the solvent should be used as the background so that only the solute will produce a change in the

recorded spectra. Narayanan et al. used antibody backgrounds for each of their antibody treated samples. To explore the effect that antibody backgrounds would have on the spectra of the samples, antibody backgrounds were prepared from the test concentrations and their absorption was measured on the spectrophotometer. Figure 7.2 shows their spectra below:

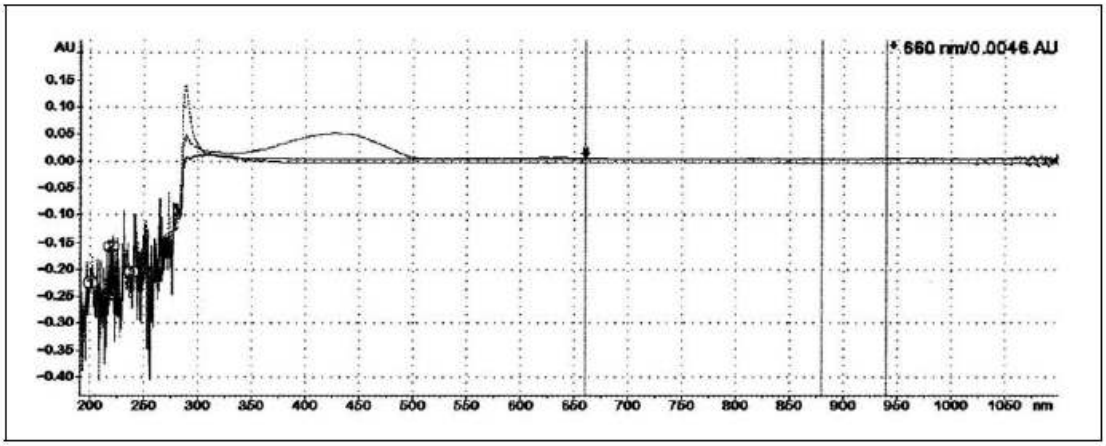


Figure 7.2 – Absorption of Antibody Background

In the bandwidth of interest (600-1000nm) it can be observed that the absorption of each sample measures below 0.02 AU. This value is close to the error of the spectrophotometer when measuring a cuvette of saline against itself. The antibody backgrounds are basically undetectable by the spectrophotometer so it is concluded that saline can be used as the background for all samples. This helps save time in the procedure which is critical when testing. The anti-B background sample does reveal a small absorption band that can be seen at 425 nm which explains its yellowish color, but is not critical because it is not in the bandwidth of interest.

7.2 System Evaluation

The first issue to address before typing blood is to evaluate how reliable the source/detector/amplifiers will be and their optimal operating conditions. Tests such as amplifier linearity, drift of LEDs, repeatability of cuvette mounts, repeatability of LED coupling, fiber attenuation and fiber bending help determine the characteristics and sources of error in a system.

Amplifier linearity was evaluated two ways, one method employed a neutral density filter and the other did not. The neutral density filter was obtained from the AERL Lab supervised by Dr. W. Roberts. This filter is manufactured by Melles Griot and has an optical

density of 0.6. The spec sheet can be referenced in Appendix D**.** In order to observe linearity, the drive current to the LED/IREDs is varied between 5 and 90 mA and the input current for the photodiode is plotted against the output voltage from the amplifier. The LED/IRED drive current was varied using an HP 3611A DC power supply while the input current was measured by a multimeter and the output voltage was recorded with the National Instruments USB-6008 data acquisition/control module. The plot is shown below and the results are quite satisfactory:

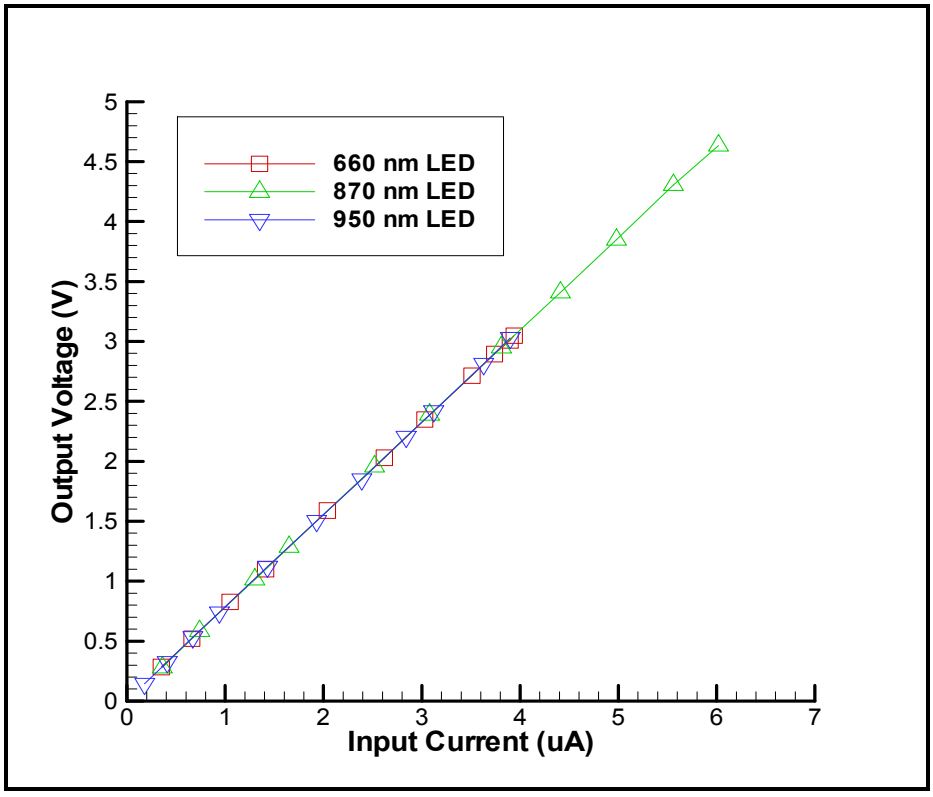


Figure 7.3 – Amplifier Linearity with Neutral Density Filter

The plot shows a linear response to the changes in incident light intensity measured by the photodiode for each light source.

These measurements were recorded in the optimal optical configuration to show that the system used to type the blood is indeed linear. The 870 nm IRED is the most powerful of the three light sources and the plot indicates this fact above. Since the end of the fiber optic cable is fixed and is never moved throughout testing, mounting misalignments are eliminated. The following plot shows the amplifier linearity without the neutral density filter and these results are favorable as well.

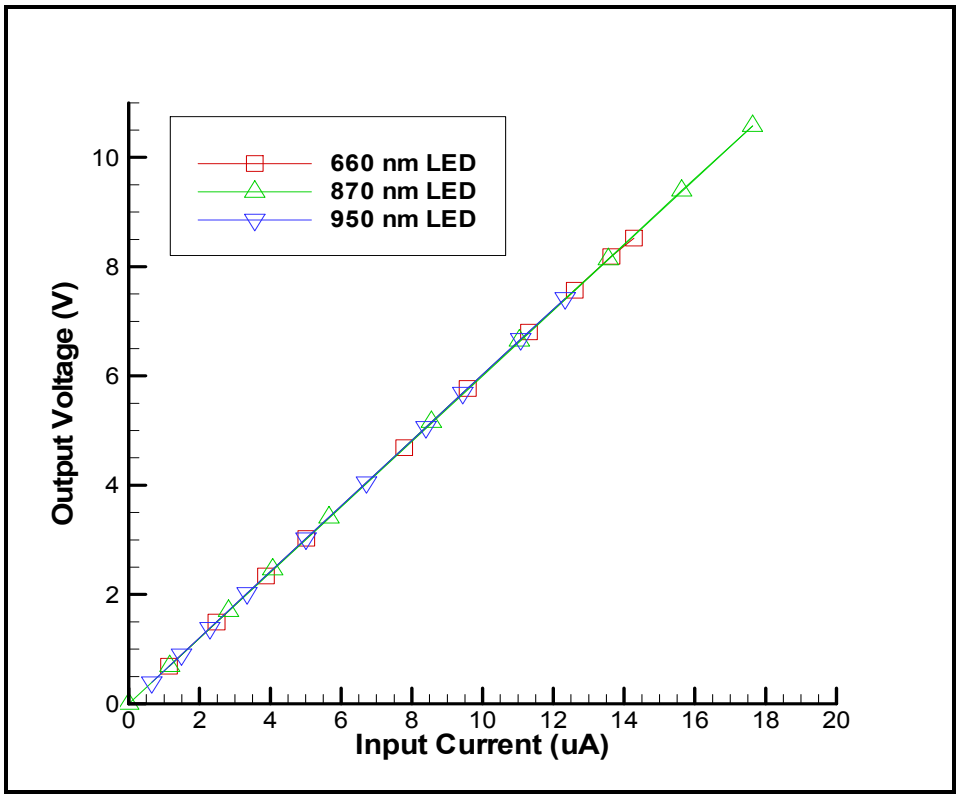


Figure 7.4 – Amplifier Linearity with no Obstruction

This plot also clearly shows that the system is linear although the LED source current could not be tested as high as the previous plot because the amplifier saturates around 11 volts. Nonetheless, this plot goes along with the previous plot in confirming the linearity of the amplifier.

Together, these plots show that the amplifier gives a linear response whether the beam is impeded or not.

The signal drift of the combined electrical system consisting of the LED driver (power supply), LED irradiance, photodiode sensitivity, and amplifier response over time can be investigated by simply observing the output voltage of the amplifiers over time. This can shed light on whether or not the system will give a consistent response over time and whether or not the system needs a "warm-up" period.

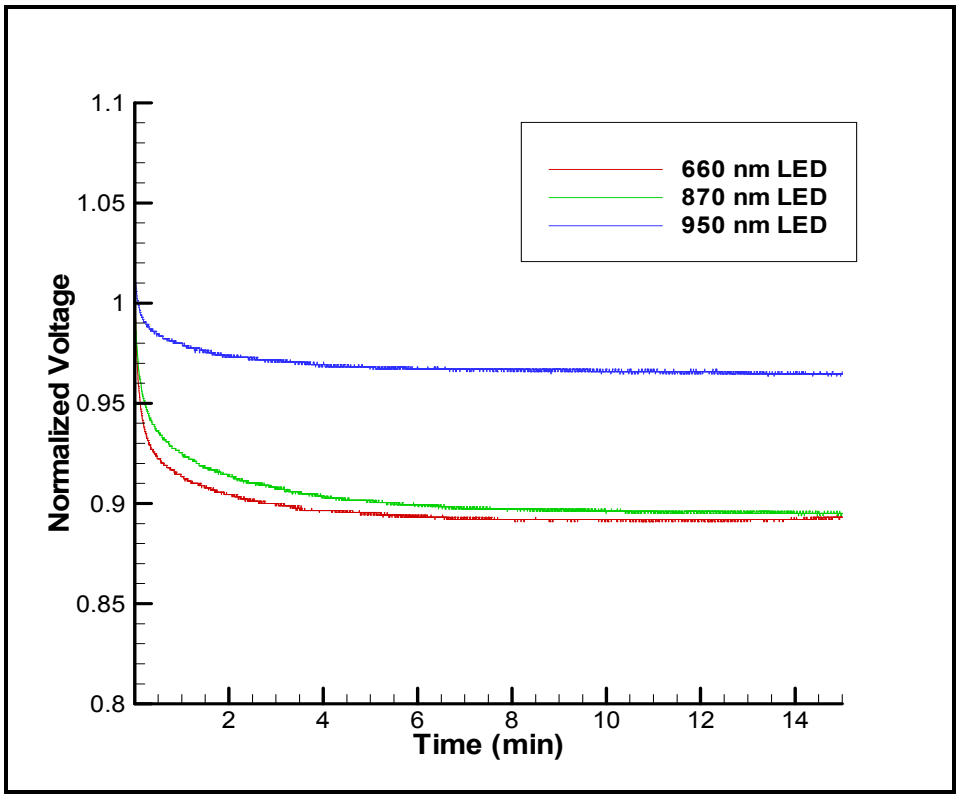


Figure 7.5 – Combined Electrical System Response over time

The plot indicates that the system does indeed need time to warm-up and stabilize. A time of about 6-8 minutes should be sufficient to adequately warm-up the system. During testing, the system was allowed to warm-up at least ten minutes before measurements were taken.

Cuvette transmission between alternate sides can vary consistently in absorption by about 0.02 AU. A marking on the cuvette allows consistent placement for each measurement. Repeatable cuvette placement is also desirable to maintain that the system does not introduce any errors that can affect the spectra of the samples. A test was conducted to insure that the cuvette mount could produce repeatable measurements with little or no deviation as the cuvette is changed in and out. The figure below shows a plot of normalized values recorded as the cuvette was mounted, dismounted, and remounted ten times over a ten minute period. Each value was recorded taking 1000 points over 2 seconds and averaging for a recorded value.

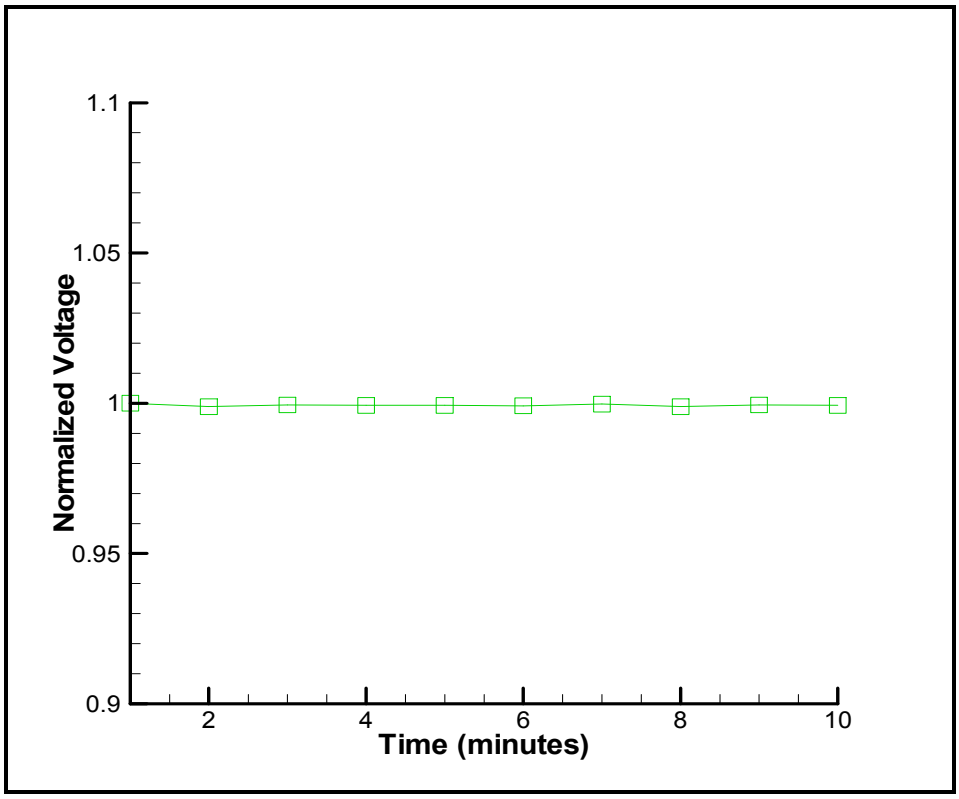


Figure 7.6 – Normalized Cuvette Mount Repeatablility Versus Time

The plot indicates that the cuvette mount is sufficient for testing and will give repeatable values and any effect on the recorded spectra is negligible. The standard deviation is around 0.000346 and the error is 0.0007% to further support this assumption.

These tests indicate that the system is linear, stable, and reliable for measurement and blood typing experimentation can now proceed.

7.3 Fiber Optic Characteristics

Fiber optics use internal reflection to keep the incident light in the core and transmit it to the desired location. In order to better understand the fiber optic cable used to transmit the radiation from the LED/IREDs a few tests were conducted to observe characteristics of the fiber and possible effects that it can have on the tests. Fiber bending, fiber mounting, and fiber attenuation will be observed and discussed.

The bending of optical fiber can cause light attenuation to increase dramatically because the confinement angle will be changed and allow some of the light to escape into the cladding. In order to explore this trait of optical fiber, the fiber was bent at an angle between

0 and 60° using a 660 nm light source. The plot of the output voltage versus the fiber angle is shown below.

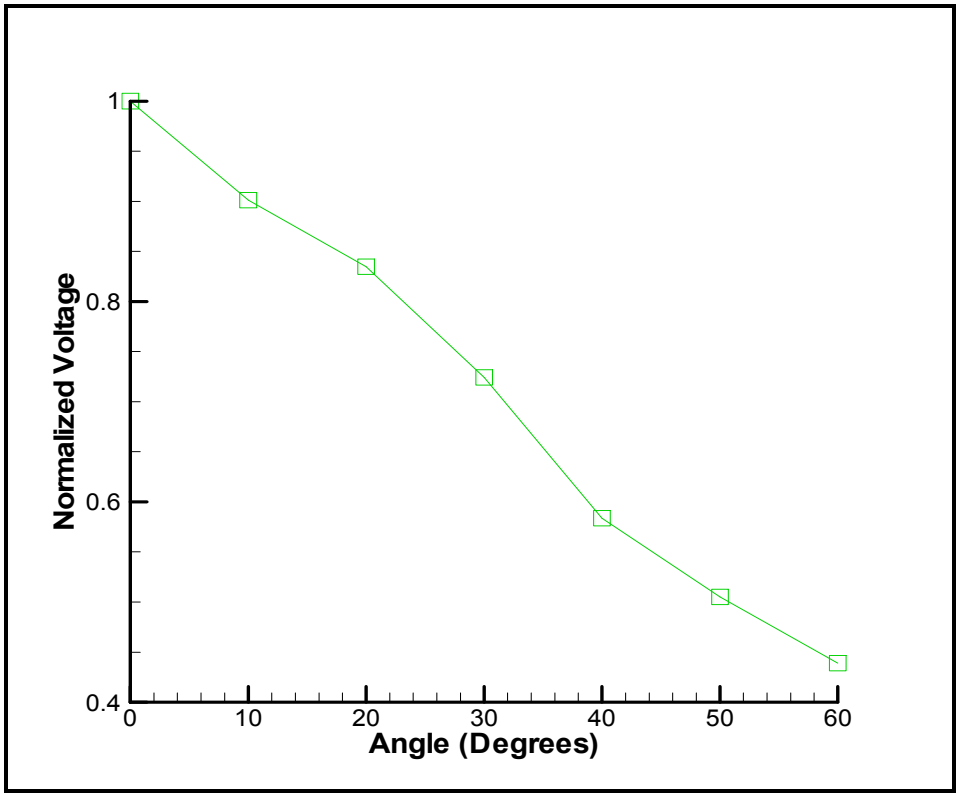


Figure 7.7 – Output Voltage Versus Optical Fiber Angle

The plot above shows that the relationship between attenuation and fiber angle is virtually linear and that bending fiber will weaken the light exiting the cable. The cable was near breaking when at the 60° measurement and it should be noted that this test was the last test conducted so it is possible that the fiber may need to be replaced because of micro-fractures that could have been induced by the deflection of the fiber. These micro-fractures could have implications on the future performance of this particular segment of fiber.

Since the prototype does not electronically switch wavelengths or employ fiber splitters to stabilize the incoming light signal, the fiber had to be manually pulled from one LED and mounted in the next respective wavelength during the test. The repeatability of this action has an effect on the intensity of the incident light yet this error can be accounted for by measuring a blank such as saline before measuring control and treated samples. When the control and treated samples are manipulated to calculate transmission values, they are

divided by the blank measurement to calculate transmission and therefore the error is eliminated. The plot below shows the repeatability of fiber/LED coupling.

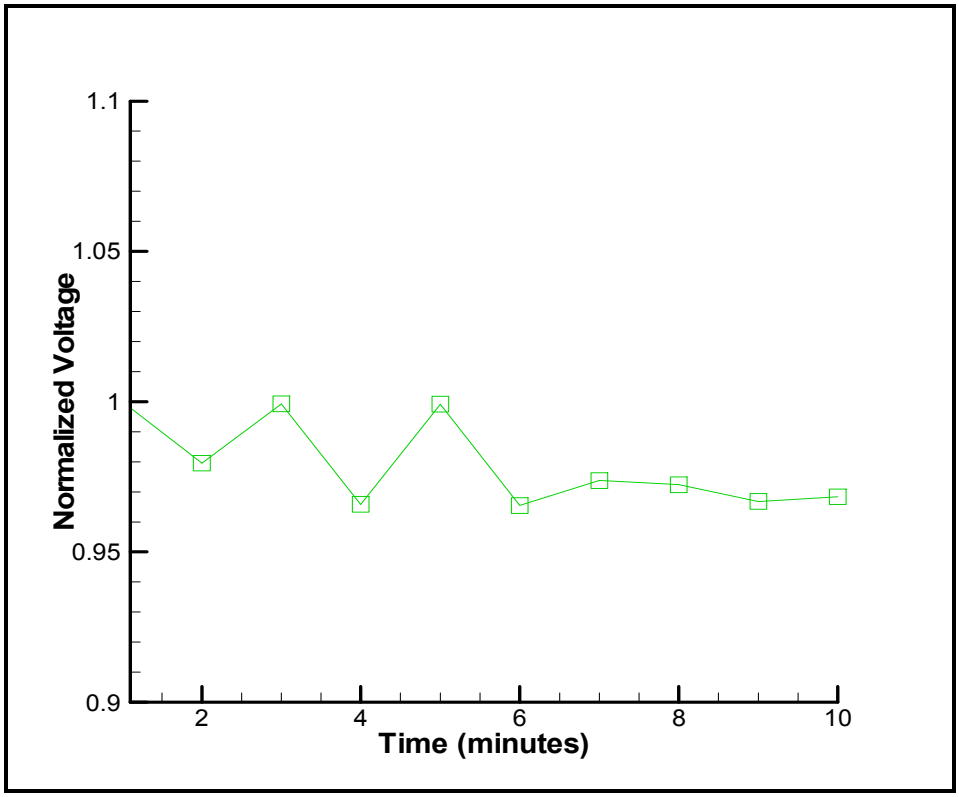


Figure 7.8 – Normalized Output Voltage Versus Time for Fiber Coupling Repeatability

The repeated coupling of the LEDs and the fiber show that the output voltage is fairly constant with a standard deviation of 0.14005 and an error of 0.97%. This shows that despite the fact this error can be accounted for with a blank measurement, it is a relatively insignificant error and can be neglected.

Fiber attenuation per unit length is another parameter that should be mentioned. Although this is a parameter that is mostly of concern for fiber that carries data over long distances, it will be addressed anyway. Attenuation is generally measured in dB/m and is basically a ratio of the difference between the power going in the cable and the power coming out. The Mitsubishi GH4001 1000 μm core jacketed step-index optical fiber used in the testing is rated at 0.15 dB/m attenuation (650 nm). Attenuation is a function of wavelength because not all wavelengths can be carried through an optical fiber. The fiber used is compatible for the visible-IR range so the variance of attenuation between the wavelengths used in the testing will be minimal. A quick comparison was done using a 3

inch segment and the 9 inch segment used for testing. A difference of about 1% was measured which again shows that attenuation is not a large factor in small systems like the prototype. Attenuation can be a large factor when splitters and couplers are used because the signal is divided by the amount of splits. For example, a 3:1 splitter that would be needed when automating this device would only allow 1/3 of the intensity to pass to the termination fiber. This may require that LEDs with more output power would need to be specified because shutters would also need to be employed to block the two unused wavelengths.

7.4 Collimation of the Beam Incident to the Detector

The optical system has been designed to collimate the diverging light beam exiting the fiber so that it enters and exits the sample collimated, passes through the aperture, and enters the offset photodetector allowing the stray light to diverge away from the sensitive face. This also helps offset effects caused by the possibility that the lens cannot maintain collimation over a distance. The accuracy of the absorption measurements is increased and allows the system to be much smaller than the previous converging/diverging beam system. The size of the collimated beam is regulated by the sample entrance and exit apertures to maintain an intensity that will not saturate the amplifiers. The apertures were varied from 2 – 4 mm in 0.5 mm increments, resulting in beam diameters of 2 mm to 4 mm into the sample cuvette. In order to increase the absorption measurements, the detector was moved 56 mm back from the aperture which decreased the possibility of recording scattered light that could dilute the measurements. The figure below shows the system collimation:

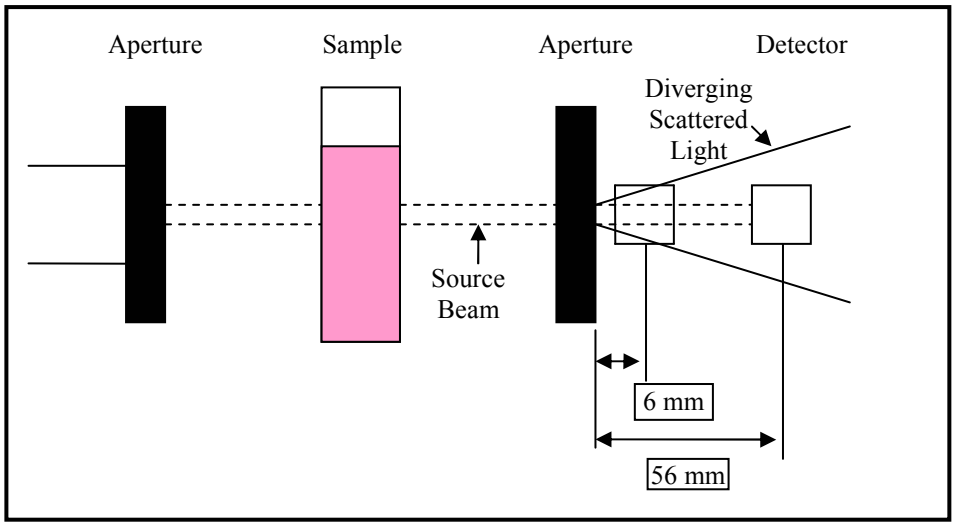


Figure 7.9 – System Collimation

A- samples were prepared using the procedure in section 7.1 . The detector was set at the optimal 56mm distance from the exit aperture and each aperture setting was evaluated. The following plots show the measured optical densities for each light source.

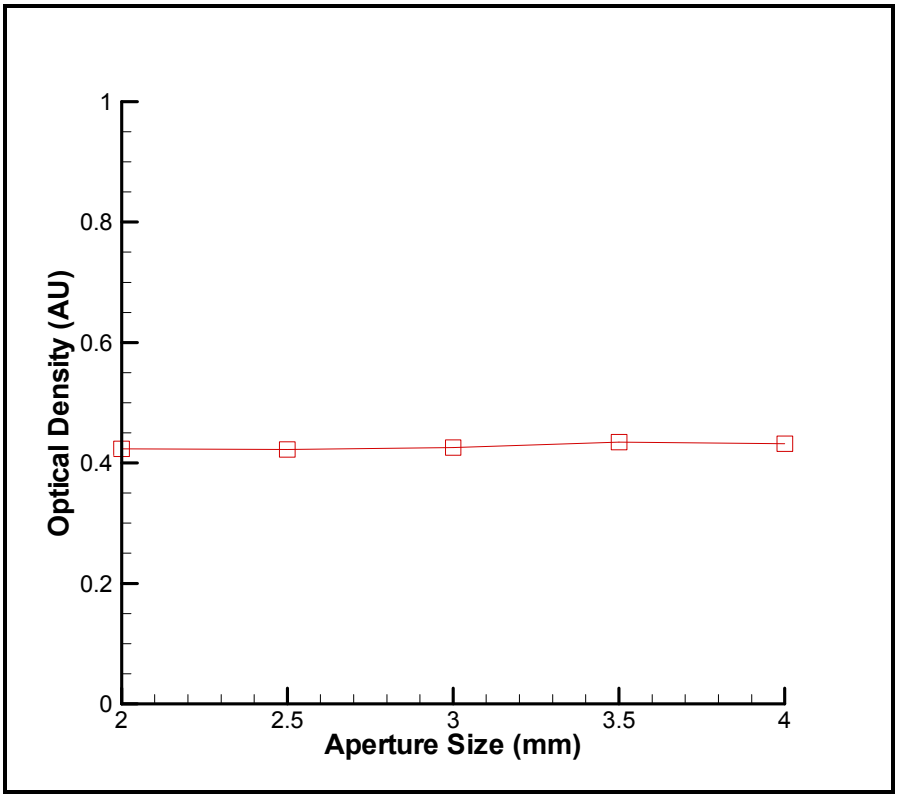


Figure 7.10 – Normalized Optical Density vs. Aperture Size at 660 nm Wavelength

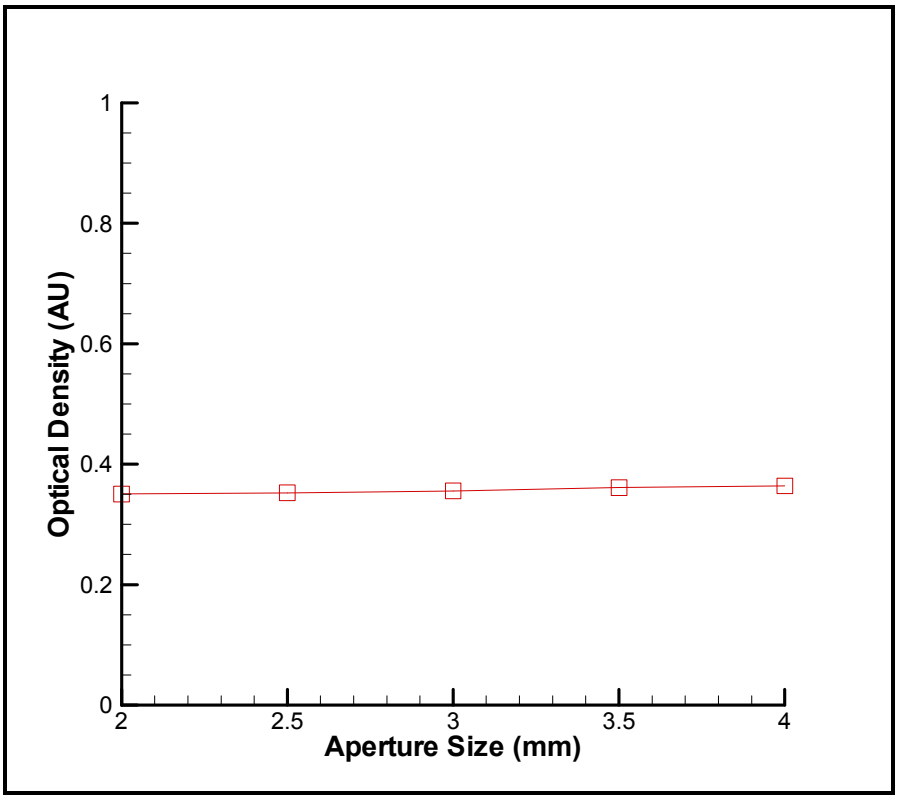


Figure 7.11 – Normalized Optical Density vs. Aperture Size at 870 nm Wavelength

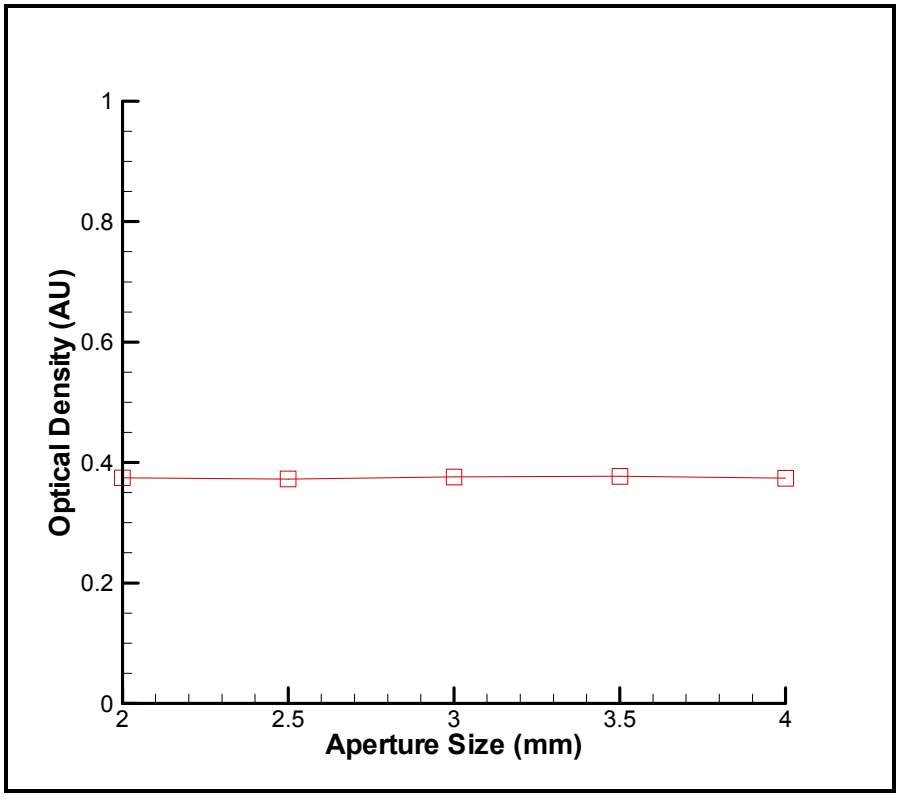


Figure 7.12- Normalized Optical Density vs. Aperture Size at 950 nm Wavelength

The plots show that changing the aperture diameter does not have a large effect on the optical density of the control sample. The 3 mm setting was used throughout the testing because it allowed for a beam to pass through the cuvette unimpeded by the cuvette walls and allow a favorable intensity to reach the detector. The 2 – 4 mm aperture size range was maintained because the amplifiers saturated above 4 mm and measurements below 2 mm could not provide the intensity needed for measurement.

The previous test established that with a collimated beam, the aperture settings will not affect the optical density significantly. This means that the apertures can be used as a way to adjust source intensity. The next test will evaluate the effect that detector distance has on the optimal aperture setting of 3mm. All system parameters will be held constant with the exception of detector distance. The following plots show the measured results with A+ blood.

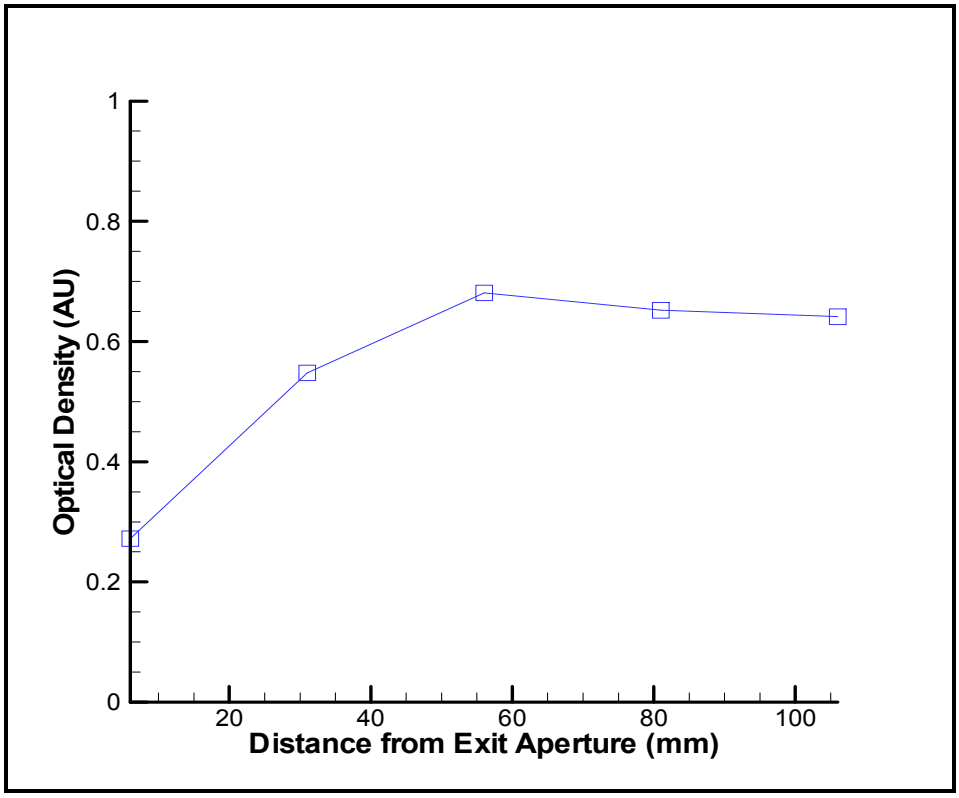


Figure 7.13– Optical Density vs. Detector Distance at 660 nm Wavelength

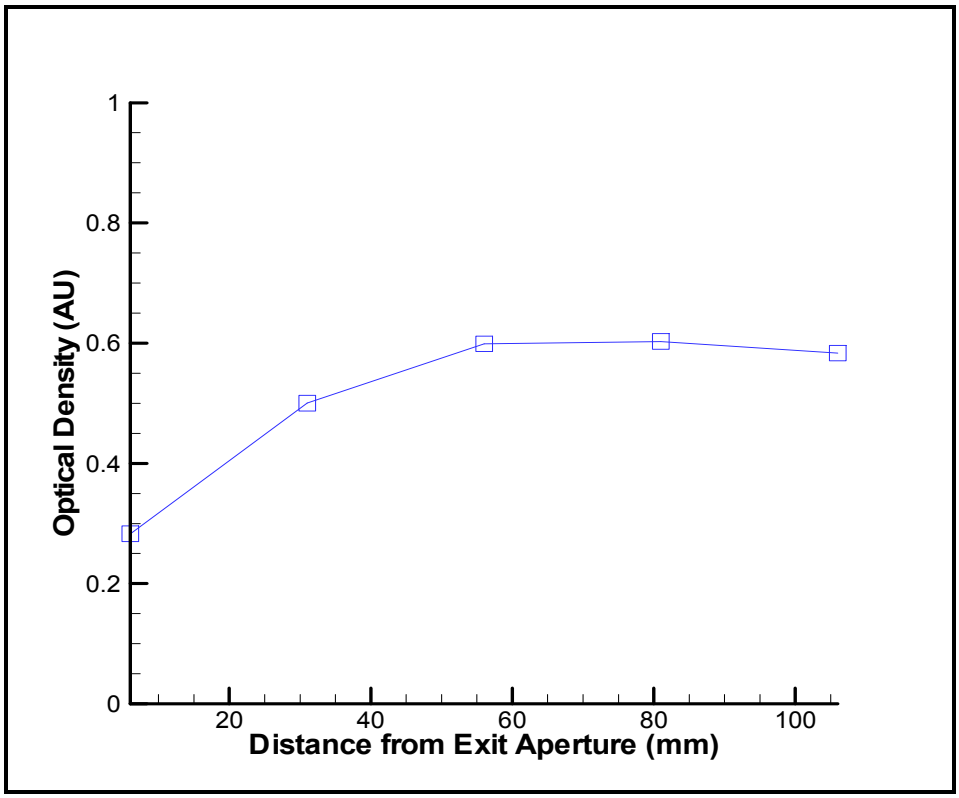


Figure 7.14 – Optical Density vs. Detector Distance at 870 nm Wavelength

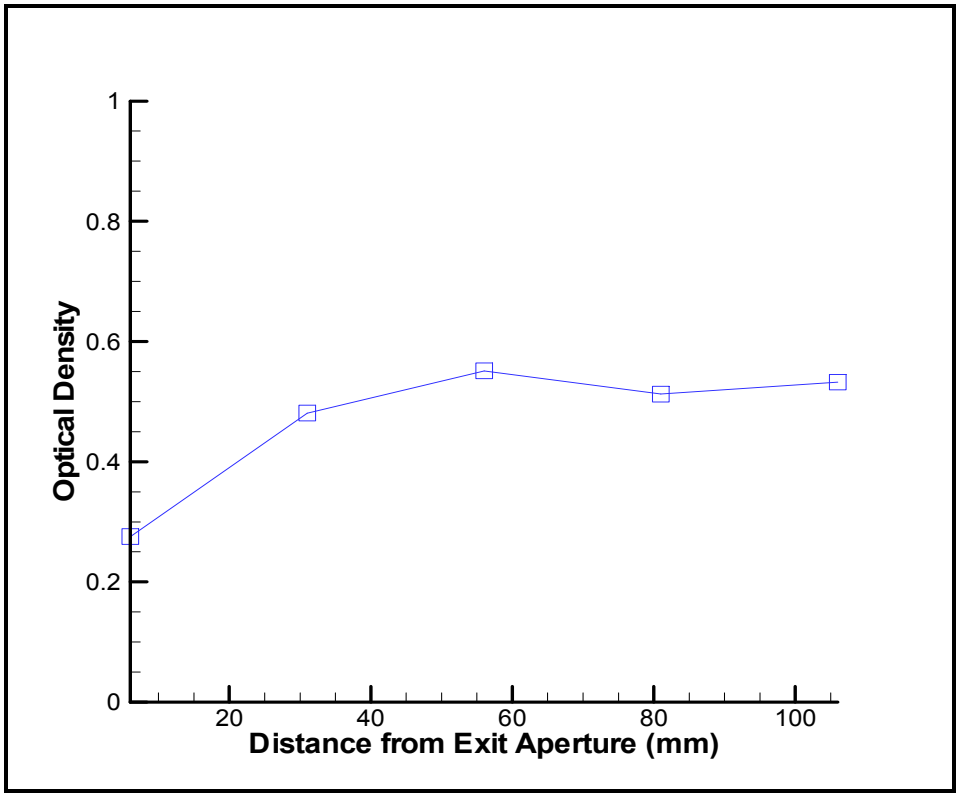


Figure 7.15 – Optical Density vs. Detector Distance at 950 nm Wavelength

The detector distance test shows that when the detector is placed directly behind the exit aperture, there is a significantly diluted absorption. This can be attributed to scattered light at small angles from the incident direction. This acceptance angle for the detector also contains the majority of light intensity scattered by the sample as well as light reflected off the walls of the cuvette. The absorption values begin to level off once the detector is 56mm beyond the exit aperture. This is because the acceptance angle is inside the incident source beam. This measurement is still contaminated by scattered light from small angles off of the incident rays, but the absorption measurement is significantly improved as well as the sensitivity of the system. The deviations in absorption for the detector distances within the stable absorption range can mostly be attributed to alignment errors associated with the detector being so far away from the exit aperture. All of the plots show a fairly constant measurement although possible errors can be attributed to the singlet lens used to collimate the light. As wavelength increases, the beam will focus farther away. This could mean that the 950 nm wavelength is focusing farther away than the 660 nm wavelength and lead to an error in the system. Although this error is present in the system, the short focal length of the lens allows for this error to not be a large factor and good results can be obtained from this system. This error can be addressed with a lens combination that eliminates the errors associated with wavelength changes. This error did not appear to be significant in this experiment and was not addressed.

Now that the optimal sensing configuration for the detector has been established the characteristics of the optical density of blood samples seen on the spectrophotometer can be observed with the experimental system. A downward sloping line will be observed for non reactive samples while a flattened line will be observed for the reactive antibody treated samples. Non-reactive antibody treated samples will show effects similar to the control samples with slightly different absorptions, but very similar slopes. With a slope similar to the control, the agglutination index of the sample will hover around zero or display a negative agglutination index. Ideally the slope of the non-reactive antibody treated sample will be about the same as the control, but it can exhibit a sharper slope which will generate negative agglutination indices. The two plots below show examples of the reactive and non-reactive spectra.

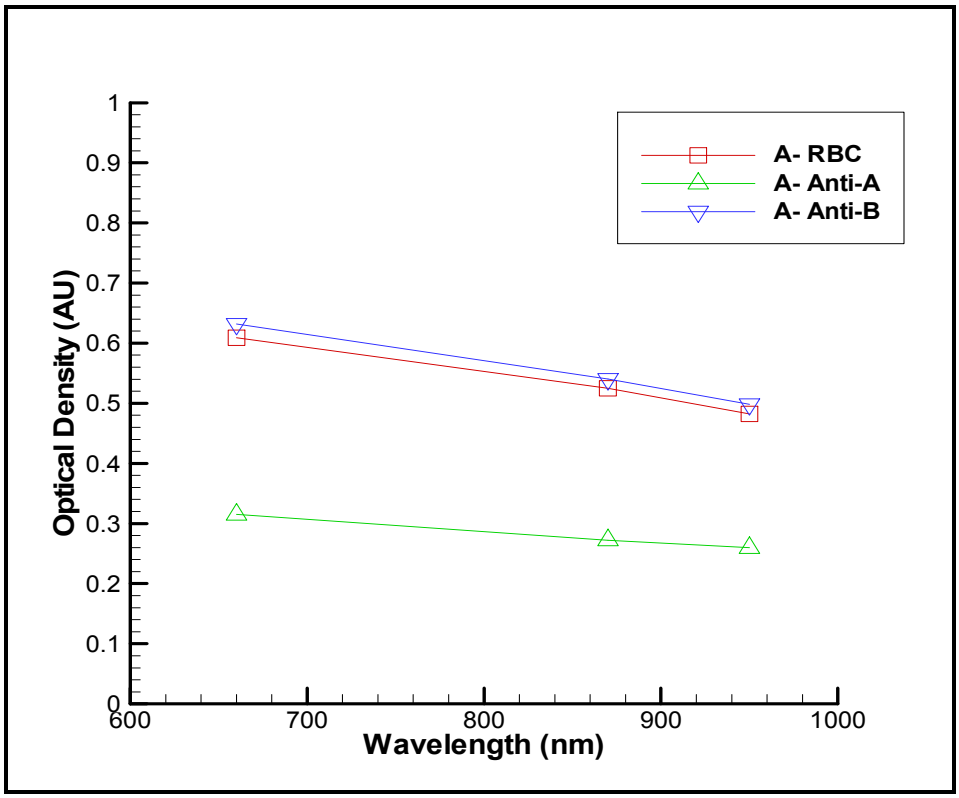


Figure 7.16 – Measured Spectra of A- Control and Antibody Treated Samples

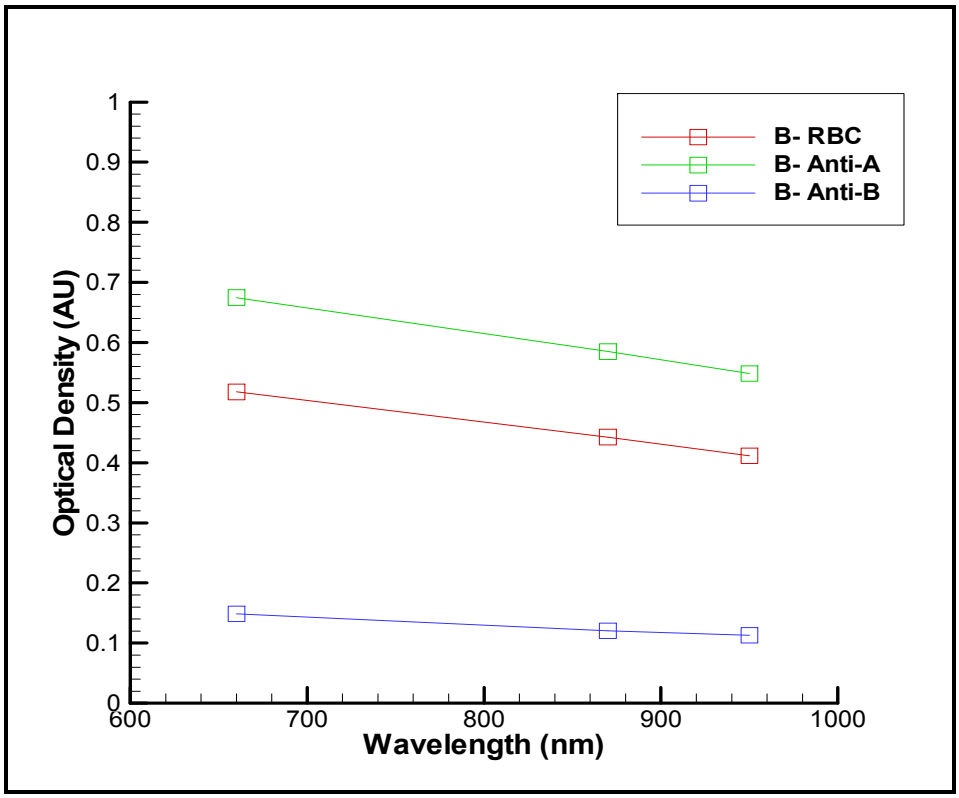


Figure 7.17 - Measured Spectra of B- Control and Antibody Treated Samples

7.5 Source Intensity Effects

Changing the aperture diameters will have an effect on the intensity of the source beam so the effects of changing the source intensity should be investigated. The detector is mounted at the 56mm distance from the exit aperture and the apertures were set to the 3mm diameter, both of which were used throughout testing. The forward current of the sources were varied between 10 and 60 mA and the spectra were measured for A- control and anti-A treated samples. The spectra are expected to vary in a manner proportional to the forward current. The following figures show the results of the experiment.

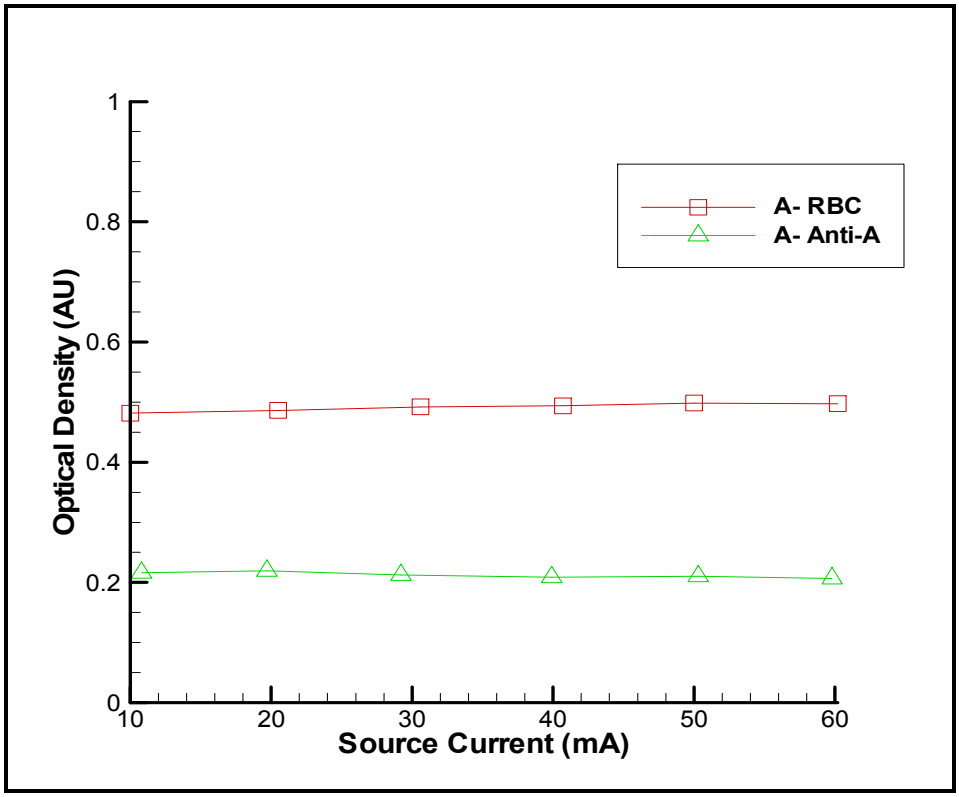


Figure 7.18– Optical Density vs. Source Intensity for 660 nm LED

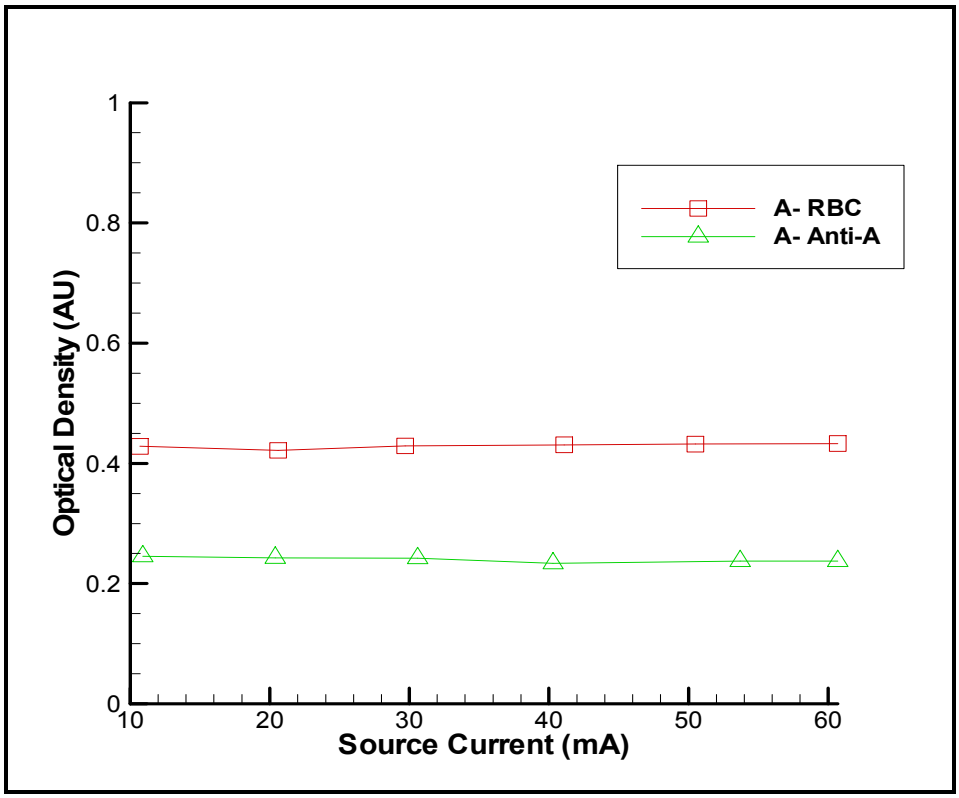


Figure 7.19 – Optical Density vs. Source Intensity for 870 nm LED

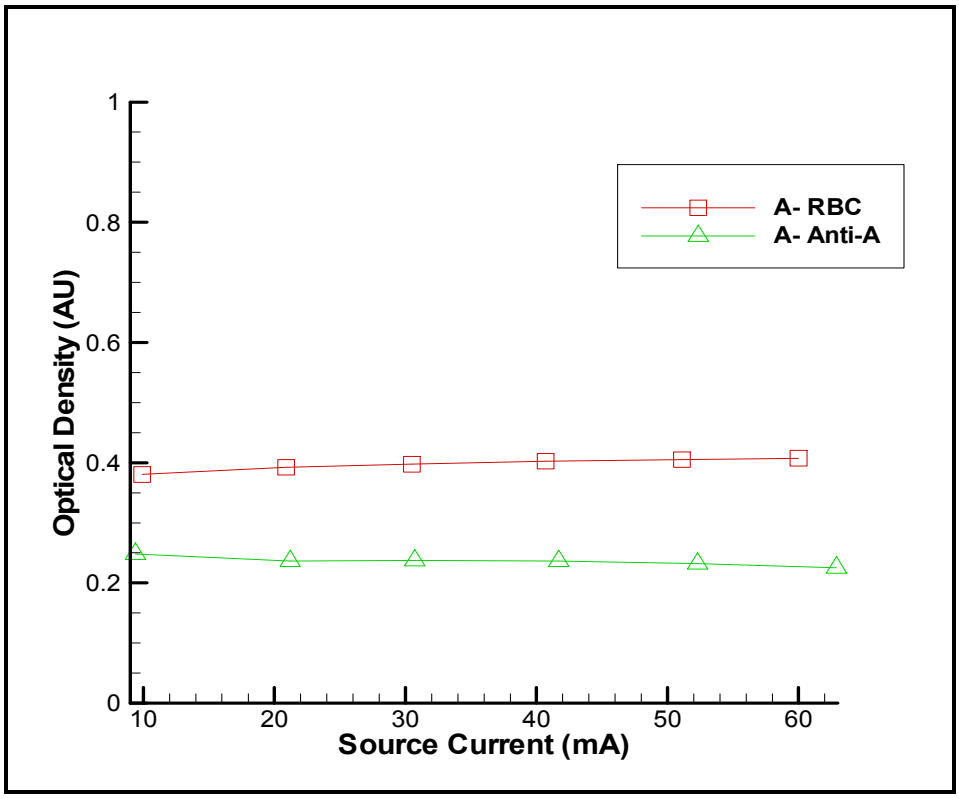


Figure 7.20 – Optical Density vs. Source Intensity for 950 nm LED

As expected, varying the forward current of the source does not have any impact on the optical density measurements. This means that intensity can be eliminated as a factor to consider when measuring samples. The intensity can be varied to make the data acquisition measurements look neat and easy to understand. This leaves the detector position, alignment, and beam size as the only relevant factors affecting measurement.

7.6 Sample Concentration

Concentration of the test sample should be investigated to explore their effects on the spectral slopes of the test samples. Samples of A+ control and anti-A treated samples were prepared according to section 7.1. Concentrations of 10, 20, 40, and 80 µL were added to 2 ml of saline in the cuvette. These concentrations resulted in blood to saline/antibody concentrations of 0.031-0.241%. The plot below shows the resulting spectra:

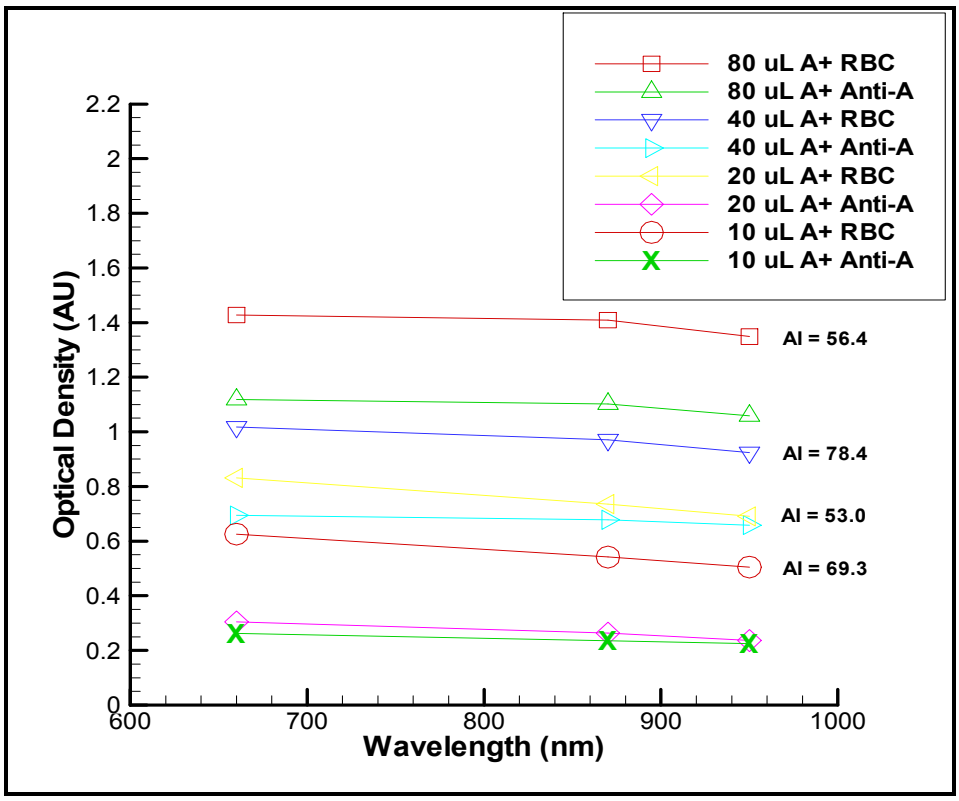


Figure 7.21 – Spectra of 10 – 80 µL A+ Concentrations

The plot shows that an increase in concentration does affect the optical density of the measurement as expected. This does not appear to be a completely linear relationship, but the concentration does have an effect on optical density. It is important to maintain a measurement range of about 0.1-1.0 AU for accuracy of measurement in absorption

spectroscopy [24]. The figure below takes a look at optical density as a function of concentration and the nonlinear deviation from the Beer-Lambert Law.

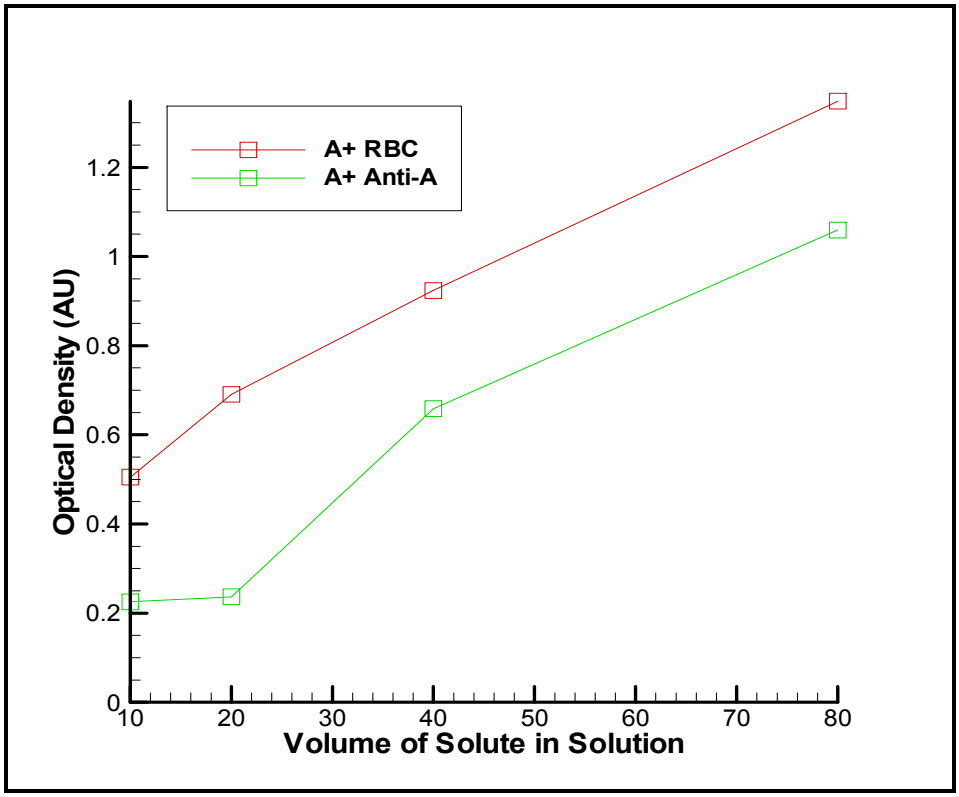


Figure 7.22 – Comparison of Control and Antibody Treated Spectra at 950 nm

The deviation from the linearity of the Beer-Lambert law is easier to see with the reactive sample, but the curves for both do not display linearity. The reactive sample allows more forward scattered light to be incident upon the detector so its behavior is less predictable. Reactive samples also do not always exhibit the same absorptions from sample to sample because the extraction method does not always produce a uniform distribution of cells as it does with the non-reactive samples. This is because the agglutination produces clumps of cells varying in size.

7.7 Sample Transience

The samples prepared, using the procedure in section 7.1, are a suspension of solid particles that are in constant motion in the solution and the light path. It is important to realize that the samples are constantly changing and do not remain in a constant state in the light path like the neutral density filter used in the amplifier linearity test. The red blood cells will sediment at rate that is a function of particle size especially in reactive samples. Untreated samples will also sediment and aggregate when left to stagnate over time. With

this in mind, a transience test will be conducted to better understand when it is the best time to take the spectra of the samples and how the samples change over time. It is assumed that taking the spectra of the samples as quickly as possible is the best approach.

Using the 660 nm LED, the spectra of saline, control, and antibody treated samples were examined over a 20 minute period. The samples were measured at a sampling rate of 5 hertz which resulted in 6000 measurements over the test interval. The normalized results are displayed in Figure 7.23:

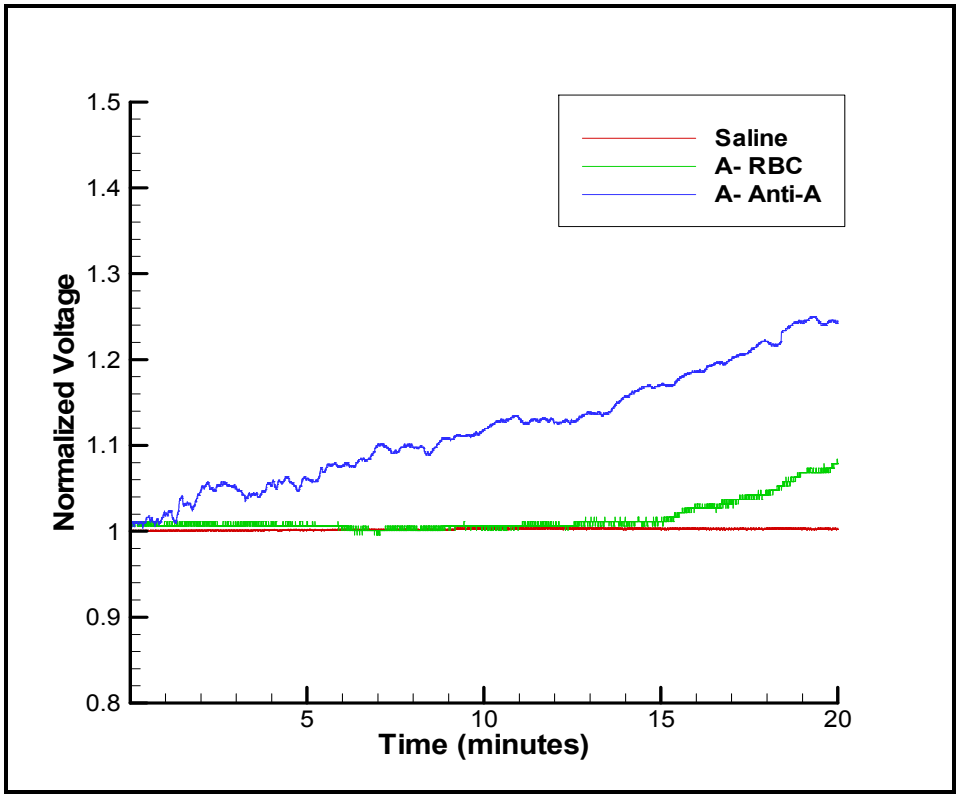


Figure 7.23 – Normalized Output Voltage Over Time for Saline and A- Samples With 660 nm Source

The plot above shows that the saline sample remains constant over time. The RBC control sample remains fairly constant until stagnation leads to aggregation at the bottom of the cuvette. As the cells settle, the transmission begins to rise in the final 5 minutes of data collection. The reactive sample begins to settle almost immediately due to the particle sizes in the suspension. It is important to note that in order to capture the spectra of the reactive sample after mixing, the spectrum needs to be recorded in the first three minutes. The automation of the procedure allows this requirement to be satisfied in the testing because a full test can be run in about 2 minutes.

Now that the sedimentation of the samples has been explored and it has been proven that time is a factor in recording spectra, agglutination index over time can now be explored. It would be expected that the agglutination index would shrink over time as the large particles sediment to the bottom of the cuvette leaving the smaller unagglutinated particles behind. This is a valid assumption, although when agglutination occurs the aggregation of the particles varies between blood types and the donor bloods. This means that each blood type can exhibit different optical densities depending on the donor and the way the blood was packaged. Samples of B- control and anti-B treated blood were prepared and the agglutination over time was recorded for all wavelengths. The linear regression agglutination indices are plotted below:

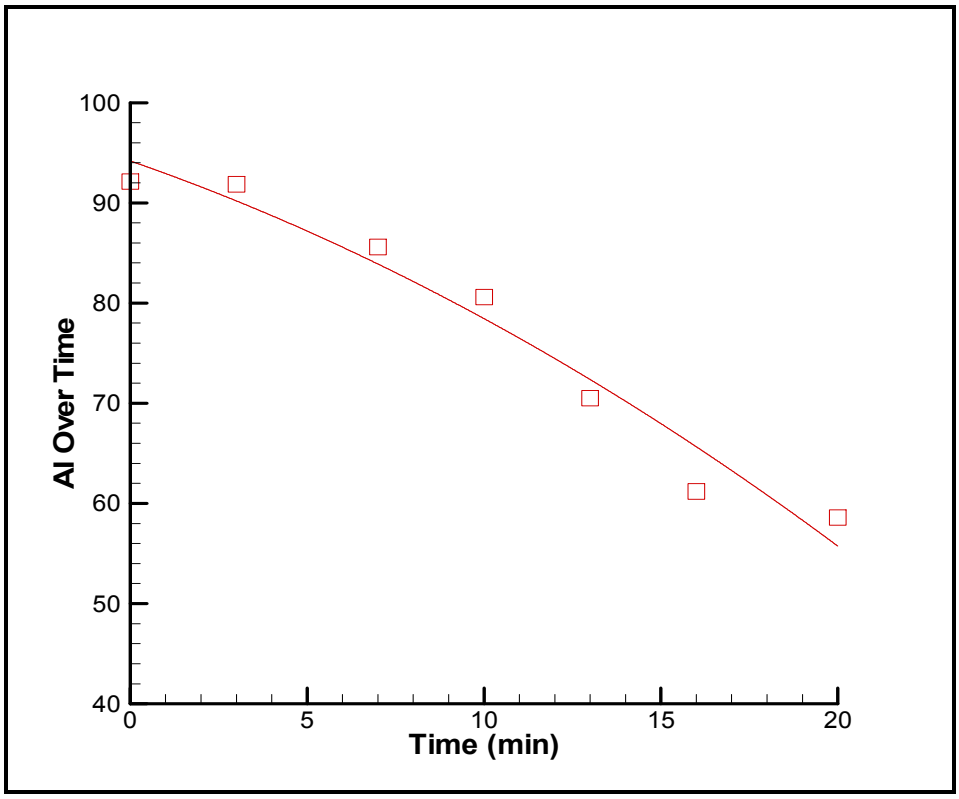


Figure 7.24 – Agglutination Index over Time

This plot was recorded using the same B- control and anti-B treated samples over a twenty minute period. The plot suggests that time is a factor when determining agglutination index. This suggests that as the large particles settle, the scattering properties change. This sample also exhibited a steadily higher transmission over time meaning that the sample was

demonstrating sedimentation. It can be concluded that it is best to test the samples as quickly as possible for maximum accuracy and efficiency.

7.8 Optimal Configuration

The results of the Mie scattering models, system evaluation, and test sample behavior suggest that the maximum collimation of the source beam and detector and forward scattering measurement are most desirable for good results and packaging of the sensor designed in the testing. Off axis measurements were proven to provide no apparent advantages in measuring the agglutination of samples in previous research and were never considered as an option [8]. The 20 μL volume or 0.062% concentration of the test sample added to 2 mL of saline is best for maintaining optical densities in the 0.1 - 1.0 AU range that is good for maximum accuracy of spectra measurements. Measuring the sample quickly and consistently preparing samples and mounting them provided the most desirable results.

The fact that the singlet lens focal point changes as a function of wavelength did not appear to hinder the measurement of spectral slopes similar to that of the spectrophotometer and moving the photodetector back from the cuvette helped keep absorption measurements from being diluted by stray light, scattered light at small angles from the incident direction, and light reflected off the walls of the cuvette.

Referring back to figure 6.9**,** the optimal dimensions are listed based on the experimental testing.

$$f_l = 12\text{mm}$$

$$d_l = 4\text{ mm}$$

$$d_{a1} = d_{a2} = 8\text{mm}$$

$$d_c = 21\text{ mm}$$

$$d_s = 56\text{ mm}$$

Measurements taken within the first 5 minutes are reliable for the agglutination index comparison. Cuvettes must be consistently oriented for each measurement. The parameters listed above were used on the prototype to arrive at the results listed in the following section.

7.9 Full ABO/Rh Results

Now that the system has been verified for reliability and tested for optimal optical parameters, it is time to compare the device against the spectrophotometer. Donor packed samples of A+, A-, B+, B-, O+, and O- were obtained from the Duke University Medical Center Transfusion Services Laboratory to facilitate the comparison. For each blood type control, anti-A, anti-B, and anti-D samples were prepared for testing and comparison following the procedure outlined in section 7.1. This process was performed on the Agilient 8453 Spectrophotometer and repeated with the LED array on the prototype device. The spectra were then plotted and agglutination indices were calculated for comparison.

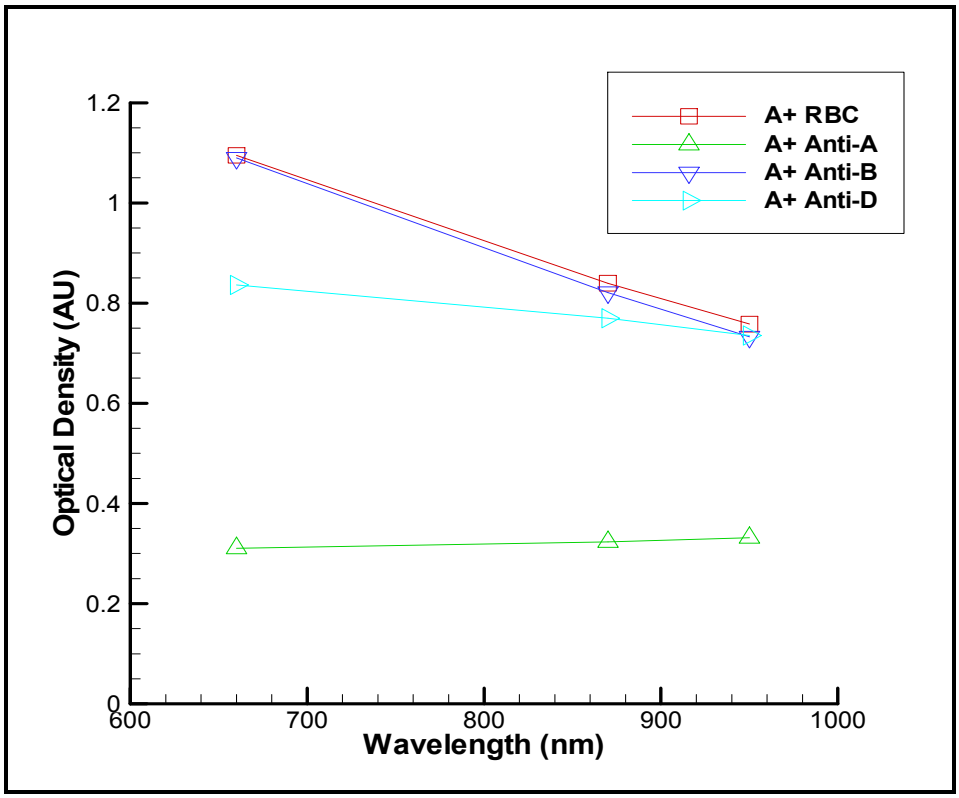


Figure 7.25 – Full Spectra of A+ Type Blood on Spectrophotometer

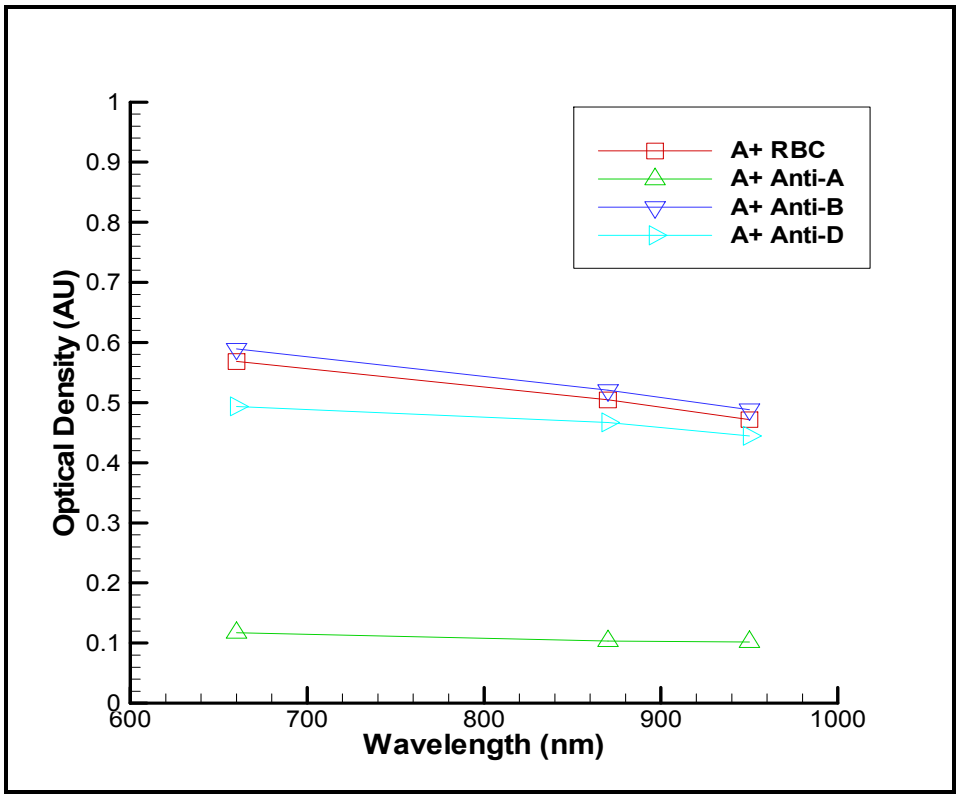


Figure 7.26 – Full Spectra of A+ Type Blood on LED Device

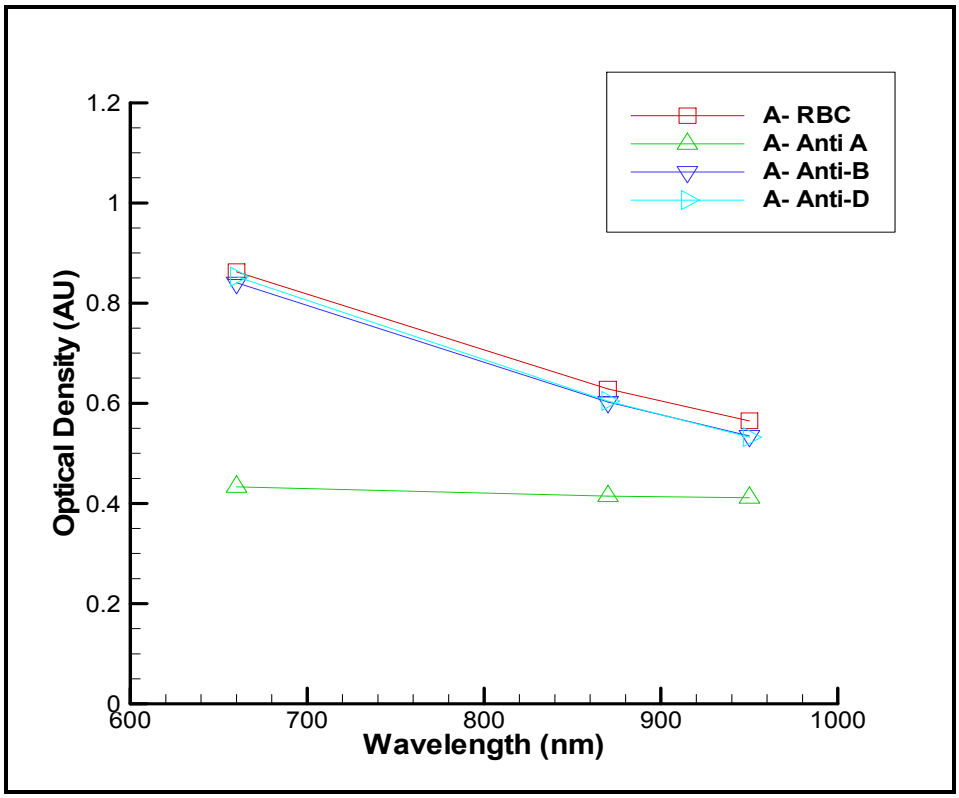


Figure 7.27 – Full Spectra of A- Type Blood on Spectrophotometer

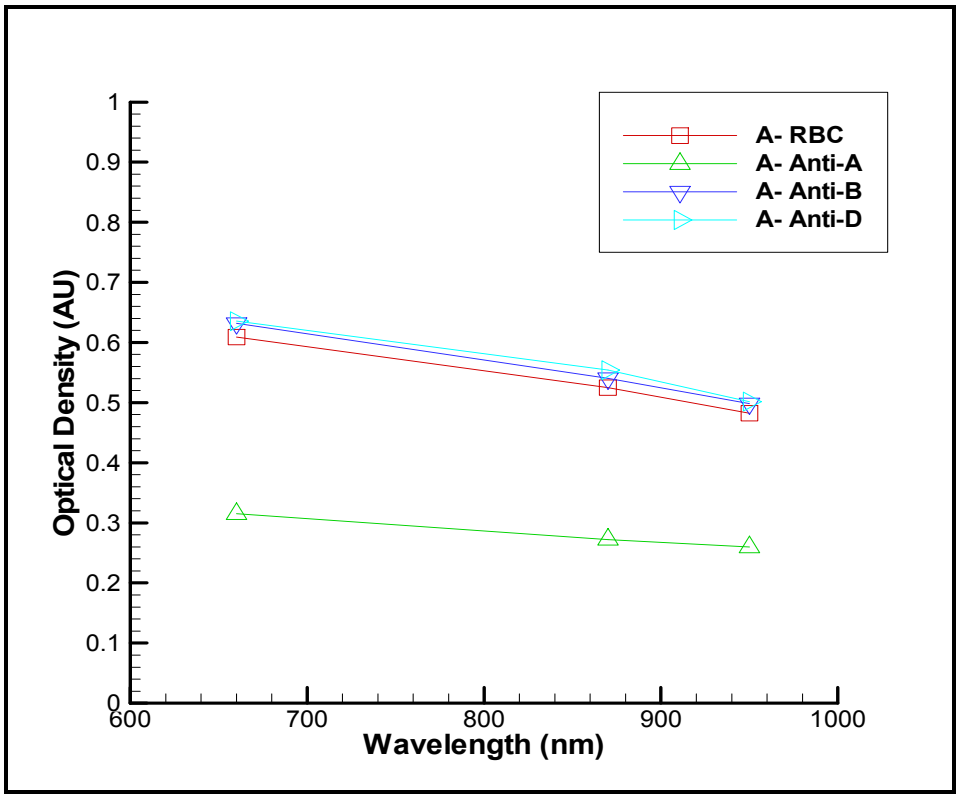


Figure 7.28 – Full Spectra of A- Type Blood on LED Device

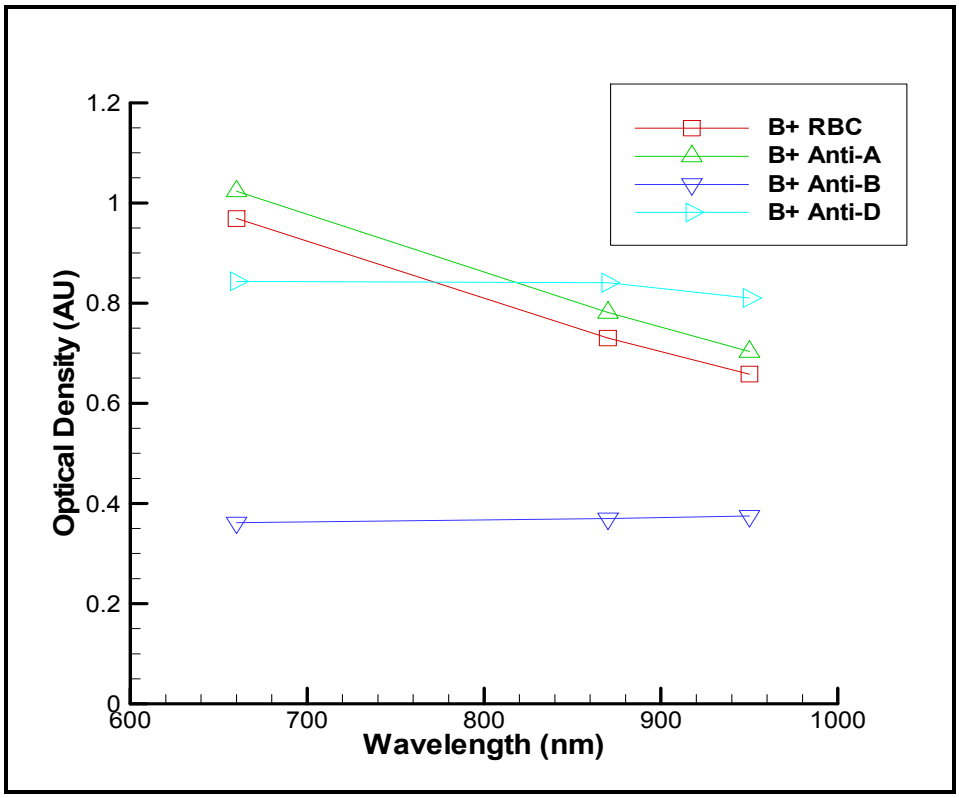


Figure 7.29 – Full Spectra of B+ Type Blood on Spectrophotometer

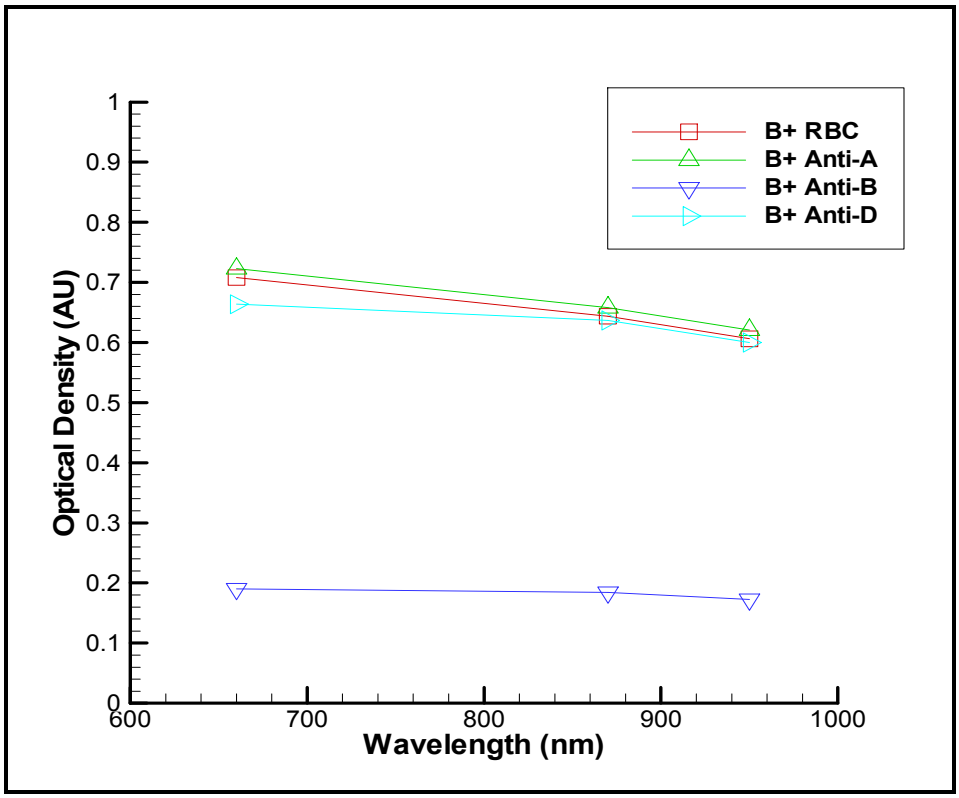


Figure 7.30 – Full Spectra of B+ Type Blood on LED Device

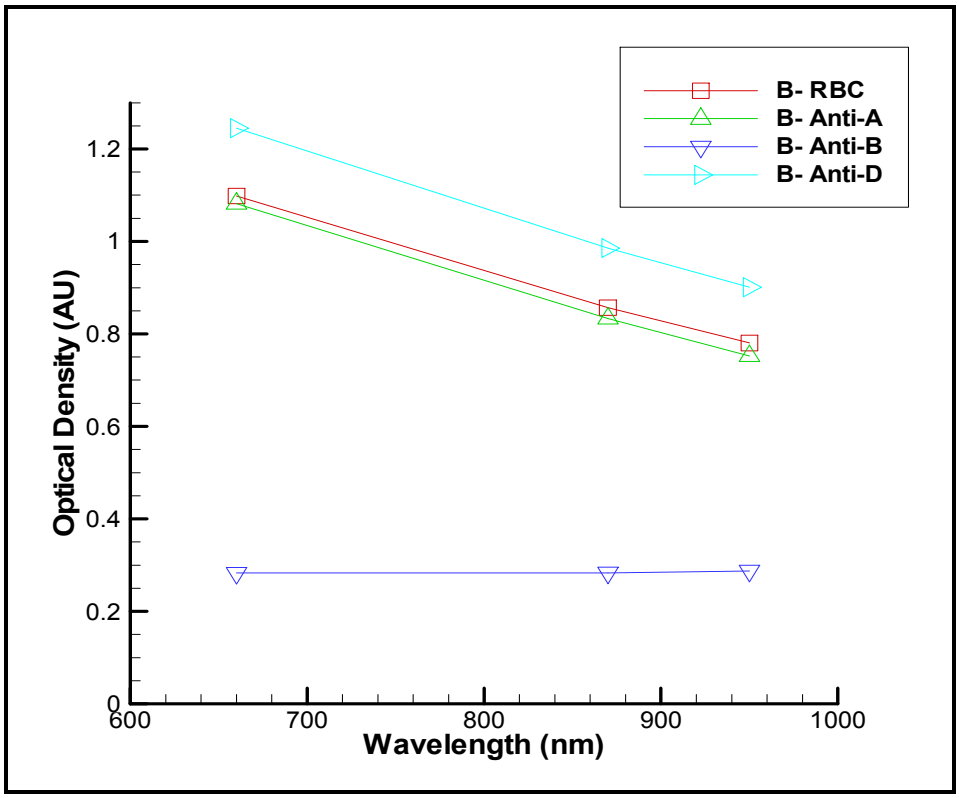


Figure 7.31 – Full Spectra of B- Type Blood on Spectrophotometer

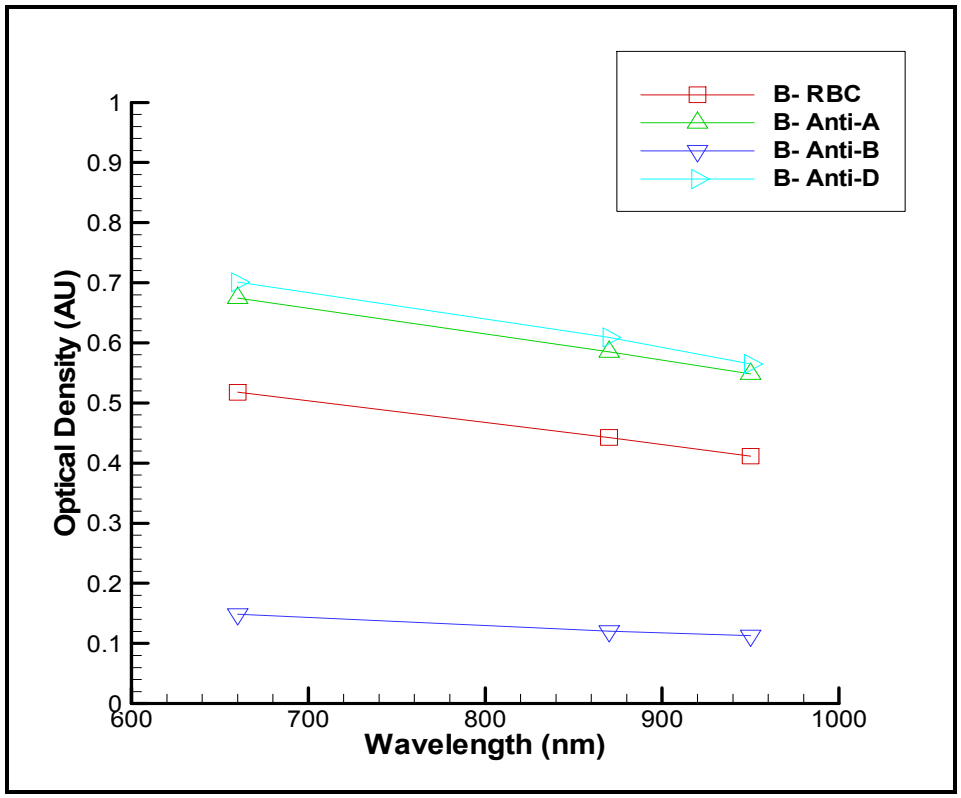


Figure 7.32 – Full Spectra of B- Type Blood on LED Device

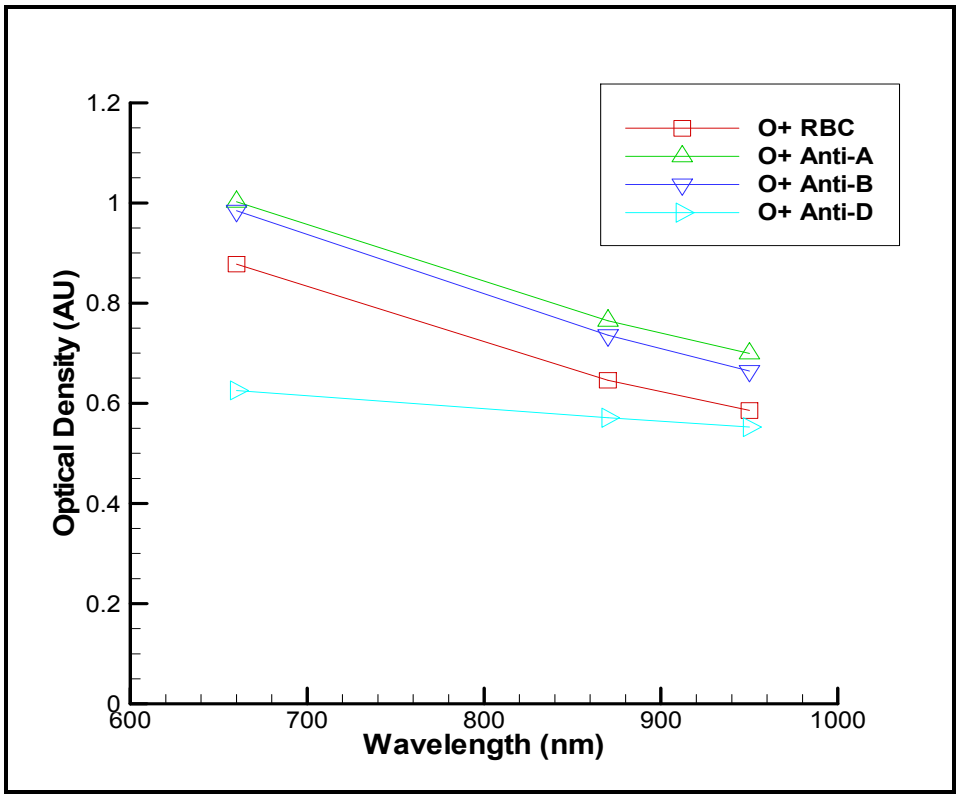


Figure 7.33 – Full Spectra of O+ Type Blood on Spectrophotometer

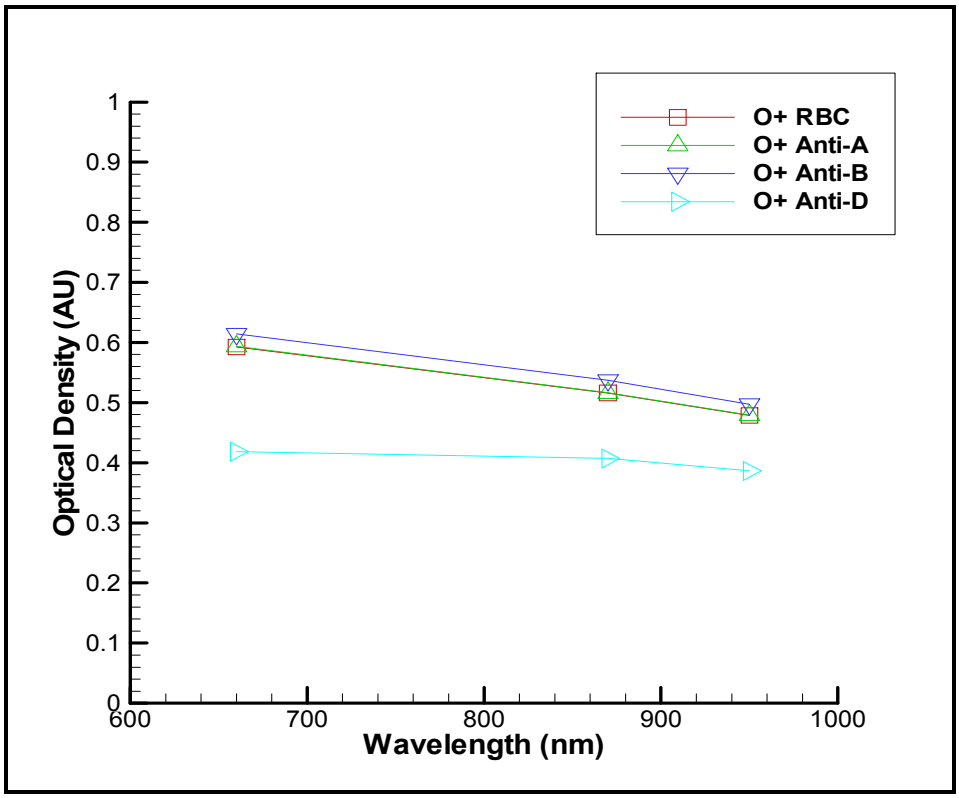


Figure 7.34 – Full Spectra of O+ Type Blood on LED Device

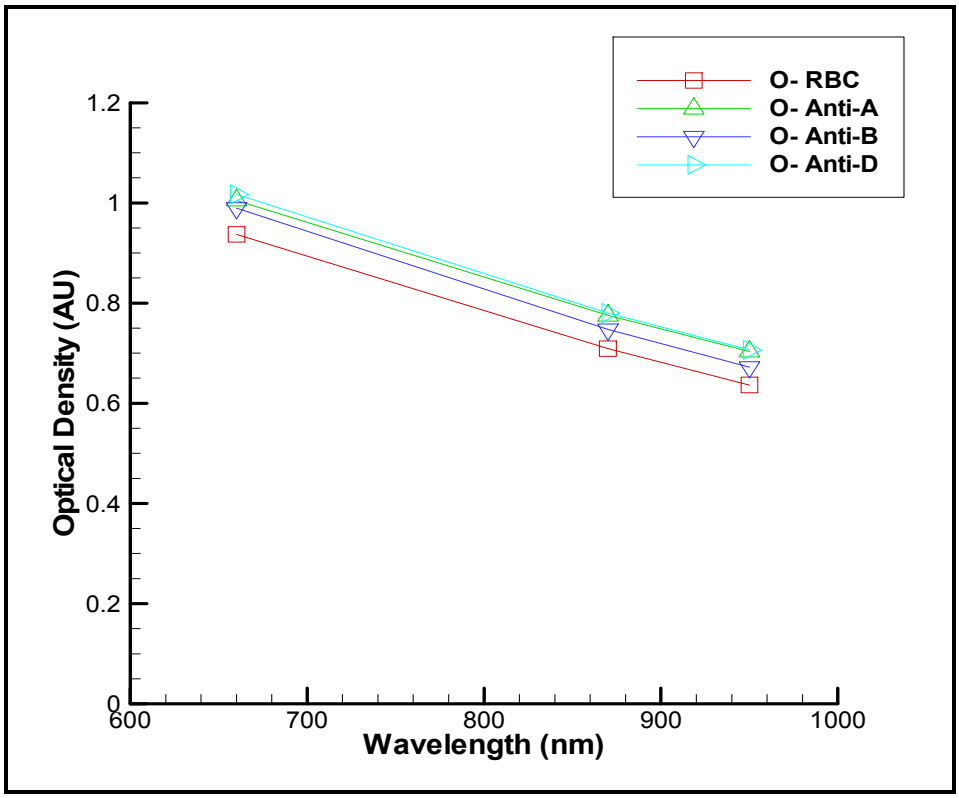


Figure 7.35 – Full Spectra of O- Type Blood on Spectrophotometer

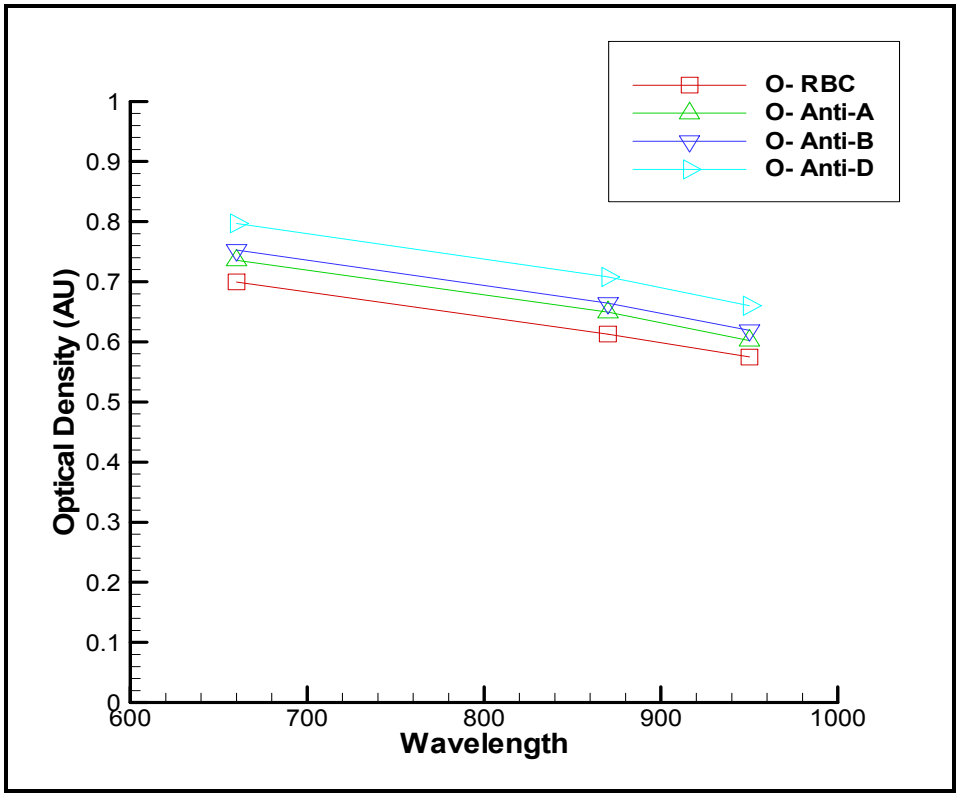


Figure 7.36 – Full Spectra of O- Type Blood on LED Device

The plots comparing the spectrophotometer and the experimental device seem to show fairly similar characteristics despite the fact that the experimental device records lower optical densities. For the purpose of this experimentation it is important to note that the experimental device does not need to record optical densities that are exactly the same as the spectrophotometer. The important factor is that the slopes of the samples between the two devices are similar. The agglutination index algorithm works based a comparison of the slopes of the treated samples and the control. The slopes recorded by the experimental device tend to be flatter than the spectrophotometer, but not by much. The experimental system was able to successfully produce the blood typing spectra for all of the blood types and the agglutination index values are very similar to the spectrophotometer.

The calculated agglutination indices for both systems are shown in table 6.1 below:

Table 7.1 – Comparison of the Agglutination Indeces between the Spectrophotometer and Experimental System

Blood Type	Method	Anti-A	Anti-B	Anti-D
A+	HP 8453	105.83	-5.84	71.11
	Experimental	82.67	-5.16	51.32
A-	HP 8453	92.50	-2.41	-7.16
	Experimental	54.53	-6.48	-3.66
B+	HP 8453	-2.65	104.00	91.87
	Experimental	0.08	84.63	42.12
B-	HP 8453	-3.55	101.09	-8.03
	Experimental	-18.96	65.45	-26.51
O+	HP 8453	-0.58	-8.81	75.36
	Experimental	0.98	-2.01	75.14
O-	HP 8453	-4.11	-5.80	-3.33
	Experimental	-4.83	-5.51	-7.82

The experimental system is able to show a distinct difference between reactive and non-reactive samples as shown in the table. These values are comparable to those of the spectrophotometer. According to Narayanan et al. an agglutination index above 17 is

considered reactive. All of these samples are well within that threshold for both test methods. There is a very distinct difference between reactive and non-reactive samples for the experimental system because the lowest agglutination index of a reactive sample is 42.12 while the highest agglutination index of a non-reactive sample is 0.98. The Rh or D antibody is known to exhibit variability in strength and does not produce consistent results like the ABO groups although the results in this test were good. There are also weak Rh variants such as D_u that are not detectable in this testing and could lead to confusion and delay at the bedside. The ABO groups are also the blood groups known to have the most immediate bedside effects where Rh generally does not. Based on these facts and the correspondence with Mr. Donald Bennett at the Duke Transfusion Services Lab (see Appendix E) it is not recommended that Rh be included in a future device.

7.10 Reactive and Non-Reactive Thresholds

The device has now been proven to replicate the relative slopes measured by the spectrophotometer and is able to measure optical densities that are within reason. Narayanan et al. specified that any sample with an agglutination index greater than 17 was considered reactive which correlates well with the results of this system. In order to prove that the system is consistently typing blood correctly, 5 segments of type A, B, and O blood were obtained from the Duke University Medical Center Transfusion Services Center. Three sets of control, anti-A, and anti-B treated samples were prepared from each segment using the procedure outlined in section 7.1. This created a total of 45 tests to create a normal distribution of results. There were a total of 30 agglutinated and 60 non-agglutinated samples for each measurement method. The full results are documented in appendix A.

The purpose of this test is to determine if only two LED/IRED comparison methods can effectively type the blood. For this test, three methods will be used to calculate the relative slopes of the samples: between the 660 and 870 nm sources, between the 660 and 950 nm sources, and a linear regression of all three LEDs. The linear regression slope of the three sources is computed using the following equation:

$$slope = \frac{n\sum XY - \sum X \sum Y}{n\sum X^2 - \left(\sum X\right)^2}$$

The results of agglutinated and non-agglutinated samples will be statistically analyzed in the following tables:

Table 7.2 – Agglutination Index Distribution for Agglutinated Samples

Parameter	660-870 nm	660-950 nm	Lin. Regression
Mean	69.685	65.567	66.548
Standard Deviation	16.474	13.776	14.017
Standard Error	3.007	2.515	2.559
Variance	271.404	189.7993	196.4996
Kurtosis	-0.474	-1.203	-1.091
Skewness	-0.389	-0.216	-0.276
Median	69.385	65.382	64.8418
Minimum	29.559	39.360	38.803
Maximum	91.514	84.048	84.632
Range	61.953	44.688	45.829
Count	30	30	30

Table 7.3 – Agglutination Index Distribution for Non-Agglutinated Samples

Parameter	660-870 nm	660-950 nm	Lin. Regression
Mean	-4.166	-5.890	-5.495
Standard Deviation	6.817	5.089	5.213
Standard Error	0.880	0.657	0.673
Variance	46.474	25.906	27.182
Kurtosis	0.265	0.080	0.379
Skewness	-0.931	-0.422	-0.706
Median	-2.669	-5.551	-5.030
Minimum	-23.373	-18.820	-19.697
Maximum	6.141	4.331	4.044
Range	29.515	23.152	23.743
Count	60	60	60

The statistical data from the non-agglutinated samples is the most important data to analyze to determine a cut-off value for agglutinated and non-agglutinated samples. It is important to realize the maximum values and the standard deviation for each data set because that exposes the likelihood of recording false positives.

In order to automate this system so that blood type can be displayed, the cut-off value must be determined to distinguish between agglutinated and non-agglutinated systems. The approach taken in this paper is to model the non-agglutinated samples as a normal distribution and set confidence intervals to estimate the probability that a non-agglutinated sample will fall within a certain range.

The normal distribution approach seems valid based on the data provided in the preceding tables with the formula below [37]:

$$P(X \le x) = P\left(\frac{X-\mu}{\sigma} \le \frac{x-\mu}{\sigma}\right) = P(Z \le z)$$

Where X is a normally distributed random variable, μ is the mean, and σ is the standard deviation. Z is the standard normal random variable and $z = (x - \mu)/\sigma$.

The z values were obtained using a standard normal distribution program where the mean, standard deviation, and confidence interval were inputs. These values were entered into the program and the values in table 7.4 were the result.

Table 7.4 – Agglutination Index Thresholds for Slope Calculation Methods

Confidence Interval	660 nm – 870 nm	660 nm – 950 nm	Linear Regression
99.9 %	16.900	9.839	10.620
99 %	11.693	5.951	6.634
98 %	9.835	4.5633	5.213
95%	7.047	2.4821	3.081

This table holds well with the full blood typing test in section 7.8, but it is important to note that the 870 nm method had a higher standard deviation than the other two methods used. The thresholds for the 870 nm method were right on target with the agglutination index of 17 that was proposed in Narayanan et al. The 950 nm method sets even tighter thresholds and may be more susceptible to a false positive if an outlier occurs. The minimum

value in the agglutinated samples table is 29.559 and the maximum value in the non-agglutinated samples table is 6.141. It is for this reason that the confidence intervals set for the 870 nm method may be the best set of confidence intervals to use because they are less susceptible to the false positive reading. Since the difference between the maximum non-agglutinated sample and the minimum agglutinated sample is 23.418, this would be a logical approach. Also, since the minimum agglutinated sample is has an agglutination index 12.659 higher than the 99.9% threshold of 16.90 for non-agglutinated samples, there is a significant differential and reduces the likelihood of false negatives with agglutinated samples.

7.11 Economic Analysis

Since reducing the cost of bedside or laboratory blood typing was a factor that initiated this project an economic analysis of the items purchased will be displayed as well as an approximation of the cost of implementing this design. Only the crucial components will be included. The mounts and stands will be are included although a custom design would not include them. Since it would be difficult to approximate what the cost of a manufactured setup, an approximation will be made. Table 7.5 lists the integral components and their costs:

Table 7.5 – Approximated Cost of Packaged Unit

Vendor	Component	Cost
Thor Labs	BK7 Plano-Convex Lens, AR Coating 650-1050nm	$29.00
Thor Labs	2 Variable Apertures	$78.00
Thor Labs	Purchased Mounts	$73.00
Industrial Fiber Optics	3 Fiber Optic LED/IRED	$9.00
Hamamatsu	1 Photodiode	$20.00
Digikey	Amplifier Parts (3 amplifiers)	$10.00
National Instruments	Data Acquisition	$150.00
Total		**$369.00**

The cost of $369.00 is much less than the cost of a $2500.00 spectrophotometer and the results are still good with this setup. The cost would be significantly reduced when a housing is designed that can integrate the apertures and mount the components. A microcontroller can be implemented to take over data acquisition and processing. A microcontroller was not used in the testing, but would need to be implemented to create a packaged unit. The demands would not be that great on a microcontroller for the current setup although it would need to do more as the system is automated further. It would need three analog to digital converters for each amplifier out and three digital outs to switch the shutters and amplifier inputs for each source. Shutters would be needed to block out two of the sources while the other is being measured. The lens and fiber optic cable could also be integrated to further optimize the system. The packaging will be discussed further in section 8.2**.** The housing cost is hard to predict because once the housing is designed and manufactured in bulk, the cost will go down.

Overall, the components used in this setup performed well at a cost much less than that of a spectrophotometer. As the unit is optimized and produced in bulk, the cost should be reduced and a profit could be made from this device.

Chapter 8

Discussion and Future Recommendations

8.1 Discussion of Testing

In order to create a miniaturized blood typing sensor the first step was to look at the previous design and attempt to shrink everything on it. Initially, this was the approach taken.

The previous design employed a converging/diverging beam that required the detector to be moved back in order to collimate the source and detector. This testing used fully collimated light to collimate the detector and source just as the spectrophotometer does. Optical fiber was chosen to guide the light to the lens because it allowed the light termination to remain the same as sources were changed. The same photodetector was used as the previous testing, but in hindsight, a detector with a smaller sensing area possibly would have been optimal. Alignment could have contributed to the tests not being accurate as possible because the alignment of all the components was fairly crude. The visible light was used to align the components which were mounted on optical posts or fabricated parts. This produced good results, but a precision machined housing would produce a better aligned setup.

Prompt testing of the sample was also critical since the sample changes so rapidly. The automation introduced by the LabView program allowed for the most rapid testing possible.

The purpose of this testing was to miniaturize the setup by exploring new ways to test the blood. The following section will discuss implementation and recommendations for the future.

8.2 Future Recommendations

When considering the packaging of this device there are two options to consider, a whole blood system and an antisera system. The whole blood system would be a more simplified system because the fluid handling would be much easier, yet the antisera system would be much more accurate and less confusing. A solid model of a proposed design with manual fluid handling will also be presented.

8.2.1 Whole Blood System

During testing the feasibility of a whole blood system became a topic of interest because it would simplify the design in the next phase of the project, the fluid handling. Before any tests were performed, Mr. Donald Bennett (see Appendix E) was contacted to explore the possibility of this method being effective. His response was not very optimistic for many reasons. Mixing whole blood to whole blood adds a dilutional factor that is not visible in the spectral measurements. A few tests were performed using each blood as a control and no difference could be detected. Assuming that the device did see agglutination, there is not a way to know which cells are reacting. When giving group compatible cells to a patient, such as an O to A, there is no way to know which cells are reacting when combining whole blood. There are also atypical antibodies from other blood groups that can give a false positive. In a blood lab, there are antibody screens that identify these blood groups and account for them. Based on the equipment and time needed to identify agglutination with this method, it does not seem to be feasible with this device. The antisera method seems to be the only method that can produce strong enough reactions for spectra measurements.

8.2.2 The Antisera Method

Based on the recommendations of medical professionals in appendix E and some simple tests on the device, it seems that antisera treatment of samples is the best way to implement this research. This would complicate the fluid handling and require that two separate tests for the donor and patient be performed, but at this point it seems to be the most feasible. The results presented in this paper show that a miniaturized device can perform effective measurements that are similar to that of the spectrophotometer.

8.2.3 A Packaged Device with Manual Fluid Handling

The scope of the project asked that a miniaturized prototype be built in the lab and tested. This was accomplished on the optical breadboard and tested. Figure 8.1 shows an exterior view of a proposed device that could be built by implementing the parameters established by the testing.

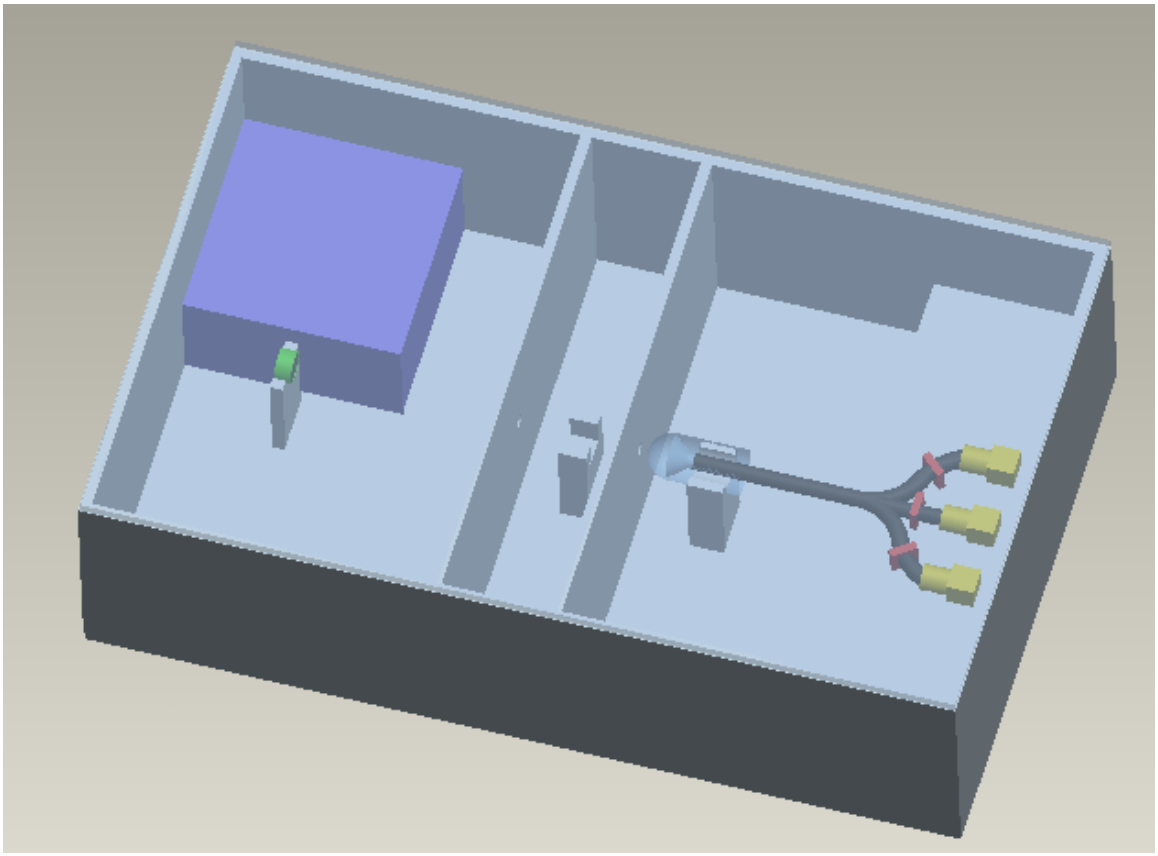


Figure 8.1 – Solid Model of Proposed Sensor with Manual Fluid Handling

This figure applies the design parameters set by the experimental device, yet eliminates much of the cost because features such as mounts and apertures are built into the housing. The light sources are coupled into a single fiber with shutters that will block the radiation from the other two sources while one is being measured. The lens can be integrated into the tip of the fiber as shown in the schematic in figure 8.2 [38].

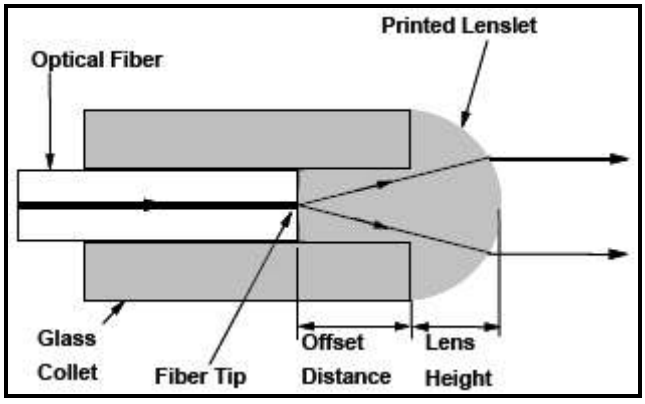


Figure 8.2 – Collimating Lens Integrated Into Fiber

This design will help eliminate some of the costs that were faced with the experimental setup and will also eliminate parts such as a lens mount and fiber mount. This will still require a post and alignment on the optical axis, but it will help the setup tremendously. The apertures are integrated into the housing using the 3 mm diameter specified by the testing. The photo-diode will be mounted on the optical axis and placed as specified. The purple box shows a proposed location for a microcontroller, the amplifiers, switching transistors, and other electronics for a possible LED display on the outside to report status although it may be possible to package the electronics underneath the raised LEDs.

The nature of the automation can include many possibilities where a fully automated setup could be implemented with transfusion apparatus at bedside or a semi-automated sample reader with pre-filled cuvette cartridges that could be inserts for brief incubation and transmission measurement.

This setup proves that the spectrophotometer measurements can be mimicked with fairly inexpensive equipment and produce good results. This setup is definitely a good step in the direction of inexpensive measurement.

Chapter 9

Conclusion

In conclusion, this setup has shown promising results in a fairly small package reducing the size of the optics by more than a half and suggesting some hardware improvements that could reduce the size even more such as integrating the lens and fiber. The LED and photodiode pairs were successful in detecting agglutination in the 660 – 1000 nm range as supported by the spectrophotometer and the Lorentz–Mie scattering theory. The alignment of the beam and placement of the photodetector in the forward scattering direction proved to be the most important factors when determining blood type.

The spectrophotometric method developed by Narayanan et al. is not a thoroughly proven method although their published results are good. With over 475 samples typed with zero errors, including samples with weak antibodies such as the A_2 and weak D types, these results are encouraging [7]. Although the test results of this experimental apparatus are not as thorough, this device has proven that it truly capable of distinguishing between reactive and non-reactive samples.

An important fact to note is that the experimental device is not as sensitive as the spectrophotometer when recording transmission measurements, but is able to record spectral slopes that are similar to that of the spectrophotometer including the slope flattening phenomena that occurs in agglutinated samples. The spectral slopes are the important factor when calculating the agglutination index and are therefore the parameter that should be focused on.

With the replacement of the spectrophotometer by a miniaturized, LED array device based on the research of this project, it may be possible in the future to create a device that can effectively improve transfusion safety or provide an alternative to other blood typing methods that is cost effective and accurate.

References

[1] Dujardin P.P., Salmi L.R., Ingrand P., "Errors in interpreting the pretransfusion bedside compatibility test", Vox Sanguinis, 78, 37-43 (2000).

[2] Migeot V, Ingrand I, Salmi RL, Ingrand P, "Reliability of bedside ABO testing before transfusion", Transfusion, 42, 1348-1355 (2002).

[3] Linden JV, Wagner K, Voytovich AE, Sheehan J. "Transfusion errors in New York State: an analysis of 10 years' experience", Transfusion, 40, 1207-1213 (2000).

[4] Voak D, "The status of new methods for the detection of red cell agglutination", Transfusion, 39, 1037-1040 (1999).

[5] Sturgeon P, "Automation: its introduction to the field of blood group serology", Immunohematology 17, 4 (2001)

[6] Narayanan S., Orton S., Leparc G.F., Garcia-Rubio L.H., Potter R.L., "Ultraviolet and visible light spectrophotometric approach to blood typing: objective analysis by agglutination index", Transfusion 39, 1051-1059 (1999).

[7] Narayanan S., Galloway L., Nonoyama A., Leparc G., Garcia-Rubio L.H., Potter R.L., "UV-visible spectrophotometric approach to blood typing II: phenotyping of subtype A2 and weak D and whole blood analysis", Transfusion 42, 619-626 (2002).

[8] Anthony, S., "A Simplified Visible/Near-Infrared Spectrophotometric Approach to Blood Typing for Automated Transfusion Safety", NCSU, (2005)

[9] Tsinopoulos S.V., Sellountos E.J., Polyzos D, "Light scattering by aggregated red blood cells," Applied Optics, 41, 1408-1417 (2002).

[10] Prakash M., Arara C.K., *Physiology of Blood*, (Anmol, New Delhi, 1998).

[11] Quinley E.D*., Immunohematology: Principles and Practice,* Second Edition, (Lippincott-Raven, Philadelphia, 1998).

[12] Daniels G., *Human Blood Groups*, Second Edition, (Blackwell Science, Oxford, 2002).

[13] Reid M.E., Lomas-Francis C., *The Blood Group Antigen Facts Book*, Second Edition, (Elsevier, New York, 2004)

[14] Hughes-Jones N.C., "Nature of the reaction between antigen and antibody", Brit. Med. Bull. 19, 3, 171-177 (1963)

[15] *Blood Policy and Technology* (Washington, DC: U.S. Congress of Technology Assessment, OTA-H-260, January 1985)

[16] *Micronics ABO Card Product Page.* 28 March, 2006. Micronics Inc. <http:www.micronics.net/products/blood.php>

[17] *Craig Medical EldonCard Product Page*. 28 March , 2006. Craig Medical Distribution Inc. <http://www.craigmedical.com/Blood_typing_kit.htm>.

[18] Tycho D.H., Metz M.H., Epstein E.A., Grinbaum A., "Flow-cytometric light scattering measurement of red blood cell volume and hemoglobin concentration", Applied Optics, 24, 1355-1365 (1985).

[19] Brown M., Wittwer C., "Flow Cytometry: Principles and Clinical Applications in Hematology", Clinical Chemistry, 48, 1221-1229 (2000)

[20] Meyer-Arendt J.R., *Introduction to Classical and Modern Optics*, Fourth Edition, (Prentice-Hall, New Jersey, 1995).

[21] Wyatt C.L., *Radiometric System Design*, (Macmillan, New York, 1987).

[22] *Agilent 8453 Spectrophotometer Service Manual*, Edition 02/00 (Agilent Technologies, Germany, 2000).

[23] Denney, C., Sinclair, R., *Visible and Ultraviolet Spectroscopy*, (John Wiley and Sons, London, 1987)

[24] Burgess C., Frost T., *Standards and Best Practice In Absorption Spectrometry*, (Blackwell Science, Oxford, 1999).

[25] Schmidt, W., *Optical Spectroscopy in Chemistry and Life Sciences*, (Wiley-VCH, Germany, 2005)

[26] Tilley R., Wiley J., *Colour and the Optical Properties of Materials*, Chichester, New York, 2000

[27] Mischchenko M.I., Travis L.D., Lacis A.A., *Scattering, Absorption, and Emission of Light by Small Particles,*(Cambridge, Cambridge, 2002).

[28] Shvalov A.N., Soini J.T., Chernsyshev A.V., Tarasov P.A., Soini E., Maltsev V.P., "Light-scattering properties of individual erythrocytes," Applied Optics 38, 230-235 (1999).

[29] Tsinopoulos S.V., Polyzos D, "Scattering of He-Ne laser light by an average sized red blood cell", Applied Optics, 38, 5499-5510 (1999).

[30] Uiga E., *Optoelectronics*, (Prentice-Hall, New Jersey, 1995).

[31] *Electromagnetic Wave.* 30 March 2006. http://www.monos.leidenuniv.nl/smo/index.html?basics/light_anim.htm

[32] Hecht, J., *Understanding Fiber Optics,* (Prentice-Hall, New Jersey, 2002)

[33] Safford, Jr., E., *The Fiber Optics and Laser Handbook,*(TAB Books, Blue Ridge Summit, 1984)

[34] Murata, H., *Handbook of Optical Fibers and Cables*, (Marcel Dekker, Inc., New York, 1988)

[35] Hecht, E., *Optics*, (Addison-Wesley, San Francisco, 2002)

[36] Greame J., *Photodiode Amplifiers: Op Amp Solutions*, (McGraw-Hill, New York, 1996).

[37] Lapin, L., *Modern Engineering Statistics,* (Duxbury Press, Belmont, 1997)

[38] Cox, W., Chen, T., Hayes, D., Grove, M., "Low Cost Fiber Collimation For MOEMS Switches By Ink Jet Printing," Proceedings, SPIE Conference on MOEMS and Minaturize Systems, 2001

Appendix A

Full Agglutination Results

Sample: A1-1

Transmission

Wave-length	RBC	Anti-A	Anti-B
660	19.67%	48.05%	18.20%
870	23.58%	51.03%	22.35%
950	25.94%	54.40%	24.72%

Optical Density

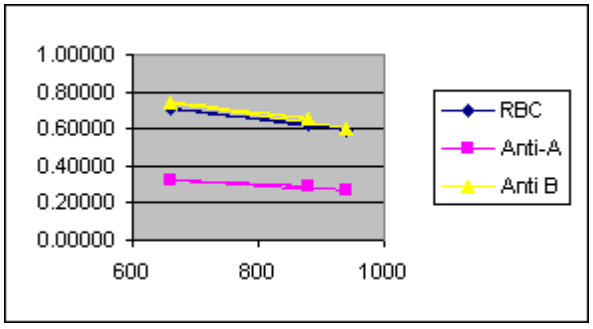
Wave-length	RBC	Anti-A	Anti-B
660	0.70615	0.31832	0.73996
870	0.62745	0.29220	0.65075
950	0.58611	0.26437	0.60703

Slopes

Sample	870	950	LR
RBC	-0.00036	-0.00043	-0.0004096
Anti-A	-0.00012	-0.00019	-0.0001727
Anti-B	-0.00041	-0.00047	-0.0004561

Agglutination Index

Method	Anti-A	Anti-B
660-870	66.81906	-13.3533
660-950	55.06122	-10.7373
Lin Reg	57.83353	-11.3541



Sample: A1-2

Transmission

Wave-length	RBC	Anti-A	Anti-B
660	20.41%	54.35%	19.37%
870	24.46%	58.75%	23.52%
950	26.47%	61.94%	25.69%

Optical Density

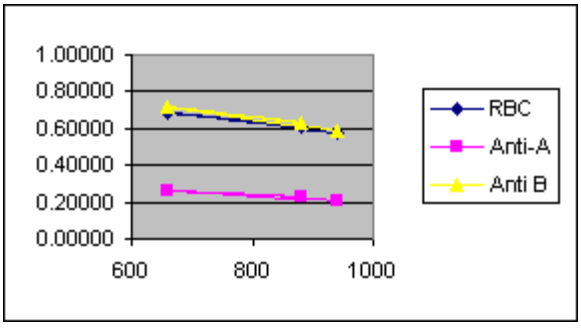
Wave-length	RBC	Anti-A	Anti-B
660	0.69022	0.26483	0.71294
870	0.61162	0.23097	0.62855
950	0.57718	0.20804	0.59022

Slopes

Sample	870	950	LR
RBC	-0.00036	-0.0004	-0.00039
Anti-A	-0.00015	-0.0002	-0.00019
Anti-B	-0.00038	-0.00044	-0.00042

Agglutination Index

Method	Anti-A	Anti-B
660-870	56.91847	-7.37455
660-950	49.76198	-8.56621
Lin Reg	51.52631	-8.27242



Sample: A1-3

Transmission

Wave-length	RBC	Anti-A	Anti-B
660	20.61%	63.61%	18.07%
870	25.19%	70.15%	22.08%
950	27.25%	72.78%	24.09%

Optical Density

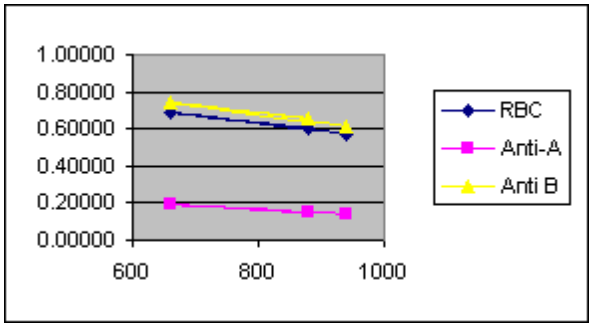
Wave-length	RBC	Anti-A	Anti-B
660	0.68590	0.19649	0.74316
870	0.59874	0.15396	0.65590
950	0.56469	0.13800	0.61814

Slopes

Sample	870	950	LR
RBC	-0.0004	-0.00043	-0.000423
Anti-A	-0.00019	-0.00021	-0.0002047
Anti-B	-0.0004	-0.00045	-0.000433

Agglutination Index

Method	Anti-A	Anti-B
660-870	51.19549	-0.11072
660-950	51.74231	-3.14148
Lin Reg	51.60406	-2.37519



Sample: A2-1

Transmission

Wave-length	RBC	Anti-A	Anti-B
660	17.39%	48.62%	15.40%
870	20.84%	50.56%	18.61%
950	23.15%	55.25%	21.05%

Optical Density

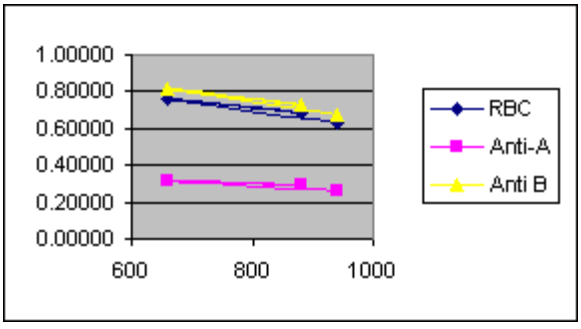
Wave-length	RBC	Anti-A	Anti-B
660	0.75973	0.31320	0.81238
870	0.68112	0.29618	0.73033
950	0.63539	0.25768	0.67680

Slopes

Sample	870	950	LR
RBC	-0.00036	-0.00044	-0.00042
Anti-A	-7.7E-05	-0.0002	-0.00017
Anti-B	-0.00037	-0.00048	-0.00045

Agglutination Index

Method	Anti-A	Anti-B
660-870	78.34777	-4.38076
660-950	55.35061	-9.04131
Lin Reg	60.62362	-7.97269



Sample: A2-2

Transmission

Wave-length	RBC	Anti-A	Anti-B
660	15.35%	44.47%	15.01%
870	18.82%	48.67%	18.81%
950	20.83%	52.35%	21.17%

Optical Density

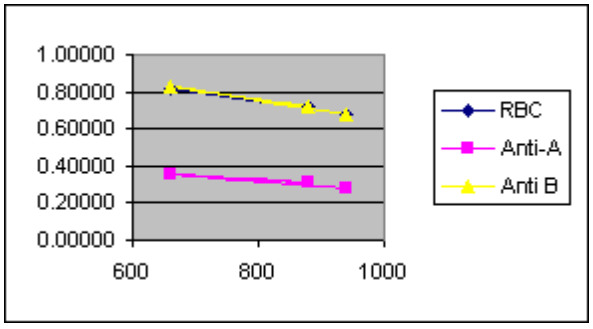
Wave-length	RBC	Anti-A	Anti-B
660	0.81381	0.35189	0.82356
870	0.72538	0.31271	0.72558
950	0.68134	0.28106	0.67432

Slopes

Sample	870	950	LR
RBC	-0.0004	-0.00047	-0.0004539
Anti-A	-0.00018	-0.00025	-0.0002327
Anti-B	-0.00045	-0.00053	-0.0005093

Agglutination Index

Method	Anti-A	Anti-B
660-870	55.69673	-10.787
660-950	46.53085	-12.6648
Lin Reg	48.72205	-12.2159



Sample: A2-3

Transmission

Wave-length	RBC	Anti-A	Anti-B
660	17.54%	47.19%	14.60%
870	21.85%	51.65%	17.94%
950	23.83%	55.26%	20.06%

Optical Density

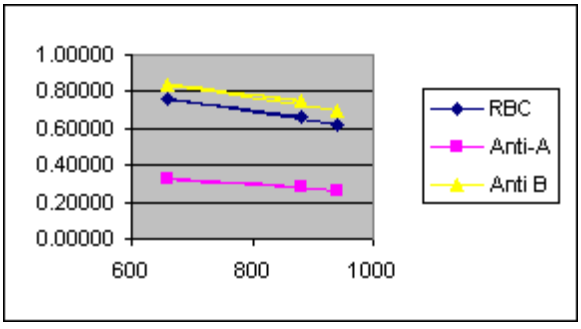
Wave-length	RBC	Anti-A	Anti-B
660	0.75587	0.32620	0.83576
870	0.66049	0.28691	0.74623
950	0.62281	0.25756	0.69770

Slopes

Sample	870	950	LR
RBC	-0.00043	-0.00048	-0.00046
Anti-A	-0.00018	-0.00025	-0.00023
Anti-B	-0.00041	-0.00049	-0.00047

Agglutination Index

Method	Anti-A	Anti-B
660-870	58.81033	6.141632
660-950	48.41953	-3.75511
Lin Reg	51.0405	-1.25876



Sample: A3-1

Transmission

Wave-length	RBC	Anti-A	Anti-B
660	35.25%	60.64%	34.37%
870	40.27%	61.33%	39.67%
950	42.41%	63.10%	42.16%

Optical Density

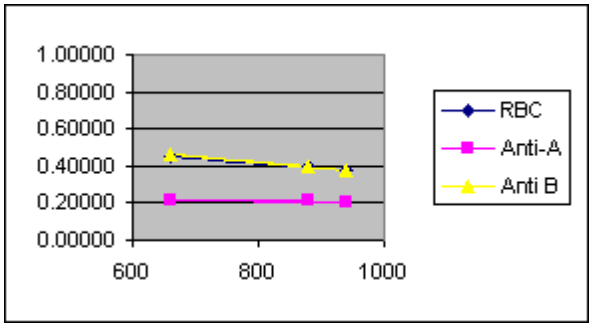
Wave-length	RBC	Anti-A	Anti-B
660	0.45278	0.21723	0.46378
870	0.39499	0.21232	0.40152
950	0.37256	0.19994	0.37507

Slopes

Sample	870	950	LR
RBC	-0.00026	-0.00029	-0.0002801
Anti-A	-2.2E-05	-6.2E-05	-5.109E-05
Anti-B	-0.00028	-0.00032	-0.0003077

Agglutination Index

Method	Anti-A	Anti-B
660-870	91.51387	-7.74315
660-950	78.45002	-10.5925
Lin Reg	81.75772	-9.87108



Sample: A3-2

Transmission

Wave-length	RBC	Anti-A	Anti-B
660	34.28%	63.87%	34.44%
870	38.65%	64.72%	38.69%
950	41.08%	66.27%	40.95%

Optical Density

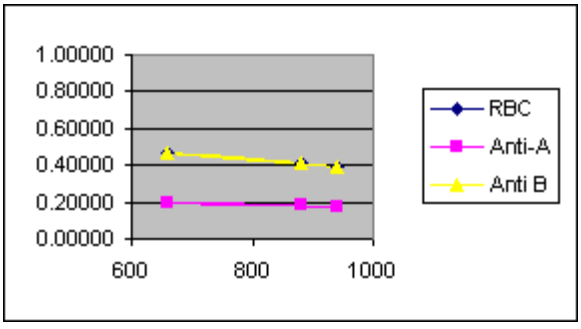
Wave-length	RBC	Anti-A	Anti-B
660	0.46501	0.19470	0.46296
870	0.41286	0.18897	0.41244
950	0.38636	0.17871	0.38772

Slopes

Sample	870	950	LR
RBC	-0.00024	-0.00028	-0.00027
Anti-A	-2.6E-05	-5.7E-05	-4.9E-05
Anti-B	-0.00023	-0.00027	-0.00026

Agglutination Index

Method	Anti-A	Anti-B
660-870	89.00914	3.127932
660-950	79.67663	4.331028
Lin Reg	81.89617	4.044897



Sample: A3-3

Transmission

Wave-length	RBC	Anti-A	Anti-B
660	34.76%	64.61%	34.14%
870	39.66%	66.23%	38.88%
950	41.72%	67.34%	41.05%

Optical Density

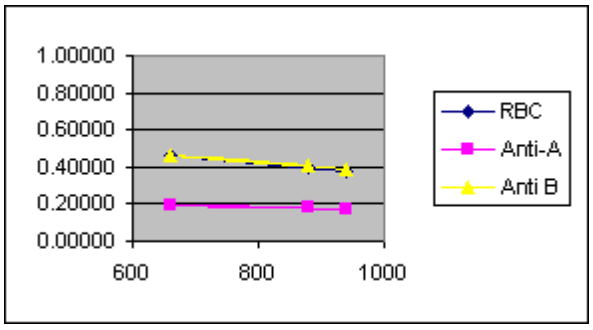
Wave-length	RBC	Anti-A	Anti-B
660	0.45897	0.18973	0.46678
870	0.40169	0.17896	0.41023
950	0.37962	0.17172	0.38669

Slopes

Sample	870	950	LR
RBC	-0.00026	-0.00028	-0.0002772
Anti-A	-4.9E-05	-6.4E-05	-6.017E-05
Anti-B	-0.00026	-0.00029	-0.0002782

Agglutination Index

Method	Anti-A	Anti-B
660-870	81.19927	1.273211
660-950	77.30433	-0.93252
Lin Reg	78.29196	-0.37322



Sample: A4-1

Transmission

Wave-length	RBC	Anti-A	Anti-B
660	27.75%	54.62%	26.78%
870	32.74%	56.67%	31.53%
950	35.07%	57.94%	33.82%

Optical Density

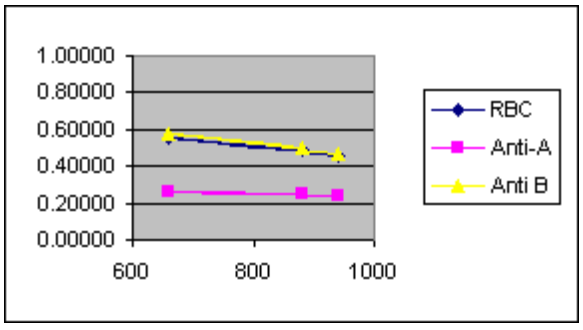
Wave-length	RBC	Anti-A	Anti-B
660	0.55678	0.26265	0.57213
870	0.48494	0.24665	0.50128
950	0.45509	0.23700	0.47088

Slopes

Sample	870	950	LR
RBC	-0.00033	-0.00036	-0.00035
Anti-A	-7.3E-05	-9.2E-05	-8.7E-05
Anti-B	-0.00032	-0.00036	-0.00035

Agglutination Index

Method	Anti-A	Anti-B
660-870	77.7257	1.378586
660-950	74.77326	0.428316
Lin Reg	75.50995	0.665426



Sample: A4-2

Transmission

Wave-length	RBC	Anti-A	Anti-B
660	27.48%	56.58%	26.89%
870	32.16%	57.55%	31.24%
950	34.52%	59.75%	33.98%

Optical Density

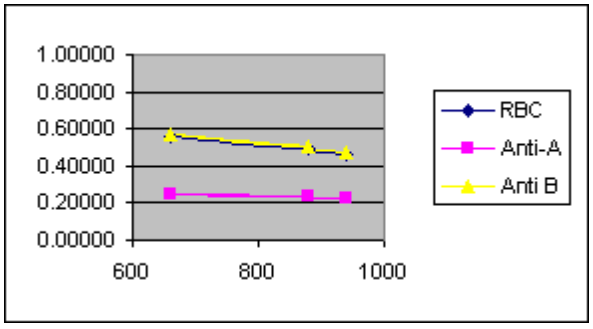
Wave-length	RBC	Anti-A	Anti-B
660	0.56102	0.24731	0.57037
870	0.49270	0.23997	0.50527
950	0.46191	0.22366	0.46879

Slopes

Sample	870	950	LR
RBC	-0.00031	-0.00035	-0.0003422
Anti-A	-3.3E-05	-8.4E-05	-7.068E-05
Anti-B	-0.0003	-0.00036	-0.0003447

Agglutination Index

Method	Anti-A	Anti-B
660-870	89.26035	4.727982
660-950	76.13361	-2.48557
Lin Reg	79.349	-0.71861



Sample: A4-3

Transmission

Wave-length	RBC	Anti-A	Anti-B
660	28.24%	54.89%	26.51%
870	32.48%	55.83%	31.25%
950	35.08%	57.37%	33.91%

Optical Density

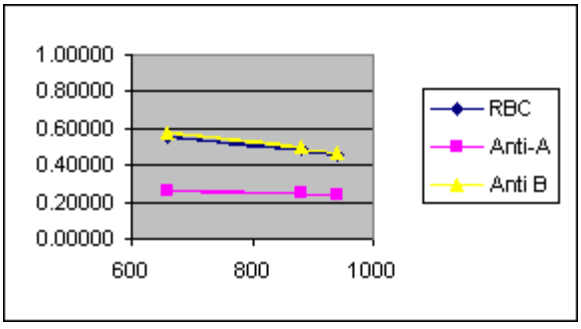
Wave-length	RBC	Anti-A	Anti-B
660	0.54920	0.26050	0.57667
870	0.48834	0.25310	0.50511
950	0.45494	0.24134	0.46966

Slopes

Sample	870	950	LR
RBC	-0.00028	-0.00034	-0.00032
Anti-A	-3.4E-05	-6.8E-05	-5.9E-05
Anti-B	-0.00033	-0.00038	-0.00037

Agglutination Index

Method	Anti-A	Anti-B
660-870	87.84165	-17.5656
660-950	79.66933	-13.519
Lin Reg	81.57386	-14.462



Sample: A5-1

Sample: A+

Transmission

Wave-length	RBC	Anti-A	Anti-B
660	0.27012	0.76339	0.25745
870	0.31297	0.78826	0.3069
950	0.33741	0.79097	0.32473

Optical Density

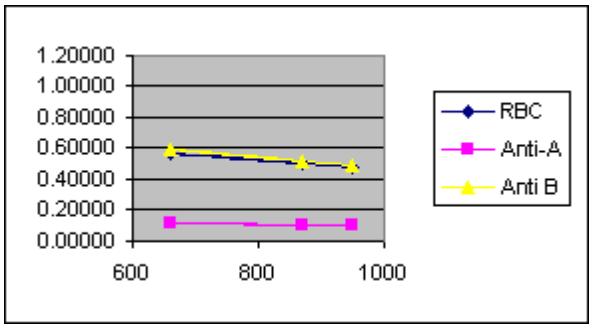
Wave-length	RBC	Anti-A	Anti-B
660	0.56844	0.11725	0.58929
870	0.50449	0.10333	0.52043
660	0.56844	0.11725	0.58929
950	0.47183	0.10184	0.48847

Slopes

Sample	880	940	LR
RBC	-0.0003	-0.00033	-0.0003303
Anti-A	-6.6E-05	-5.3E-05	-5.726E-05
Anti-B	-0.00033	-0.00035	-0.0003474

Agglutination Index

Method	Anti-A	Anti-B
660-800	78.23456	-7.68256
660-940	84.04811	-4.36839
Lin Reg	82.66723	-5.1556



Sample: A5-2

Sample: A-

Transmission

Wave-length	RBC	Anti-A	Anti-B
660	0.246	0.4816	0.233331
870	0.29869	0.53422	0.28827
950	0.32926	0.55	0.31734

Optical Density

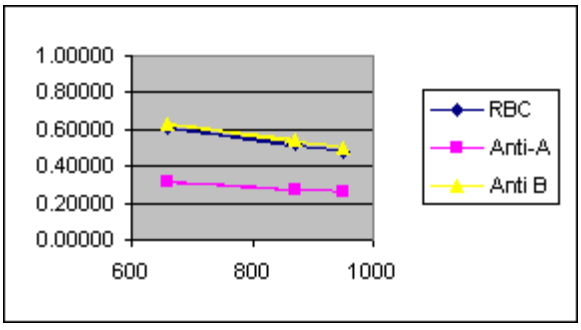
Wave-length	RBC	Anti-A	Anti-B
660	0.60893	0.31501	0.63206
870	0.52478	0.27227	0.54019
660	0.60893	0.31501	0.63206
950	0.48245	0.25961	0.49846

Slopes

Sample	880	940	LR
RBC	-0.0004	-0.00044	-0.00043
Anti-A	-0.0002	-0.00019	-0.0002
Anti-B	-0.00044	-0.00046	-0.00046

Agglutination Index

Method	Anti-A	Anti-B
660-800	49.20673	-9.18058
660-940	56.19371	-5.63273
Lin Reg	54.52777	-6.47867



Sample: A5-3

Transmission

Wave-length	RBC	Anti-A	Anti-B
660	25.63%	55.46%	24.26%
870	30.11%	58.78%	29.41%
950	32.56%	63.84%	31.47%

Optical Density

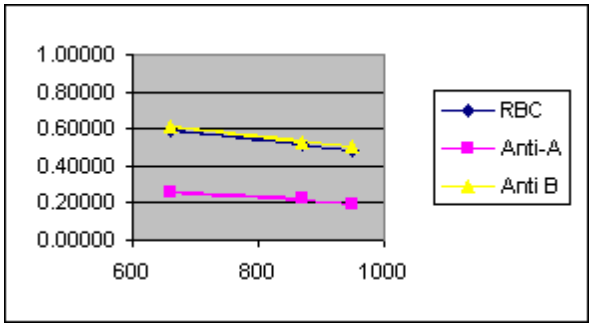
Wave-length	RBC	Anti-A	Anti-B
660	0.59120	0.25606	0.61517
870	0.52133	0.23077	0.53156
660	0.59120	0.25606	0.61517
950	0.48729	0.19490	0.50203

Slopes

Sample	870	950	LR
RBC	-0.00033	-0.00036	-0.0003567
Anti-A	-0.00012	-0.00021	-0.0001905
Anti-B	-0.0004	-0.00039	-0.0003976

Agglutination Index

Method	Anti-A	Anti-B
660-870	63.81356	-19.663
660-950	41.14473	-8.87574
Lin Reg	46.59344	-11.4686



Sample: B1-1

Transmission

Wave-length	RBC	Anti-A	Anti-B
660	21.47%	20.60%	61.53%
870	24.91%	23.95%	64.49%
950	26.94%	26.06%	66.92%

Optical Density

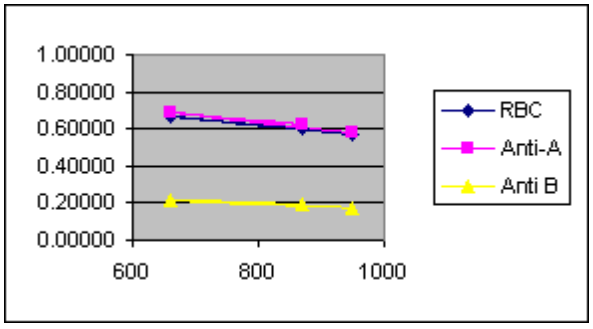
Wave-length	RBC	Anti-A	Anti-B
660	0.66819	0.68611	0.21095
870	0.60355	0.62072	0.19048
660	0.66819	0.68611	0.21095
950	0.56957	0.58404	0.17442

Slopes

Sample	870	950	LR
RBC	-0.00031	-0.00034	-0.0003365
Anti-A	-0.00031	-0.00035	-0.0003463
Anti-B	-9.7E-05	-0.00013	-0.0001203

Agglutination Index

Method	Anti-A	Anti-B
660-870	-1.14843	68.33538
660-950	-3.48758	62.96661
Lin Reg	-2.93618	64.23219



Sample: B1-2

Transmission

Wave-length	RBC	Anti-A	Anti-B
660	18.51%	20.63%	57.80%
870	21.65%	24.24%	60.25%
950	23.51%	26.10%	60.48%

Optical Density

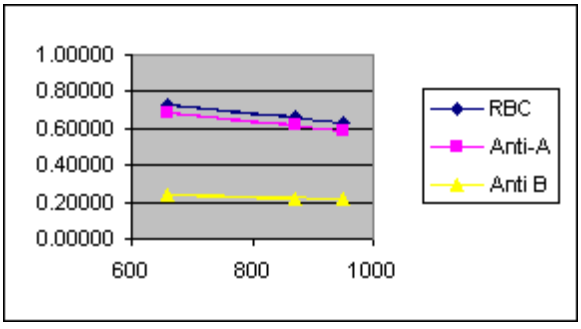
Wave-length	RBC	Anti-A	Anti-B
660	0.73261	0.68560	0.23808
870	0.66459	0.61545	0.22006
660	0.73261	0.68560	0.23808
950	0.62877	0.58328	0.21838

Slopes

Sample	870	950	LR
RBC	-0.00032	-0.00036	-0.00035
Anti-A	-0.00033	-0.00035	-0.00035
Anti-B	-8.6E-05	-6.8E-05	-7.3E-05

Agglutination Index

Method	Anti-A	Anti-B
660-870	-3.13441	73.51321
660-950	1.469491	81.03074
Lin Reg	0.384762	79.25953



Sample: B1-3

Transmission

Wave-length	RBC	Anti-A	Anti-B
660	21.62%	20.88%	57.94%
870	25.46%	24.46%	62.18%
950	27.31%	26.83%	62.74%

Optical Density

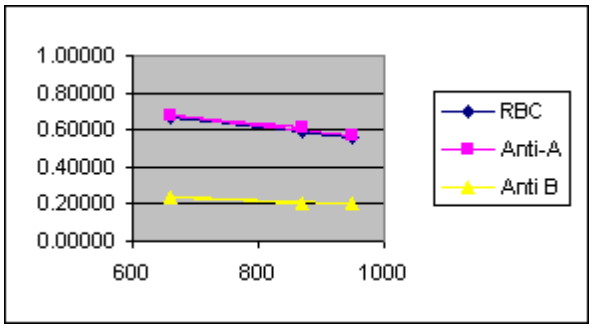
Wave-length	RBC	Anti-A	Anti-B
660	0.66516	0.68031	0.23701
870	0.59410	0.61146	0.20635
660	0.66516	0.68031	0.23701
950	0.56364	0.57143	0.20247

Slopes

Sample	870	950	LR
RBC	-0.00034	-0.00035	-0.0003519
Anti-A	-0.00033	-0.00038	-0.0003683
Anti-B	-0.00015	-0.00012	-0.0001277

Agglutination Index

Method	Anti-A	Anti-B
660-870	3.115382	56.85204
660-950	-7.24095	65.97558
Lin Reg	-4.67504	63.71511



Sample: B2-1

Transmission

Wave-length	RBC	Anti-A	Anti-B
660	20.00%	20.93%	54.24%
870	23.34%	24.37%	57.82%
950	25.54%	26.61%	59.76%

Optical Density

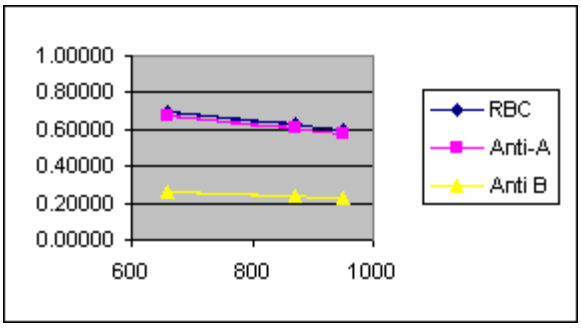
Wave-length	RBC	Anti-A	Anti-B
660	0.69895	0.67920	0.26570
870	0.63191	0.61314	0.23793
660	0.69895	0.67920	0.26570
950	0.59285	0.57491	0.22362

Slopes

Sample	870	950	LR
RBC	-0.00032	-0.00037	-0.00036
Anti-A	-0.00031	-0.00036	-0.00035
Anti-B	-0.00013	-0.00015	-0.00014

Agglutination Index

Method	Anti-A	Anti-B
660-870	1.45354	58.57603
660-950	1.696535	60.33123
Lin Reg	1.640841	59.92894



Sample: B2-2

Transmission

Wave-length	RBC	Anti-A	Anti-B
660	21.36%	20.70%	55.99%
870	25.03%	24.10%	57.09%
950	27.36%	26.54%	60.40%

Optical Density

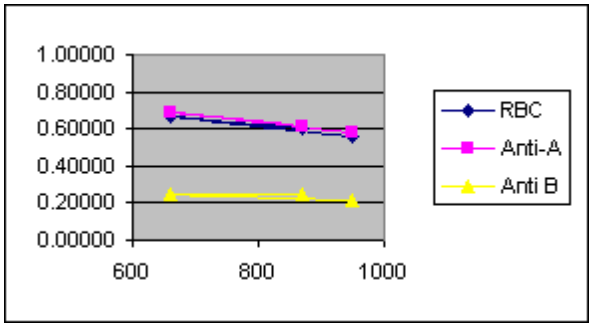
Wave-length	RBC	Anti-A	Anti-B
660	0.67033	0.68397	0.25192
870	0.60160	0.61800	0.24341
660	0.67033	0.68397	0.25192
950	0.56292	0.57611	0.21895

Slopes

Sample	870	950	LR
RBC	-0.00033	-0.00037	-0.0003644
Anti-A	-0.00031	-0.00037	-0.0003622
Anti-B	-4.1E-05	-0.00011	-9.639E-05

Agglutination Index

Method	Anti-A	Anti-B
660-870	4.015602	87.61975
660-950	-0.4248	69.30878
Lin Reg	0.602879	73.54665



Sample: B2-3

Transmission

Wave-length	RBC	Anti-A	Anti-B
660	21.44%	20.67%	58.50%
870	24.95%	23.98%	62.15%
950	27.23%	26.72%	64.20%

Optical Density

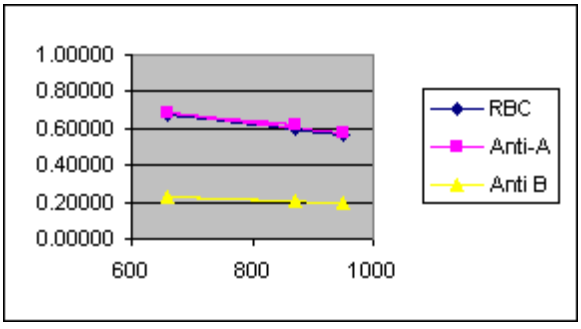
Wave-length	RBC	Anti-A	Anti-B
660	0.66880	0.68466	0.23285
870	0.60291	0.62020	0.20658
660	0.66880	0.68466	0.23285
950	0.56501	0.57324	0.19245

Slopes

Sample	870	950	LR
RBC	-0.00031	-0.00036	-0.00035
Anti-A	-0.00031	-0.00038	-0.00037
Anti-B	-0.00013	-0.00014	-0.00014

Agglutination Index

Method	Anti-A	Anti-B
660-870	2.177663	60.13605
660-950	-7.34092	61.08067
Lin Reg	-5.15146	60.86338



Sample: B3-1

Transmission

Wave-length	RBC	Anti-A	Anti-B
660	13.87%	12.88%	49.83%
870	17.02%	15.81%	50.97%
950	18.84%	17.69%	53.14%

Optical Density

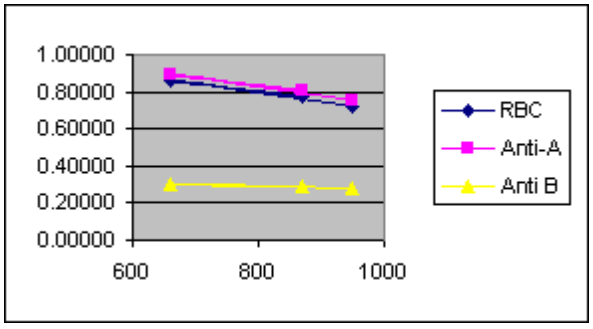
Wave-length	RBC	Anti-A	Anti-B
660	0.85785	0.89004	0.30252
870	0.76900	0.80111	0.29267
660	0.85785	0.89004	0.30252
950	0.72494	0.75232	0.27461

Slopes

Sample	870	950	LR
RBC	-0.00042	-0.00046	-0.0004556
Anti-A	-0.00042	-0.00047	-0.0004682
Anti-B	-4.7E-05	-9.6E-05	-8.486E-05

Agglutination Index

Method	Anti-A	Anti-B
660-870	-0.10138	88.9179
660-950	-3.61866	78.99962
Lin Reg	-2.777	81.37299



Sample: B3-2

Transmission

Wave-length	RBC	Anti-A	Anti-B
660	13.38%	13.73%	64.91%
870	16.24%	16.49%	68.74%
950	18.00%	18.32%	72.06%

Optical Density

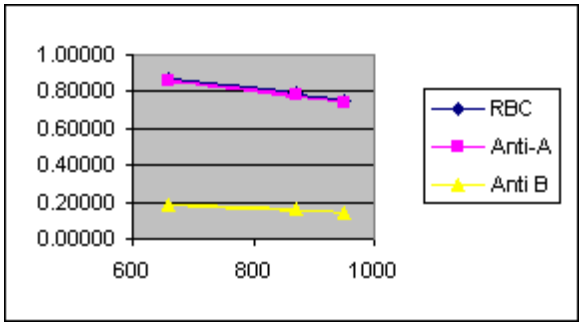
Wave-length	RBC	Anti-A	Anti-B
660	0.87369	0.86219	0.18770
870	0.78948	0.78272	0.16280
660	0.87369	0.86219	0.18770
950	0.74475	0.73703	0.14229

Slopes

Sample	870	950	LR
RBC	-0.0004	-0.00044	-0.00044
Anti-A	-0.00038	-0.00043	-0.00042
Anti-B	-0.00012	-0.00016	-0.00015

Agglutination Index

Method	Anti-A	Anti-B
660-870	5.634134	70.43577
660-950	2.933281	64.78822
Lin Reg	3.568215	66.11589



Sample: B3-3

Transmission

Wave-length	RBC	Anti-A	Anti-B
660	14.27%	13.66%	49.85%
870	17.14%	16.50%	53.94%
950	19.02%	18.50%	56.92%

Optical Density

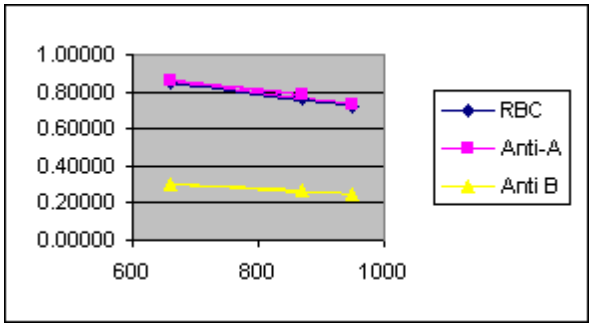
Wave-length	RBC	Anti-A	Anti-B
660	0.84563	0.86444	0.30231
870	0.76592	0.78244	0.26806
660	0.84563	0.86444	0.30231
950	0.72086	0.73284	0.24476

Slopes

Sample	870	950	LR
RBC	-0.00038	-0.00043	-0.0004231
Anti-A	-0.00039	-0.00045	-0.0004437
Anti-B	-0.00016	-0.0002	-0.0001921

Agglutination Index

Method	Anti-A	Anti-B
660-870	-2.8674	57.03497
660-950	-5.47094	53.88032
Lin Reg	-4.86915	54.60949



Sample: B4-1

Transmission

Wave-length	RBC	Anti-A	Anti-B
660	13.81%	14.35%	48.92%
870	16.91%	17.47%	52.70%
950	18.79%	19.49%	55.57%

Optical Density

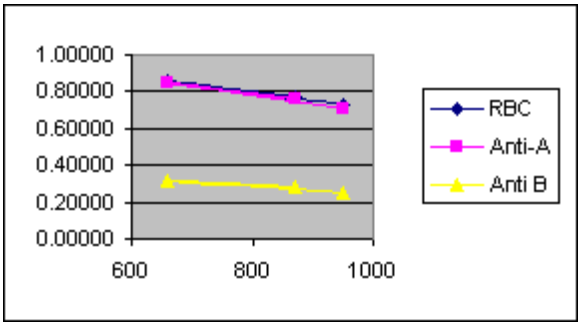
Wave-length	RBC	Anti-A	Anti-B
660	0.85989	0.84321	0.31049
870	0.77179	0.75760	0.27816
660	0.85989	0.84321	0.31049
950	0.72605	0.71018	0.25513

Slopes

Sample	870	950	LR
RBC	-0.00042	-0.00046	-0.00046
Anti-A	-0.00041	-0.00046	-0.00045
Anti-B	-0.00015	-0.00019	-0.00018

Agglutination Index

Method	Anti-A	Anti-B
660-870	2.838728	63.30585
660-950	0.610242	58.63566
Lin Reg	1.137303	59.74021



Sample: B4-2

Transmission

Wave-length	RBC	Anti-A	Anti-B
660	14.65%	13.45%	44.25%
870	17.83%	16.72%	50.80%
950	19.83%	18.46%	52.80%

Optical Density

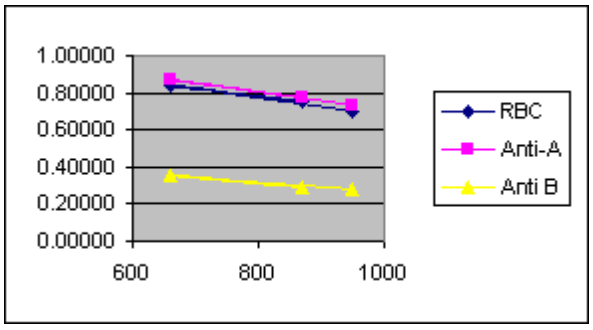
Wave-length	RBC	Anti-A	Anti-B
660	0.83406	0.87131	0.35414
870	0.74884	0.77663	0.29411
660	0.83406	0.87131	0.35414
950	0.70261	0.73365	0.27740

Slopes

Sample	870	950	LR
RBC	-0.00041	-0.00045	-0.0004473
Anti-A	-0.00045	-0.00047	-0.0004751
Anti-B	-0.00029	-0.00026	-0.0002737

Agglutination Index

Method	Anti-A	Anti-B
660-870	-11.1062	29.55999
660-950	-4.72275	41.62368
Lin Reg	-6.21488	38.80377



Sample: B4-3

Transmission

Wave-length	RBC	Anti-A	Anti-B
660	14.69%	13.50%	44.78%
870	17.88%	16.36%	50.21%
950	19.40%	18.22%	53.01%

Optical Density

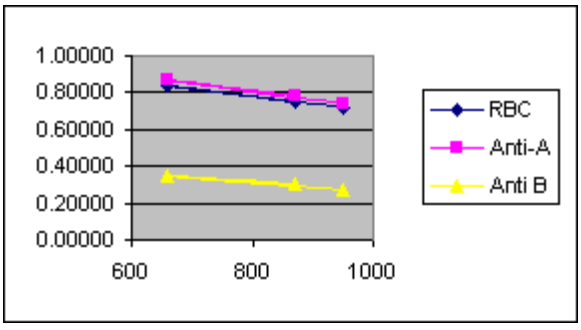
Wave-length	RBC	Anti-A	Anti-B
660	0.83291	0.86963	0.34887
870	0.74769	0.78630	0.29920
660	0.83291	0.86963	0.34887
950	0.71221	0.73953	0.27568

Slopes

Sample	870	950	LR
RBC	-0.00041	-0.00042	-0.00042
Anti-A	-0.0004	-0.00045	-0.00044
Anti-B	-0.00024	-0.00025	-0.00025

Agglutination Index

Method	Anti-A	Anti-B
660-870	2.217943	41.71934
660-950	-7.78535	39.35986
Lin Reg	-5.29048	39.94833



Sample: B5-1

Transmission

Wave-length	RBC	Anti-A	Anti-B
660	0.1958	0.189338	0.64535
870	0.22719	0.21971	0.65402
950	0.24765	0.23939	0.67208

Optical Density

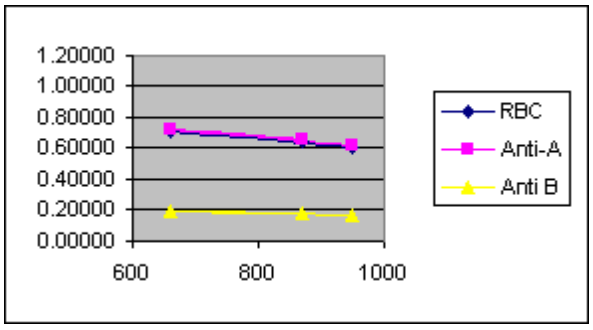
Wave-length	RBC	Anti-A	Anti-B
660	0.70817	0.72276	0.19020
870	0.64361	0.65815	0.18440
660	0.70817	0.72276	0.19020
950	0.60615	0.62087	0.17258

Slopes

Sample	880	940	LR
RBC	-0.00031	-0.00035	-0.0003452
Anti-A	-0.00031	-0.00035	-0.0003449
Anti-B	-2.8E-05	-6.1E-05	-5.306E-05

Agglutination Index

Method	Anti-A	Anti-B
660-800	-0.08209	91.01976
660-940	0.127426	82.72692
Lin Reg	0.079348	84.62991



Sample: B5-2

Transmission

Wave-length	RBC	Anti-A	Anti-B
660	0.30347	0.21152	0.71023
870	0.36082	0.26007	0.7578
950	0.38764	0.28292	0.77104

Optical Density

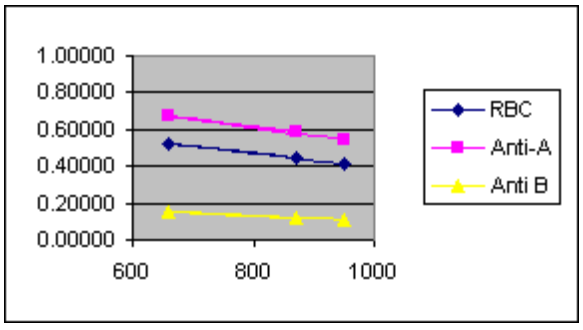
Wave-length	RBC	Anti-A	Anti-B
660	0.51787	0.67464	0.14860
870	0.44270	0.58491	0.12040
660	0.51787	0.67464	0.14860
950	0.41156	0.54832	0.11292

Slopes

Sample	880	940	LR
RBC	-0.00036	-0.00037	-0.00037
Anti-A	-0.00043	-0.00044	-0.00044
Anti-B	-0.00013	-0.00012	-0.00013

Agglutination Index

Method	Anti-A	Anti-B
660-800	-19.3678	62.48819
660-940	-18.8206	66.43746
Lin Reg	-18.9572	65.45143



Sample: B5-3

Transmission

Wave-length	RBC	Anti-A	Anti-B
660	16.95%	16.35%	63.63%
870	20.30%	20.09%	64.79%
950	22.84%	22.14%	66.97%

Optical Density

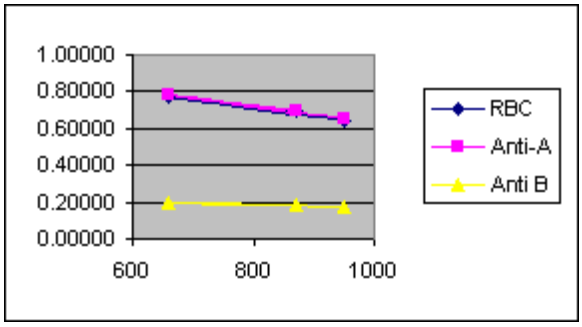
Wave-length	RBC	Anti-A	Anti-B
660	0.77089	0.78638	0.19636
870	0.69246	0.69694	0.18850
660	0.77089	0.78638	0.19636
950	0.64129	0.65473	0.17411

Slopes

Sample	870	950	LR
RBC	-0.00037	-0.00045	-0.00043
Anti-A	-0.00043	-0.00045	-0.00045
Anti-B	-3.7E-05	-7.7E-05	-6.8E-05

Agglutination Index

Method	Anti-A	Anti-B
660-870	-14.0317	89.9775
660-950	-1.58391	82.83503
Lin Reg	-4.34327	84.41833



Sample: O1-1

Transmission

Wave-length	RBC	Anti-A	Anti-B
660	18.79%	18.82%	19.72%
870	22.63%	23.44%	24.07%
950	24.86%	25.57%	26.70%

Optical Density

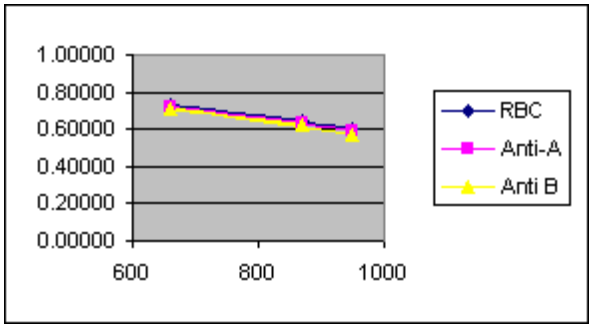
Wave-length	RBC	Anti-A	Anti-B
660	0.72598	0.72541	0.70518
870	0.64532	0.63000	0.61849
660	0.72598	0.72541	0.70518
950	0.60445	0.59220	0.57343

Slopes

Sample	870	950	LR
RBC	-0.00038	-0.00042	-0.0004158
Anti-A	-0.00045	-0.00046	-0.0004644
Anti-B	-0.00041	-0.00045	-0.0004499

Agglutination Index

Method	Anti-A	Anti-B
660-870	-18.2933	-7.48623
660-950	-9.62173	-8.4211
Lin Reg	-11.6856	-8.1986



Sample: O1-2

Transmission

Wave-length	RBC	Anti-A	Anti-B
660	18.51%	18.88%	18.72%
870	22.72%	23.16%	23.08%
950	25.02%	25.50%	25.53%

Optical Density

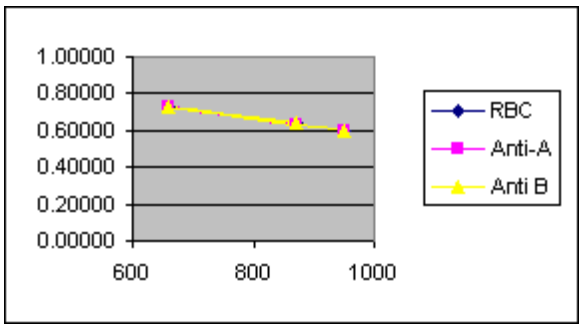
Wave-length	RBC	Anti-A	Anti-B
660	0.73258	0.72398	0.72773
870	0.64351	0.63524	0.63670
660	0.73258	0.72398	0.72773
950	0.60166	0.59352	0.59303

Slopes

Sample	870	950	LR
RBC	-0.00042	-0.00045	-0.00045
Anti-A	-0.00042	-0.00045	-0.00045
Anti-B	-0.00043	-0.00046	-0.00046

Agglutination Index

Method	Anti-A	Anti-B
660-870	0.364783	-2.20185
660-950	0.34616	-2.88654
Lin Reg	0.350676	-2.72049



Sample: O1-3

Transmission

Wave-length	RBC	Anti-A	Anti-B
660	20.15%	19.72%	19.33%
870	24.32%	23.83%	23.49%
950	26.54%	26.31%	26.24%

Optical Density

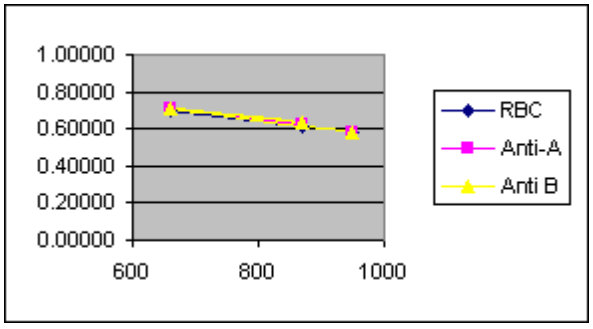
Wave-length	RBC	Anti-A	Anti-B
660	0.69576	0.70517	0.71377
870	0.61397	0.62281	0.62912
660	0.69576	0.70517	0.71377
950	0.57618	0.57995	0.58099

Slopes

Sample	870	950	LR
RBC	-0.00039	-0.00041	-0.0004121
Anti-A	-0.00039	-0.00043	-0.0004275
Anti-B	-0.0004	-0.00046	-0.0004501

Agglutination Index

Method	Anti-A	Anti-B
660-870	-0.69533	-3.49914
660-950	-4.71618	-11.0416
Lin Reg	-3.7371	-9.20497



Sample: O2-1

Transmission

Wave-length	RBC	Anti-A	Anti-B
660	20.70%	18.45%	19.84%
870	24.97%	22.27%	24.09%
950	27.05%	24.60%	26.60%

Optical Density

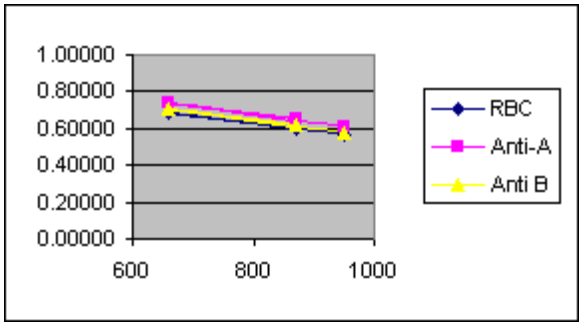
Wave-length	RBC	Anti-A	Anti-B
660	0.68406	0.73397	0.70251
870	0.60253	0.65225	0.61814
660	0.68406	0.73397	0.70251
950	0.56789	0.60906	0.57509

Slopes

Sample	870	950	LR
RBC	-0.00039	-0.0004	-0.0004
Anti-A	-0.00039	-0.00043	-0.00043
Anti-B	-0.0004	-0.00044	-0.00044

Agglutination Index

Method	Anti-A	Anti-B
660-870	-0.22516	-3.47567
660-950	-7.51783	-9.67489
Lin Reg	-5.70731	-8.13584



Sample: O2-2

Transmission

Wave-length	RBC	Anti-A	Anti-B
660	20.54%	19.31%	19.41%
870	24.43%	23.66%	23.25%
950	26.70%	26.19%	25.65%

Optical Density

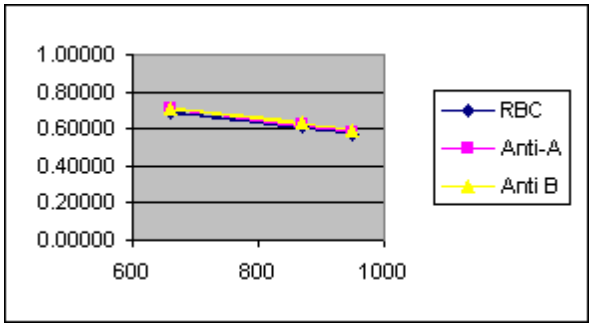
Wave-length	RBC	Anti-A	Anti-B
660	0.68730	0.71411	0.71188
870	0.61216	0.62603	0.63363
660	0.68730	0.71411	0.71188
950	0.57351	0.58188	0.59093

Slopes

Sample	870	950	LR
RBC	-0.00036	-0.00039	-0.0003889
Anti-A	-0.00042	-0.00046	-0.0004528
Anti-B	-0.00037	-0.00042	-0.0004114

Agglutination Index

Method	Anti-A	Anti-B
660-870	-17.2181	-4.14265
660-950	-16.2009	-6.29001
Lin Reg	-16.442	-5.78093



Sample: O2-3

Transmission

Wave-length	RBC	Anti-A	Anti-B
660	20.18%	19.23%	20.10%
870	24.21%	23.12%	23.98%
950	26.42%	25.53%	26.39%

Optical Density

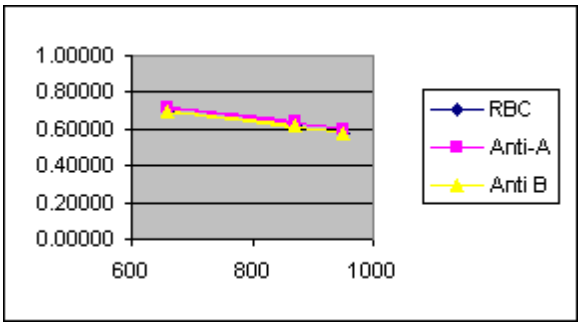
Wave-length	RBC	Anti-A	Anti-B
660	0.69511	0.71591	0.69676
870	0.61595	0.63599	0.62022
660	0.69511	0.71591	0.69676
950	0.57804	0.59294	0.57864

Slopes

Sample	870	950	LR
RBC	-0.00038	-0.0004	-0.0004
Anti-A	-0.00038	-0.00042	-0.00042
Anti-B	-0.00036	-0.00041	-0.0004

Agglutination Index

Method	Anti-A	Anti-B
660-870	-0.95503	3.315616
660-950	-5.04838	-0.90048
Lin Reg	-4.06023	0.117302



Sample: O3-1

Transmission

Wave-length	RBC	Anti-A	Anti-B
660	35.13%	33.39%	33.38%
870	39.62%	38.39%	38.71%
950	41.99%	40.64%	41.23%

Optical Density

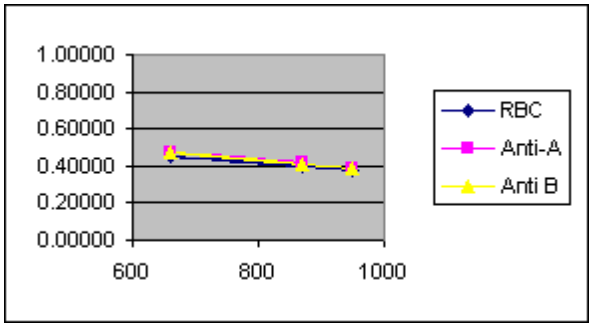
Wave-length	RBC	Anti-A	Anti-B
660	0.45431	0.47639	0.47654
870	0.40214	0.41574	0.41218
660	0.45431	0.47639	0.47654
950	0.37691	0.39109	0.38480

Slopes

Sample	870	950	LR
RBC	-0.00025	-0.00027	-0.0002658
Anti-A	-0.00029	-0.00029	-0.0002968
Anti-B	-0.00031	-0.00032	-0.0003182

Agglutination Index

Method	Anti-A	Anti-B
660-870	-16.2509	-23.3735
660-950	-10.2045	-18.5322
Lin Reg	-11.6604	-19.6979



Sample O3-2

Transmission

Wave-length	RBC	Anti-A	Anti-B
660	34.57%	33.96%	32.94%
870	39.07%	38.53%	37.78%
950	41.39%	40.86%	40.37%

Optical Density

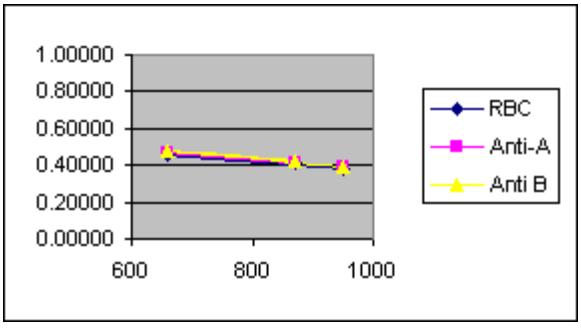
Wave-length	RBC	Anti-A	Anti-B
660	0.46134	0.46901	0.48234
870	0.40819	0.41423	0.42268
660	0.46134	0.46901	0.48234
950	0.38312	0.38869	0.39389

Slopes

Sample	870	950	LR
RBC	-0.00025	-0.00027	-0.00027
Anti-A	-0.00026	-0.00028	-0.00028
Anti-B	-0.00028	-0.0003	-0.0003

Agglutination Index

Method	Anti-A	Anti-B
660-870	-3.05912	-12.2426
660-950	-2.67562	-13.066
Lin Reg	-2.76853	-12.8665



Sample: O3-3

Transmission

Wave-length	RBC	Anti-A	Anti-B
660	34.18%	33.60%	33.27%
870	39.44%	39.01%	39.01%
950	41.47%	41.16%	41.07%

Optical Density

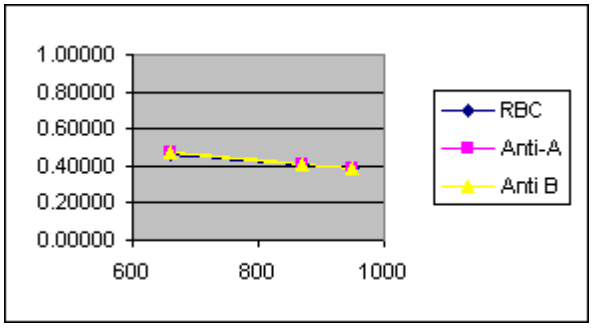
Wave-length	RBC	Anti-A	Anti-B
660	0.46619	0.47370	0.47796
870	0.40402	0.40886	0.40888
660	0.46619	0.47370	0.47796
950	0.38229	0.38550	0.38649

Slopes

Sample	870	950	LR
RBC	-0.0003	-0.00029	-0.0002951
Anti-A	-0.00031	-0.0003	-0.0003096
Anti-B	-0.00033	-0.00032	-0.0003233

Agglutination Index

Method	Anti-A	Anti-B
660-870	-4.29194	-11.106
660-950	-5.1247	-9.01547
Lin Reg	-4.90939	-9.55599



Sample: O4-1

Transmission

Wave-length	RBC	Anti-A	Anti-B
660	36.84%	34.88%	35.15%
870	41.79%	39.96%	40.05%
950	43.87%	42.12%	42.61%

Optical Density

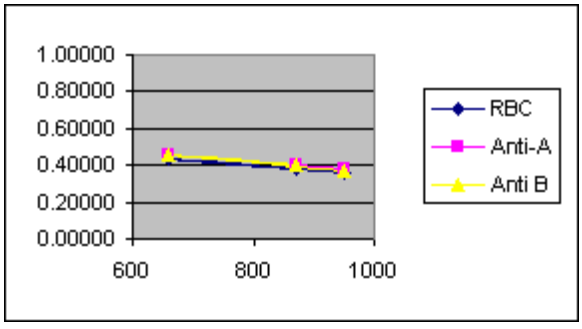
Wave-length	RBC	Anti-A	Anti-B
660	0.43374	0.45745	0.45405
870	0.37894	0.39842	0.39735
660	0.43374	0.45745	0.45405
950	0.35784	0.37555	0.37049

Slopes

Sample	870	950	LR
RBC	-0.00026	-0.00026	-0.00027
Anti-A	-0.00028	-0.00028	-0.00029
Anti-B	-0.00027	-0.00029	-0.00029

Agglutination Index

Method	Anti-A	Anti-B
660-870	-7.73442	-3.48645
660-950	-7.90274	-10.1012
Lin Reg	-7.86006	-8.42379



Sample: O4-2

Transmission

Wave-length	RBC	Anti-A	Anti-B
660	35.14%	34.69%	35.89%
870	39.83%	39.43%	40.84%
950	42.22%	41.99%	43.41%

Optical Density

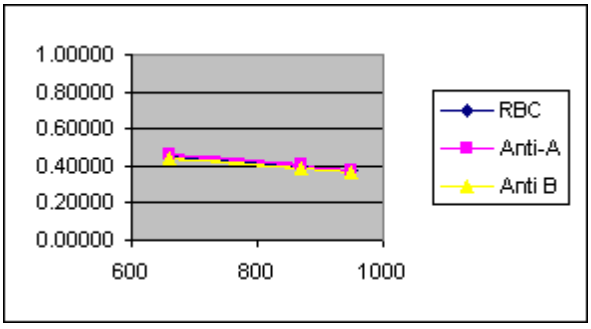
Wave-length	RBC	Anti-A	Anti-B
660	0.45415	0.45981	0.44508
870	0.39983	0.40415	0.38897
660	0.45415	0.45981	0.44508
950	0.37451	0.37685	0.36243

Slopes

Sample	870	950	LR
RBC	-0.00026	-0.00027	-0.0002743
Anti-A	-0.00027	-0.00029	-0.0002846
Anti-B	-0.00027	-0.00028	-0.0002843

Agglutination Index

Method	Anti-A	Anti-B
660-870	-2.47183	-3.31027
660-950	-4.17281	-3.7736
Lin Reg	-3.75953	-3.66103



Sample: O4-3

Transmission

Wave-length	RBC	Anti-A	Anti-B
660	35.11%	35.39%	34.56%
870	40.06%	40.59%	40.18%
950	42.35%	43.16%	42.83%

Optical Density

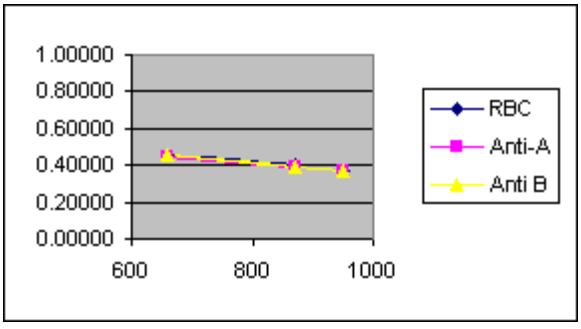
Wave-length	RBC	Anti-A	Anti-B
660	0.45456	0.45106	0.46146
870	0.39727	0.39156	0.39595
660	0.45456	0.45106	0.46146
950	0.37311	0.36496	0.36825

Slopes

Sample	870	950	LR
RBC	-0.00027	-0.00028	-0.00028
Anti-A	-0.00028	-0.0003	-0.0003
Anti-B	-0.00031	-0.00032	-0.00032

Agglutination Index

Method	Anti-A	Anti-B
660-870	-3.88007	-14.3709
660-950	-5.721	-14.4483
Lin Reg	-5.2632	-14.429



Sample: O5-1

Transmission

Wave-length	RBC	Anti-A	Anti-B
660	0.25549	0.25487	0.24312
870	0.30474	0.30117	0.29028
950	0.3322	0.33174	0.31818

Optical Density

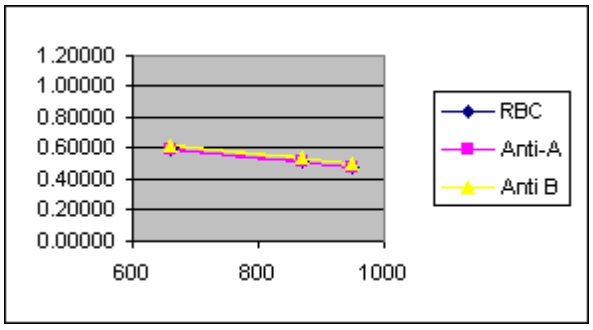
Wave-length	RBC	Anti-A	Anti-B
660	0.59263	0.59368	0.61416
870	0.51606	0.51619	0.53717
660	0.59263	0.59368	0.61416
950	0.47859	0.47919	0.49732

Slopes

Sample	880	940	LR
RBC	-0.00036	-0.00039	-0.0003913
Anti-A	-0.00037	-0.00039	-0.0003936
Anti-B	-0.00037	-0.0004	-0.0003991

Agglutination Index

Method	Anti-A	Anti-B
660-800	-1.20682	-0.5577
660-940	-0.39462	-2.46332
Lin Reg	-0.58963	-2.00578



Sample: O5-2

Transmission

Wave-length	RBC	Anti-A	Anti-B
660	0.19964	0.18384	0.1767
870	0.24386	0.22425	0.21659
950	0.266215	0.24987	0.24033

Optical Density

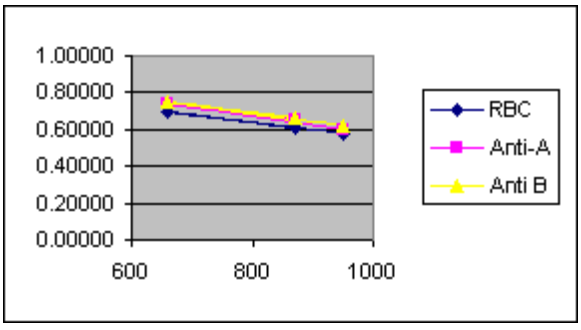
Wave-length	RBC	Anti-A	Anti-B
660	0.69974	0.73555	0.75265
870	0.61285	0.64927	0.66435
660	0.69974	0.73555	0.75265
950	0.57477	0.60229	0.61919

Slopes

Sample	880	940	LR
RBC	-0.00041	-0.00043	-0.00043
Anti-A	-0.00041	-0.00046	-0.00045
Anti-B	-0.00042	-0.00046	-0.00046

Agglutination Index

Method	Anti-A	Anti-B
660-800	0.697434	-1.61814
660-940	-6.63669	-6.78952
Lin Reg	-4.82862	-5.51463



Sample: O5-1

Transmission

Wave-length	RBC	Anti-A	Anti-B
660	18.12%	17.18%	16.83%
870	22.15%	20.94%	20.48%
950	24.34%	23.18%	22.96%

Optical Density

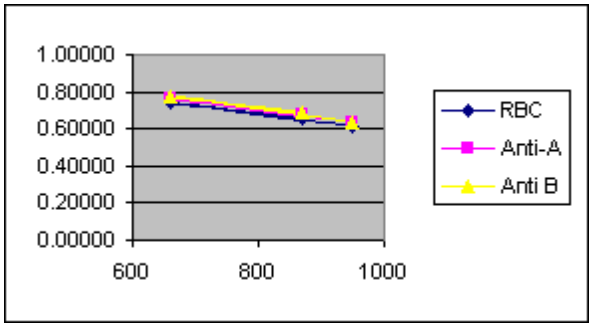
Wave-length	RBC	Anti-A	Anti-B
660	0.74180	0.76504	0.77387
870	0.65457	0.67899	0.68858
660	0.74180	0.76504	0.77387
950	0.61359	0.63495	0.63899

Slopes

Sample	870	950	LR
RBC	-0.00042	-0.00044	-0.0004413
Anti-A	-0.00041	-0.00045	-0.0004448
Anti-B	-0.00041	-0.00047	-0.0004563

Agglutination Index

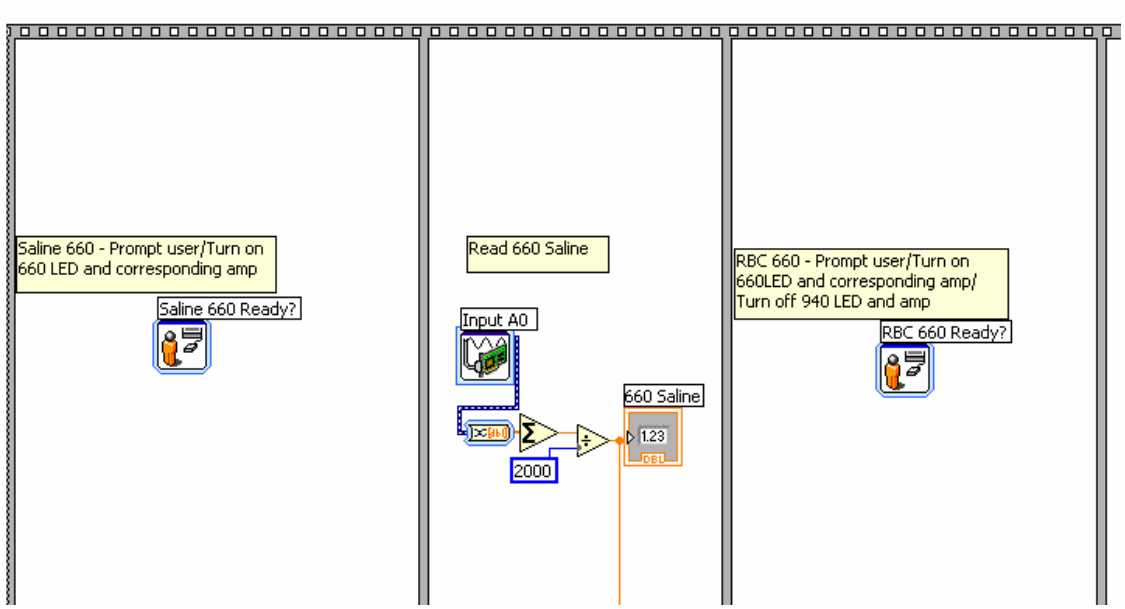
Method	Anti-A	Anti-B
660-870	1.359921	2.220707
660-950	-1.46885	-5.20471
Lin Reg	-0.78278	-3.40382



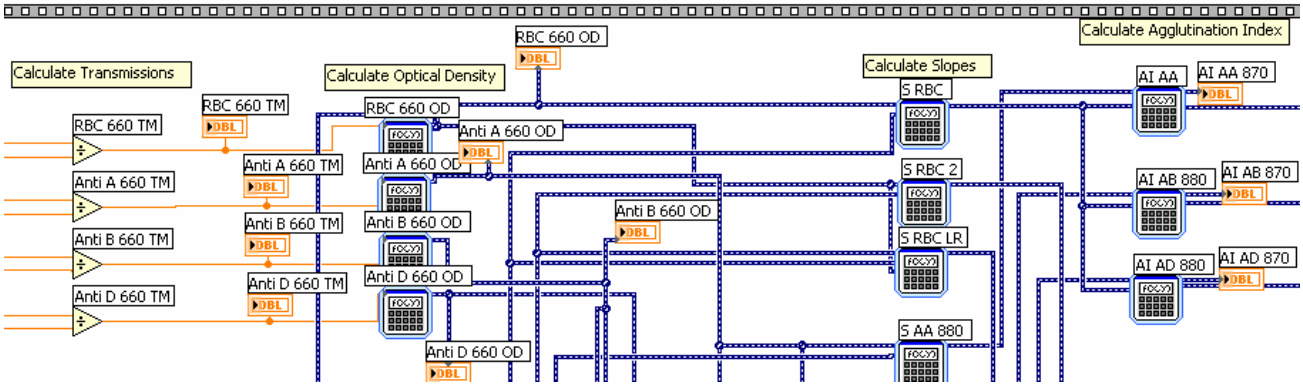
Appendix B

Sample LabView Code

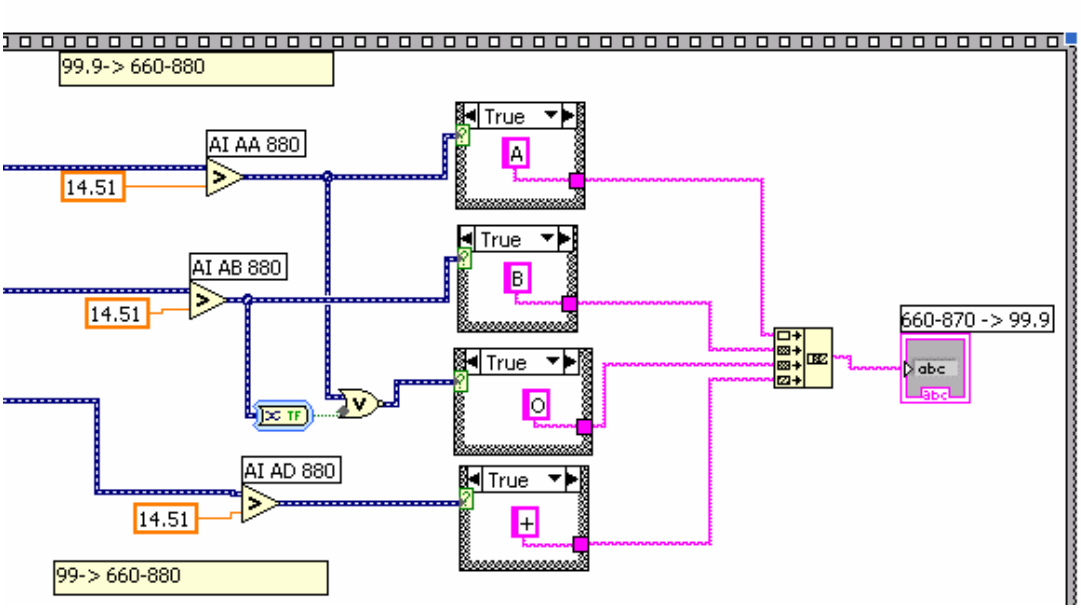
This section shows the Lab View code out of one sequence.



User Prompts



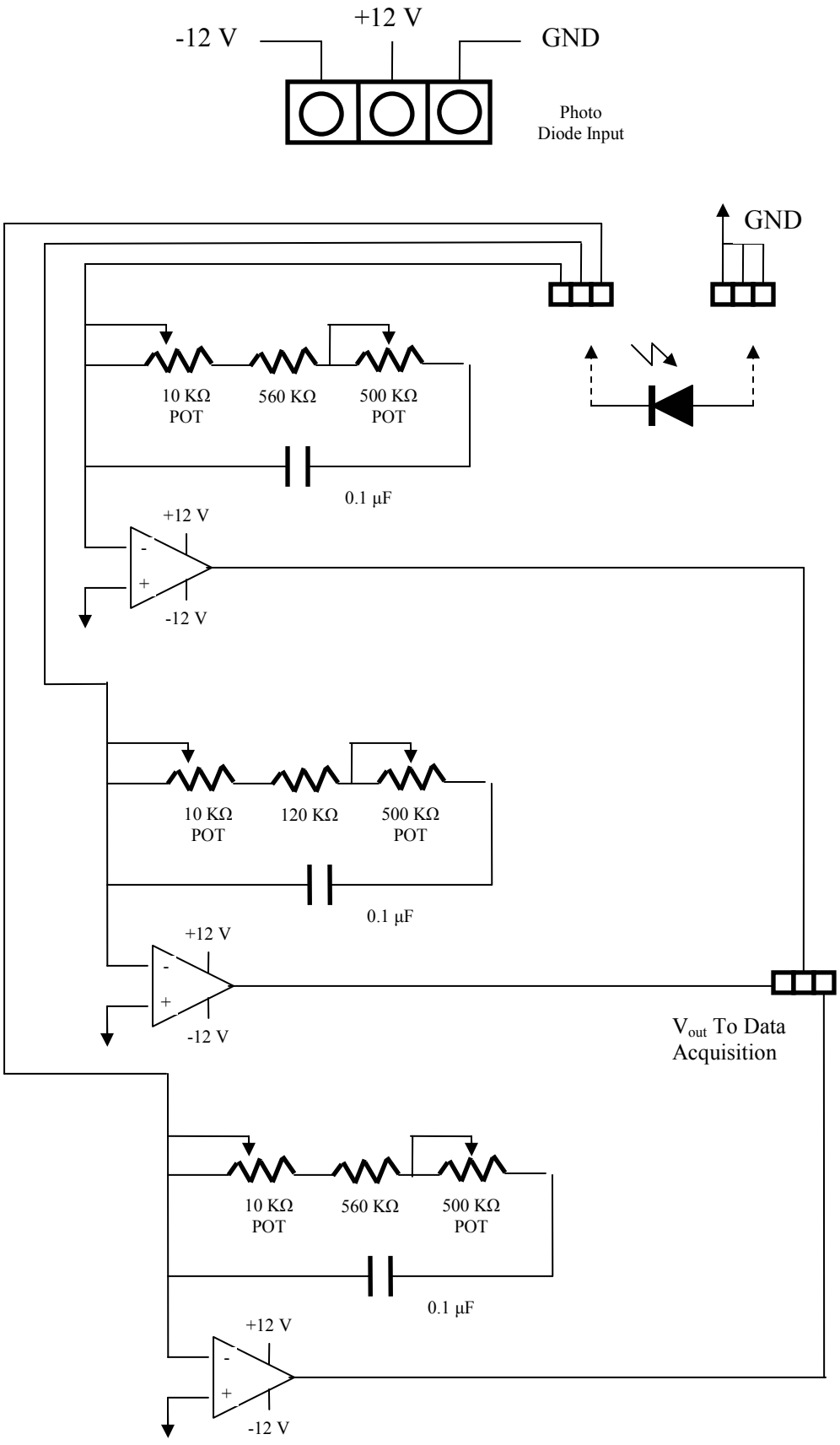
Calculations



Case State to Select Blood Type

Appendix C

Experimental Circuit Diagram


-12 V
+12 V
GND
Photo
Diode Input
GND
10 KΩ
POT
560 KΩ
500 KΩ
POT
0.1 µF
+12 V
-12 V
10 KΩ
POT
120 KΩ
500 KΩ
POT
0.1 µF
+12 V
-12 V
V_{out} To Data
Acquisition
10 KΩ
POT
560 KΩ
500 KΩ
POT
0.1 µF
+12 V
-12 V

Appendix D

Hardware Datasheets

Plastic Fiber Optic Red LED — IF-E96



Applications

- Low Cost Analog and Digital Data Links
- Automotive Electronics
- Digitized Audio
- Medical Instruments
- PC-to-Peripheral Data Links
- Robotics Communications
- Motor Controller Triggering
- EMC/EMI Signal Isolation
- Local Area Networks
- Intra-System Links: Board-to-Board, Rack-to-Rack

Description

The IF-E96 is a low-cost, high-speed, visible red LED housed in a "connector-less" style plastic fiber optic package. The output spectrum is produced by a GaAlAs die which peaks at 660 nm, one of the optimal transmission windows of PMMA plastic optical fiber. The device package features an internal micro-lens and a precision-molded PBT housing to maximize optical coupling into standard 1000 µm core plastic fiber cable.

Application Highlights

The performance/price ratio of the IF-E96 is particularly attractive for high volume design applications. The visible red output has low attenuation in PMMA plastic fiber and aids in troubleshooting installations. When used with an IF-D96 photologic detector the IF-E96 can achieve data rates of 5 Mbps. Fast transition times and low attenuation make the IF-E96 an excellent device selection for low cost analog and digital data links up to 75 meters.

Features

- High Performance at Low Cost
- Visible Red Output Aids Troubleshooting
- Low Transmission Loss with PMMA Plastic Fiber
- Fast Transition Times
- Mates with standard 1000 µm core jacketed plastic fiber cable
- No Optical Design required
- Internal Micro-Lens for Efficient Optical Coupling
- Inexpensive Plastic Connector Housing
- Connector-Less Fiber Termination
- Light-Tight Housing Provides Interference-Free Transmission
- RoHS Compliant

Maximum Ratings

(T_A=25°C)

Operating and Storage Temperature Range (T_{OP}, T_{STG}) ..... -40° to 85°C

Junction Temperature (T_J) ..... 85°C

Soldering Temperature (2mm from case bottom) (T_S) t ≤ 5 s ..... 240°C

Reverse Voltage (V_R) ..... 5 V

Power Dissipation (P_{TOT}) T_A=25°C ..... 60 mW

De-rate Above 25°C ..... 1.1 mW/°C

Forward Current, DC (I_F) ..... 35 mA

Surge Current (I_{FSM}) t ≤ 10 µs ..... 150 mA

Characteristics (T_A=25°C)

Parameter	Symbol	Min.	Typ.	Max.	Unit
Peak Wavelength	λ_{PEAK}	650	660	670	nm
Spectral Bandwidth (50% of λ_{MAX})	$\Delta\lambda$	–	20	–	nm
Output Power Coupled into Plastic Fiber (1 mm core diameter). Distance Lens to Fiber ≤0.1 mm, 1 m SH4001 fiber, I_F=20 mA	Φ_{min}	125 -9.0	200 -7.0	300 -5.2	µW dBm
Switching Times (10% to 90% and 90% to 10%) (I_F=20 mA)	t_r, t_f	–	.1	–	µs
Capacitance (F=1 MHz)	C_0	–	30	–	pF
Forward Voltage (I_F=20 mA)	V_f	–	–	1.8	V
Temperature Coefficient, λ_{PEAK}	TC_λ		0.2		nm/K

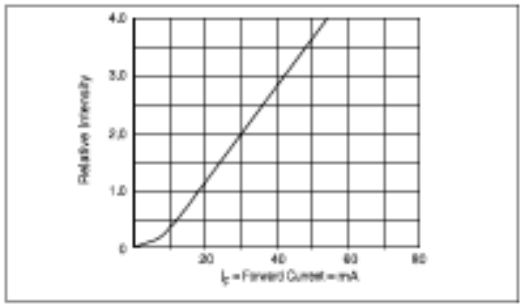


FIGURE 1. Normalized power launched versus forward current.

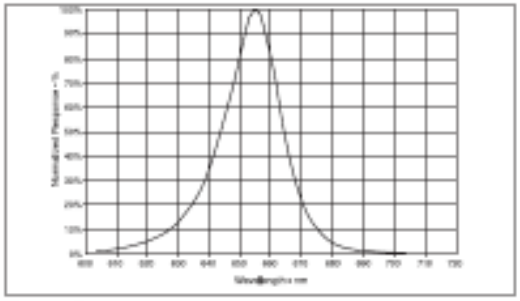


FIGURE 2. Typical spectral output versus wavelength.

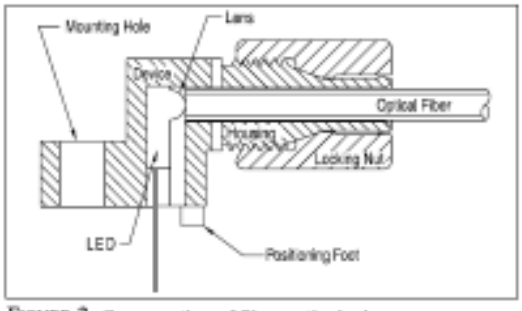
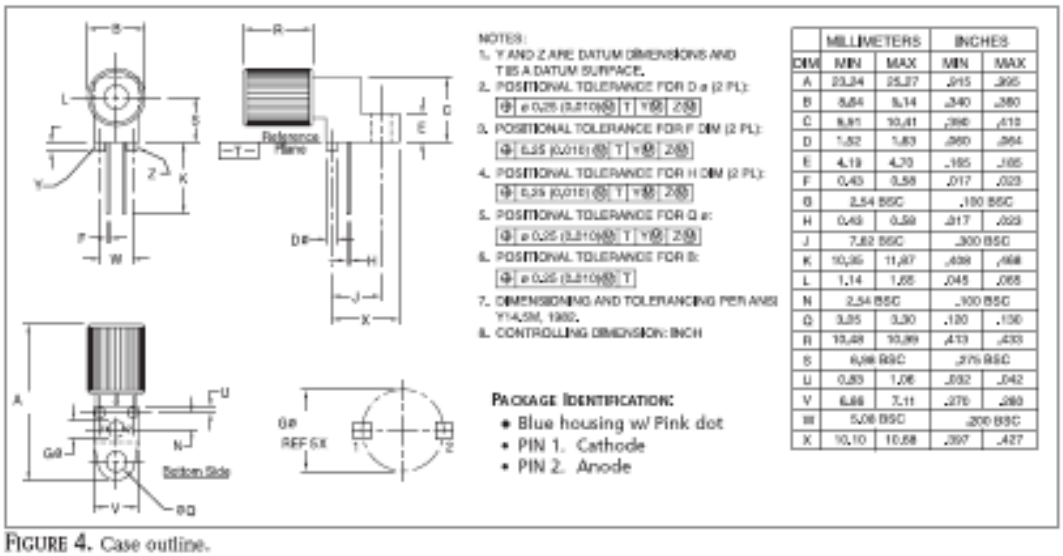


FIGURE 3. Cross-section of fiber optic device.

FIBER TERMINATION INSTRUCTIONS

1. Cut off the ends of the optical fiber with a single-edge razor blade or sharp knife. Try to obtain a precise 90-degree angle (square).
2. Insert the fiber through the locking nut and into the connector until the core tip seats against the internal micro-lens.
3. Screw the connector locking nut down to a snug fit, locking the fiber in place.



DIM	MILLIMETERS MIN	MAX	INCHES MIN	MAX
A	23,24	25,27	.915	.995
B	5,84	6,14	.340	.360
C	8,81	10,41	.286	.410
D	1,52	1,83	.060	.064
E	4,19	4,70	.165	.185
F	0,43	0,58	.017	.023
G	2,54 BSC		.100 BSC	
H	0,43	0,58	.017	.023
J	7,62 BSC		.300 BSC	
K	10,36	11,87	.408	.468
L	1,14	1,65	.045	.065
N	2,54 BSC		.100 BSC	
Q	3,05	3,30	.120	.130
R	10,68	10,89	.413	.433
S	6,98 BSC		.275 BSC	
U	0,80	1,06	.032	.042
V	6,86	7,11	.270	.280
W	5,08 BSC		.200 BSC	
X	10,10	10,68	.397	.427

FIGURE 4. Case outline.

100 Mbps Plastic Fiber Optic IR LED — IF-E91D



Description

The IF-E91D is a high-optical-output, high-speed, infrared LED housed in a "connectorless" style plastic fiber optic package. High performance at economical cost is provided by the IF-E91D in a variety of applications. The device package features an internal micro-lens and a precision-molded PBT housing to ensure efficient optical coupling with standard 1000 µm core plastic fiber cable.

Application Highlights

The high output and fast transition times of the IF-E91D make it suitable for low-cost digital data links. Using standard 1000 µm core plastic fiber, the IF-E91D LED is ideally suited for distances up to 10 meters at data rates of 100 Mbps. The drive circuit design is simpler than required for laser diodes, making the IF-E91D a good low-cost device in a variety of short distance analog and digital applications.

Applications

- Low-Cost Digital Data Links
- Optical Sensors
- Audio Systems
- Medical Instruments
- Automotive Electronics
- Robotics Communications
- Local Area Networks (LANs)
- Wavelength Multiplexing
- Electronic Games

Features

- High Infrared Optical Power
- Fast Rise and Fall Times
- Economically Priced
- Mates with Standard 1000 µm Core Jacketed Plastic Fiber Cable
- Internal Micro-Lens for Maximum Coupling
- Inexpensive Plastic Connector Housing
- Connector-Less Fiber Termination
- Light-Tight Housing Provides Interference-Free Transmission
- RoHS Compliant

Maximum Ratings

(T_A=25°C)

Operating and Storage Temperature Range (T_{OP}, T_{STG}) ..... -40° to 85°C

Junction Temperature (T_J) ..... 85°C

Soldering Temperature (2 mm from case bottom) (T_S) t ≤ 5 s ..... 240°C

Reverse Voltage (V_R) ..... 3 V

Power Dissipation (P_{TOT}) T_A = 25°C ..... 60 mW

De-rate Above 25°C ..... 1.33 mW/°C

Forward Current, DC (I_F) ..... 60 mA

Surge Current (I_{FSM}) t ≤ 10 µsec duty cycle <5% ..... 1 A

Characteristics (T_A=25°C)

Parameter	Symbol	Min.	Typ.	Max.	Unit
Peak Wavelength	λ_{PEAK}	865	870	875	nm
Spectral Bandwidth (50% of I_{MAX})	$\Delta\lambda$	–	30	–	nm
Output Power Coupled into Plastic Fiber (1 mm core diameter). Distance Lens to Fiber ≤0.1 mm, 1 m SH4001 polished fiber, I_F=20 mA	Φ_{min}	200 -7.0	300 -5.2	400 -4.0	µW dBm
Switching Times (10% to 90% and 90% to 10%) (I_F=20 mA)	t_r, t_f	–	7.0	–	ns
Capacitance (F=1 MHz)	C_O	–	120	–	pF
Forward Voltage (I_F=20 mA)	V_F	–	1.85	2.05	V
Temperature Coefficient, λ_{PEAK}	TC_λ		0.3		nm/K

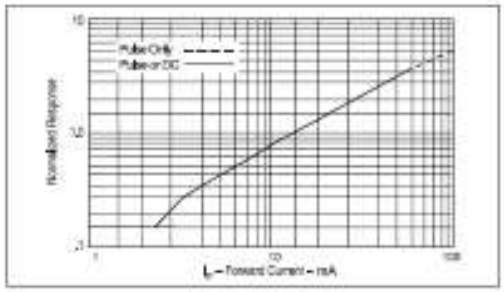


FIGURE 1. Normalized power launched versus forward current.

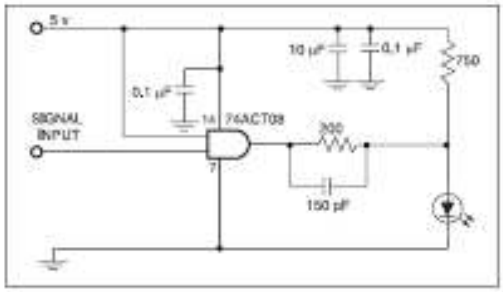


FIGURE 3. Test drive circuit (I_F = 22mA).

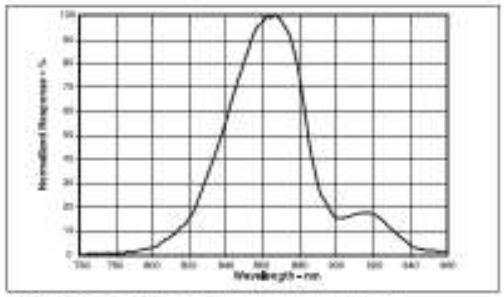
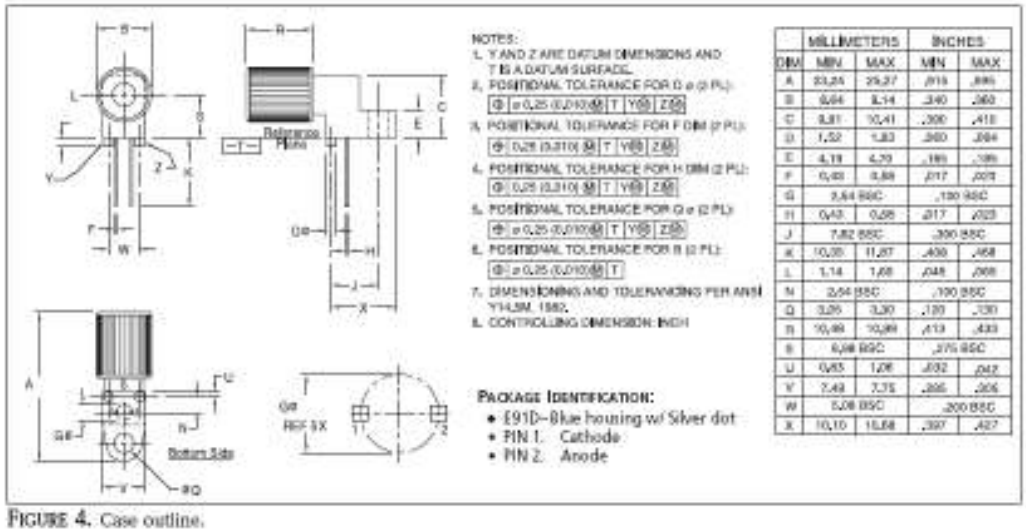


FIGURE 2. Typical spectral output vs. wavelength.

FIBER TERMINATION INSTRUCTIONS

1. Cut off the ends of the optical fiber with a single-edge razor blade or sharp knife. Try to obtain a precise 90-degree angle (square).
2. Insert the fiber through the locking nut and into the connector until the core tip seats against the internal micro-lens.
3. Screw the connector locking nut down to a snug fit, locking the fiber in place.



NOTES:
1. Y AND Z ARE DATUM DIMENSIONS AND T IS A DATUM SURFACE.
2. POSITIONAL TOLERANCE FOR Ø (2 PL):
⌖ ø 0.25 (0.010) M | T | Y M | Z M
3. POSITIONAL TOLERANCE FOR F DIM (2 PL):
⌖ 0.25 (0.010) M | T | Y M | Z M
4. POSITIONAL TOLERANCE FOR H DIM (2 PL):
⌖ 0.25 (0.010) M | T | Y M | Z M
5. POSITIONAL TOLERANCE FOR Ø (2 PL):
⌖ ø 0.25 (0.010) M | T | Y M | Z M
6. POSITIONAL TOLERANCE FOR B (2 PL):
⌖ ø 0.25 (0.010) M | T
7. DIMENSIONING AND TOLERANCING PER ANSI Y14.5M, 1982.
8. CONTROLLING DIMENSION: INCH

	MILLIMETERS		INCHES	
DIM	MIN	MAX	MIN	MAX
A	23,24	23,27	.915	.916
B	8,64	8,14	.340	.360
C	8,81	10,41	.300	.410
D	1,52	1,83	.060	.064
E	4,19	4,70	.165	.185
F	0,40	0,58	.017	.023
G	2,54 BSC		.100 BSC	
H	0,43	0,66	.017	.023
J	7,62 BSC		.300 BSC	
K	10,20	11,67	.400	.460
L	1,14	1,68	.045	.066
N	2,54 BSC		.100 BSC	
Q	3,05	3,30	.120	.130
R	10,99	10,99	.433	.433
S	6,98 BSC		.275 BSC	
U	0,65	1,06	.032	.042
V	7,49	7,75	.295	.305
W	5,08 BSC		.200 BSC	
X	10,10	10,68	.397	.427

PACKAGE IDENTIFICATION:
- E91D–Blue housing w/ Silver dot
- PIN 1. Cathode
- PIN 2. Anode

FIGURE 4. Case outline.

Plastic Fiber Optic IR LEDS — IF-E91A

rev 10/21/04



Description

The IF-E91A is a high-output medium-speed infrared LED in a "connector-less" style plastic fiber optic package. The output spectrum peaks at 950 nm for the IF-E91A. The device package features an internal micro-lens, and a precision-molded PBT housing ensures efficient optical coupling with standard 1000 µm plastic fiber cable.

Application Highlights

The high output and fast transition times of the IF-E91A is suitable for low-cost analog and digital data links. Used with an IF-D96 photologic detector, the IF-E91A can achieve data rates of 500 kbps at link distances up to 7 m. The drive circuit design is simpler than required for laser diodes, making the IF-E91A an excellent low-cost alternative in a variety of analog and digital applications.

Applications

- Low-Cost Analog and Digital Data Links
- Digitized Audio
- Optical Sensors
- Medical Instruments
- Robotics Communications
- Motor Controller Triggering
- EMC/EMI Signal Isolation
- Electronic Games
- Intra-System Links: Board-to-Board, Rack-to-Rack

Features

- Excellent Linearity
- No Optical Design Required
- Mates with Standard 1000 µm Core Jacketed Plastic Fiber Cable
- Internal Micro-Lens for Efficient Coupling
- Inexpensive Plastic Connector Housing
- Connector-Less Fiber Termination and Connection
- Interference-Free Transmission from Light-Tight Housing

Maximum Ratings

(T_A=25°C)

Operating and Storage Temperature Range (T_{OP}, T_{STG}) ..... -40° to 85°C

Junction Temperature (T_J) ..... 85°C

Soldering Temperature (2 mm from case bottom) (T_S) t≤5 s ..... 240°C

Reverse Voltage (V_R) ..... 3 V

Power Dissipation (P_{TOT}) T_A=25°C ..... 100 mW

De-rate Above 25°C ..... 1.33 mW/°C

Forward Current, DC (I_F)
IF-E91A ..... 50 mA

Surge Current (I_{FSM}) t≤10 µsec
IF-E91A ..... 2 A

Characteristics (T_A=25°C)

Parameter	Symbol	Min.	Typ.	Max.	Unit
Peak Wavelength	λ_{PEAK}		950		nm
Spectral Bandwidth (50% of I_{MAX})	$\Delta\lambda$	–	±20	–	nm
Output Power Coupled into Plastic Fiber (1 mm core diameter). Distance Lens to Fiber≤0.1 mm, 1 m SH4001 fiber, I_F=20 mA	Φ_{min}	50 -13	70 -11.6	95 -10.2	µW dBm
Switching Times (10% to 90% and 90% to 10%) (R_L=47Ω, I_F=10 mA)	t_r, t_f	–	1.0	–	µs
Capacitance (f=1 MHz)	C_0	–	25	–	pF
Forward Voltage	V_f (I_F=20 mA) (I_F=50mA)	–	1.2 1.24	1.5 1.5	V

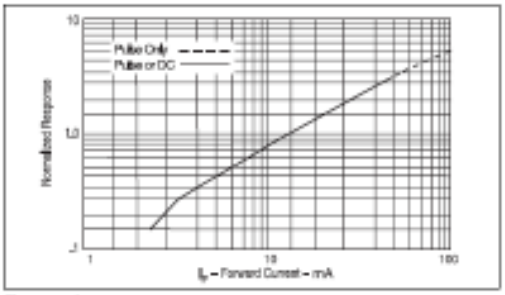


FIGURE 1. Normalized power launched versus forward current.

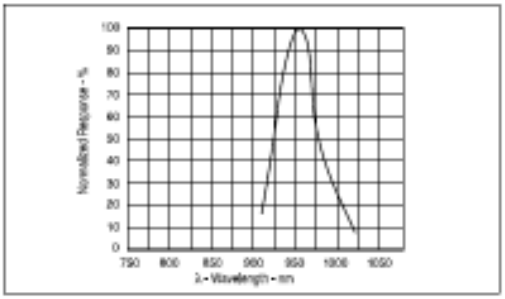


FIGURE 2. Typical spectral output vs. wavelength.

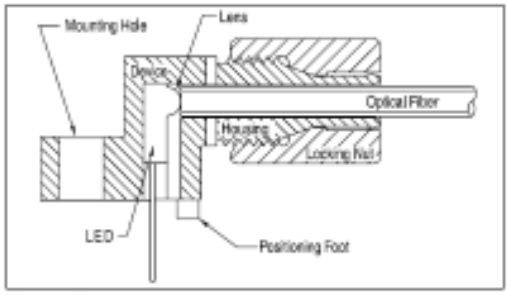
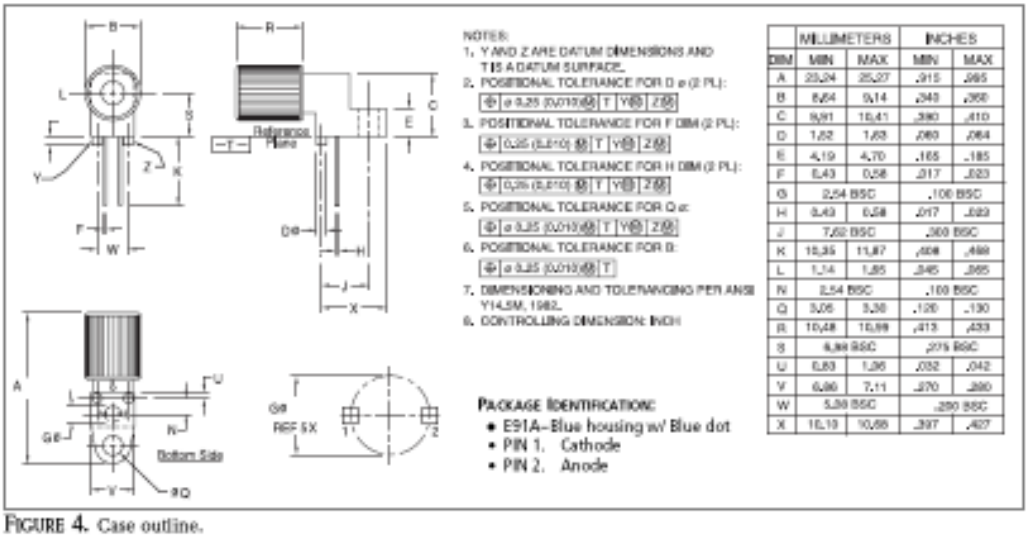


FIGURE 3. Cross-section of fiber optic device.

FIBER TERMINATION INSTRUCTIONS

1. Cut off the ends of the optical fiber with a single-edge razor blade or sharp knife. Try to obtain a precise 90-degree angle (square).
2. Insert the fiber through the locking nut and into the connector until the core tip seats against the internal micro-lens.
3. Screw the connector locking nut down to a snug fit, locking the fiber in place.



NOTES:
1. Y AND Z ARE DATUM DIMENSIONS AND T IS A DATUM SURFACE.
2. POSITIONAL TOLERANCE FOR D ø (2 PL):
⌖ ø 0,25 (0,010) Ⓜ T Ⓨ Ⓜ Z Ⓜ
3. POSITIONAL TOLERANCE FOR F DIM (2 PL):
⌖ 0,25 (0,010) Ⓜ T Ⓨ Ⓜ Z Ⓜ
4. POSITIONAL TOLERANCE FOR H DIM (2 PL):
⌖ 0,25 (0,010) Ⓜ T Ⓨ Ⓜ Z Ⓜ
5. POSITIONAL TOLERANCE FOR Q ø:
⌖ ø 0,25 (0,010) Ⓜ T Ⓨ Ⓜ Z Ⓜ
6. POSITIONAL TOLERANCE FOR S:
⌖ ø 0,25 (0,010) Ⓜ T
7. DIMENSIONING AND TOLERANCING PER ANSI Y14.5M, 1982.
8. CONTROLLING DIMENSION: INCH

PACKAGE IDENTIFICATION:
- E91A–Blue housing w/ Blue dot
- PIN 1. Cathode
- PIN 2. Anode

	MILLIMETERS		INCHES	
DIM	MIN	MAX	MIN	MAX
A	23,24	25,27	.915	.995
B	8,64	9,14	.340	.360
C	9,91	10,41	.390	.410
D	1,52	1,63	.060	.064
E	4,19	4,70	.165	.185
F	0,43	0,58	.017	.023
G	2,54 BSC		.100 BSC	
H	0,43	0,58	.017	.023
J	7,62 BSC		.300 BSC	
K	10,35	11,87	.408	.468
L	1,14	1,85	.045	.065
N	2,54 BSC		.100 BSC	
Q	3,05	3,30	.120	.130
R	10,48	10,99	.413	.433
S	8,89 BSC		.375 BSC	
U	0,80	1,06	.032	.042
V	6,86	7,11	.270	.280
W	5,38 BSC		.250 BSC	
X	10,13	10,66	.397	.427

FIGURE 4. Case outline.

PHOTODIODE

Si photodiode
S2386 series

For visible to IR, general-purpose photometry



Features

- High sensitivity
- Low dark current
- High reliability
- High linearity

Applications

- Analytical equipment
- Optical measurement equipment

■ General ratings / Absolute maximum ratings

Type No.	Dimensional outline/ Window material *	Package	Active area size	Effective active area	Absolute maximum ratings		
					Reverse voltage V_R Max. (V)	Operating temperature Topr (°C)	Storage temperature Tstg (°C)
		(mm)	(mm)	(mm^2)			
S2386-18K	①/K	TO-18	1.1 × 1.1	1.2	30	-40 to +100	-55 to +125
S2386-18L	②/L						
S2386-5K	③/K	TO-5	2.4 × 2.4	5.7			
S2386-44K			3.6 × 3.6	13			
S2386-45K			3.9 × 4.6	17.9			
S2386-8K	④/L	TO-8	5.8 × 5.8	33			

■ Electrical and optical characteristics (Typ. Ta=25 °C, unless otherwise noted)

Type No.	Spectral response range λ	Peak sensitivity wavelength λp	Photo sensitivity S (A/W)				Short circuit current Isc 100 lx		Dark current I_D V_R=10 mV Max.	Temp. coefficient of I_D T_{CID}	Rise time tr V_R=0 V R_L=1 kΩ	Terminal capacitance Ct V_R=0 V f=10 kHz	Shunt resistance Rsh V_R=10 mV		NEP
			λp	GaP LED 560 nm	He-Ne laser 633 nm	GaAs LED 930 nm	Min. (μA)	Typ. (μA)					Min. (GΩ)	Typ. (GΩ)	
	(nm)	(nm)							(pA)	(times/°C)	(μs)	(pF)			(W/$Hz^{1/2}$)
S2386-18K	320 to 1100	960	0.6	0.38	0.43	0.59	1	1.3	2	1.12	0.4	140	5	100	6.8 × 10^{-16}
S2386-18L							4	5.7							
S2386-5K							4.4	6.0	5		1.8	730	2	50	9.6 × 10^{-16}
S2386-44K							9.6	12	20		3.6	1600	0.5	25	1.4 × 10^{-15}
S2386-45K							12	17	30		5.5	2300	0.3		
S2386-8K							26	33	50		10	4300	0.2	10	2.1 × 10^{-15}

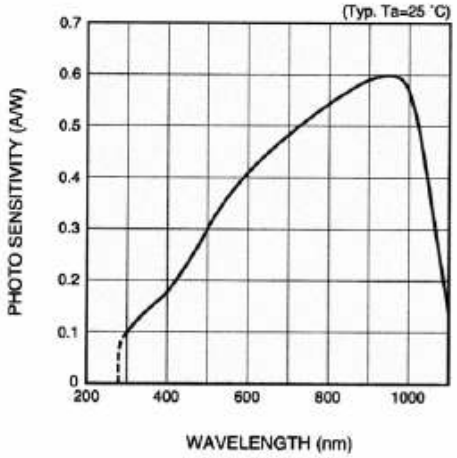
* Window material K: borosilicate glass, L: lens type borosilicate glass

SOLID STATE DIVISION

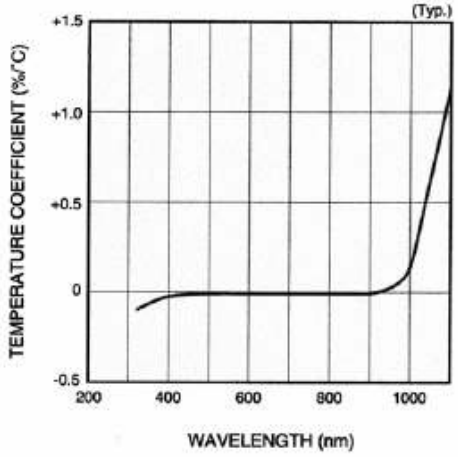
HAMAMATSU

1

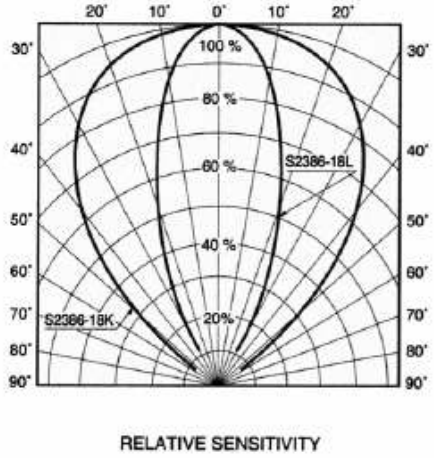
■ Spectral response



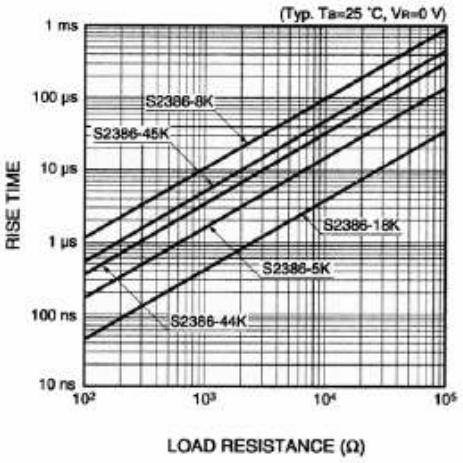
■ Photo sensitivity temperature characteristic



■ Directivity



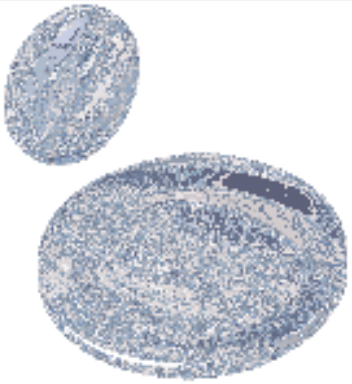
■ Rise time vs. load resistance



Part Number: **LA1576-B**

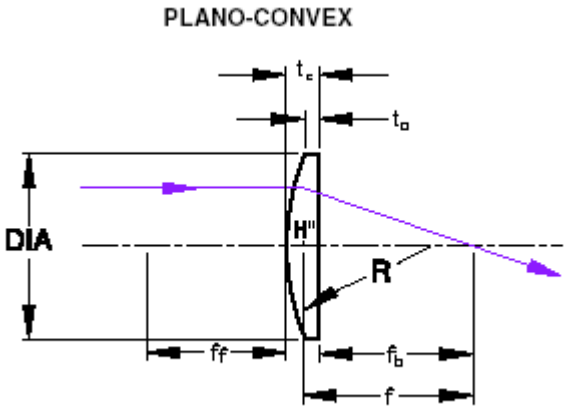
Related	**BK7 B Coated Plano Convex Lens, D 9.00, F 12.00**

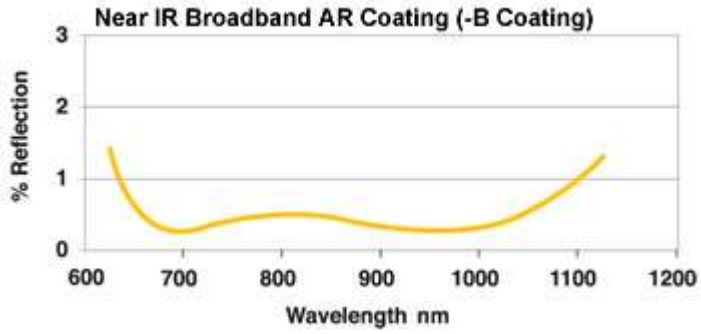
LMR05
LMRA9



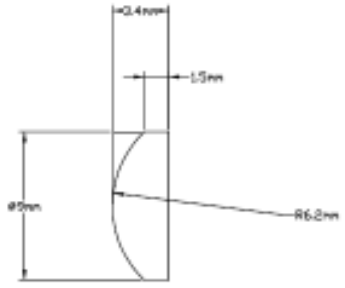
- Material: BK7
- AR Coating: 650-1050nm
- Wavelength Range: 350nm-2.0µm
- Design Wavelength: 633nm n=1.515082
- Diameter Tolerance: +0.00/-0.10mm
- Focal Length Tolerance: ±1%
- Scratch/Dig: 40/20
- Centration: 3 Arc Min
- Clear Aperture: >90%
- Center Thickness tc: ±1mm
- Edge Thickness Given Before 0.2mm @ 45° typ. Chamfer

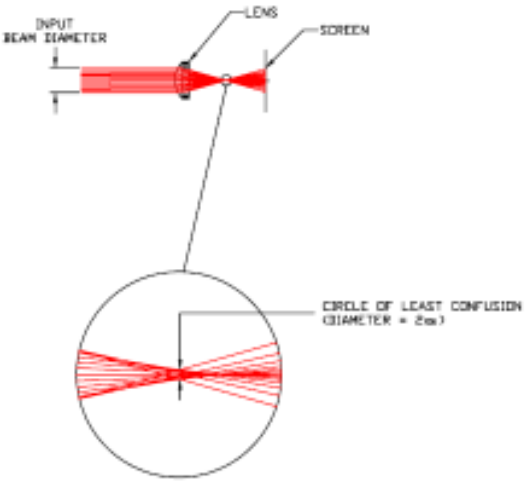
Plano-Convex optics are best used where one conjugate point (object distance, **S** or image distance **S'**) is more than five times the other. This lens shape is near best-form for either focusing collimated light or for collimating a point source.





COPYRIGHT © 2000 by THORLABS INC.





LA1576

SCALE: 4X

FOCAL LENGTH: 12.0mm
DESIGN WAVELENGTH: 633nm, n=1.515882
SCRATCH/DIG: 40/20
DIAMETER TOLERANCE: +0.00mm/-0.10mm
CLEAR APERATURE: >90%
CENTRATION: 3 ARC MIN.
CENTER THICKNESS TOLERANCE: ±0.1mm

CIRCLE OF LEAST CONFUSION

SCALE: 20X

COEFFICIENT OF LINEAR THERMAL EXPANSION

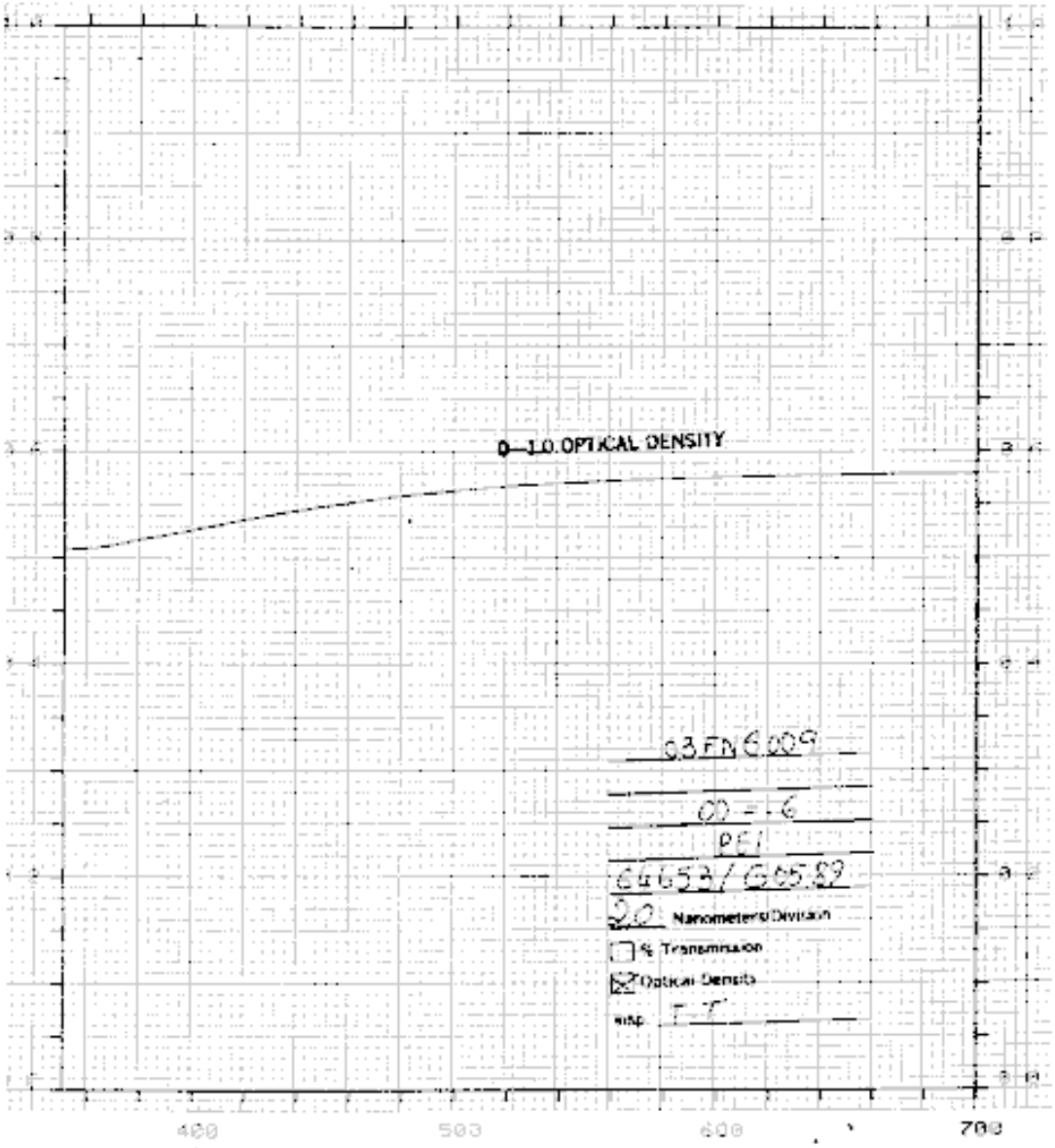
α (-38°c to +73° c) = 7.1 x 10^{-6}/°c

α (+20°c to 300°c) = 8.3 x 10^{-6}/°c

INPUT BEAM DIAMETER	2ω
2mm	Ø4µm
4mm	Ø31µm
5mm	Ø114µm

NOTE: ALL UNITS ARE GIVEN IN MILLIMETERS

INFORMATION ONLY, NOT FOR MANUFACTURING



MELLES GRIOT

Neutral Density Filter

Appendix E

Correspondence Concerning Blood Typing

Jeremy Lambert:

I am concerned about the weak reactions with anti D. Any comments?

Mr. Bennett:

Your samples and antisera are ready. Martha Rae and I were talking about your project and might make the recommendation that you consider not doing Rh. The reason is that ABO are the antigens that can cause immediate transfusion reactions and Rh generally does not. If it does, we have Rh Immune globulin to give them. The major reason is the variability in strength of the Rh antigen, hence a large variability in reaction strength.
There are quite a few weak Rh variants such as Du that you will not find in your tests but the patient will get Rh positive blood based on our more sensitive testing. You can see how that would lead to bedside confusion and lost time. Anyway, to make the test work with your machine is fine; you just may want to consider practicality and efficacy at the bedside.

Jeremy Lambert:

This email is unrelated to my request this morning, but I would like to ask an opinion on one of the final experiments I will run. I would like to be able to simulate a patient receiving RBCs. The way I understand it is that the blood you give me is just RBCs. Is there anyway we can get blood that has not been refined? I would like to be able to mix that blood with incompatible RBCs and see if I can sense the reaction. This would go a long way in actually applying this apparatus. If we cannot sense a reaction, then I guess the next step in this project will require mixtures with anti serums like I am currently doing. Any comments on this experiment?

Mr. Bennett:

You have a microcosm of whole blood in the segment. A seg is sealed off at the time of donation with blood directly from the donor. This is prior to manipulating the unit to produce a packed red cell so this is equivalent to a patient. What you are doing with mixing blood from donor and recipient is basically a crossmatch. In the real world, a crossmatch is performed by mixing only donor plasma with recipient red cells in a tube or card (and automation), then spinning them to bring the cells in contact with the antibodies in the plasma, hence increasing agglutination. ABO antibodies are strong reacting so are usually very visible. Mixing whole blood to whole blood adds a dilutional factor that may not be visible macroscopically, but may be detectable with your procedure. The problem as I see it, would be that you won't know which cells are reacting. This is a real problem when giving group compatible rather than type specific red cells (an O to an A, for example). Again due to the variability in Rh reactivity, you may end up with an unacceptable rate of false negatives.

Antisera, to my way of thinking, would be the best way of going, but whole blood testing as you propose would be interesting. It's good to remember that any testing system has false positives and false negatives due to a variety of reasons such as cross-reactivity,

antibody strength, plasma protein interference, disease interference, and temperature of reactivity (cold agglutinin interference). These should be minimal with ABO, but be aware that they exist, especially with other blood groups. Hope this helps, but if not, let me know.

Jeremy Lambert:

Thank you for setting me straight on the segs. It seems that the whole blood crossmatch is going to be hard to detect. The absorption values between different blood types can differ and therefore it is hard to set a control. Would it be more effective if I simulated the donor with red cells and the patient with whole blood using the patient whole blood mixture as the control? I am going to run a few more tests before I conclude this method is ineffective, but I would still like to know what you think about it.

Mr. Bennett:

You would be getting closer to a classic crossmatch (check for ABO compatibility) by using donor red cells and patient whole blood with the plasma. You're still going to have a variance in results due to the strength of the antibody, especially Rh if you're still trying to test for that, and a dilutional effect of the patient red cells. One serious problem is the interference of atypical antibodies from other blood groups that may agglutinate the donor cells giving a false positive. This could possibly lead to a misinterpretation and delay. These antibodies would be detected by an antibody screen which is done prior to a crossmatch and theculprit identified using specific panels and procedures. Another question would be: how are you going to get donor red cells at bedside without entering the unit, which cannot be done. To be honest, I've wondered how this process can be performed at bedside considering the equipment required, time to perform and interpretative accuracy, when most units of blood are transfused under varying time limits and multiple units at one time (trauma, surgery). Quality control in the lab ensures compatibility, and the bedside check is always a clerical check of doctor's orders, patient id, unit number association with patient, special modifications ordered (irradiation, washing, etc.), and pre-transfusion vitals. It occurs to me that a possible application for your research may be in the lab instead of bedside. Maybe it's an alternative to serological testing, but I honestly doubt it knowing all the variations in antigen/antibody relationships. I don't know if this has been looked at before as there is no current commercial application. It certainly is an interesting approach, and one you've had success with. You might want to contact some of the manufacturers to see what they think of the technology-- companies such as Ortho Clinical Diagnostics and Immucor. I hope this helps. It sounds like you've done an excellent job of research and development. I've enjoyed working with you. Good luck on your presentation.